University of Oklahoma

Graduate College

Mechanisms in Determining Erythrocyte Senescence and Membrane Damage Caused by Supra-Physiological Flow Conditions

A Dissertation

Submitted to the Graduate Faculty

in fulfillment of the requirements for the

Degree of

Doctor of Philosophy

By

James Patrick Buerck

Norman, Oklahoma

2020

Mechanisms in Determining Erythrocyte Senescence and Membrane Damage Caused by Supra-Physiological Flow Conditions

A Dissertation approved for the School of Chemical, Biological and Materials Engineering

By the committee consisting of

Dr. Edgar A. O'Rear, Chair

Dr. Dimitrios Papavassiliou

Dr. Matthias Nollert

Dr. Rong Gan

Dr. Phillip Coghill

Acknowledgements

My deepest gratitude goes out to my advising professor, Dr. Edgar O'Rear, for his guidance, support and friendship throughout my PhD studies. Without his continued care and encouragement my studies at the University of Oklahoma would not have been as enjoyed nor as fruitful.

I would also like to thank the other members of my committee, Dr. Dimitrios Papavissiliou, Dr. Matthias Nollert, Dr. Rong Gan and Dr. Phillip Coghill. Their advice and fresh outlook on my research allowed for a more well-rounded project and complete dissertation.

A special thank you goes out to Terri Colliver and Donna King for their unprecedented assistance and kind conversation. Without their help the work done on not only my research but the entirety of the CBME Department would be extremely limited.

The friendships I built during my time at the University of Oklahoma are also very important to me and would like to thank the lifelong friends I've made: John Gramlich, Patrick McKernan, Aaron Simmons, Alexis Woodward, Michael Felder, Brandon Abbott and Jin Liu.

Finally, I'd like to thank my family. My parents support of my curiosity in the sciences and encouragement to pursue my interests will forever be the greatest gift I'll receive. I'd also like to recognize my younger siblings, Adaline and Mitchell, for the love they've given me throughout my life to this point, whether deserved or not.

Table of Contents

List of Figures

List of Abbreviations

Abbreviation	Definition
ATP	Adenosine Triphosphate
ANOVA	Analysis of Variance
CVD	Cardiovascular Diseases
ErMP	Erythrocyte microparticle
FB	Fibrin
FG	Fibrinogen
FSC	Forward scatter
GPA	Glycophorin A
HSD	Honest significant difference
IgG	Immunoglobulin G
IRB	Internal Review Board
LDH	Lactate dehydrogenase
MP	Microparticle
Nabs	Naturally occurring antibodies
NO	Nitric oxide
PDMS	Poly-dimethyl siloxane
PMP	Platelet microparticle
PS	phosphatidylserine
RBC	Red Blood Cell

RES	Reticulo-endothelial system
Rh	Rhesus
SEM	Scanning Electron Microscopy
SK	Streptokinase
SSC	Side Scatter
TF	Tissue Factor
VAD	Ventricular Assist Device
vWF	von Willebrand Factor

Abstract

Incidence of cardiovascular diseases (CVDs) is growing more prevalent in today's society as a result of changes of three basic factors: the increasing age of the general population, declines in mortality as a result of these CVDs and increasing rate of obesity. As we see the predictable increase in CVDs across the population, the current gold standard for treatment of heart transplant becomes less viable. Therefor the current solution of implanted devices such as Ventricular Assist Devices (VADs) and prosthetic heart valves to either alleviate work required by the heart will become increasingly more common. Since their early use, the level of blood damage seen as a result of VAD implantation has steadily decreased to near negligible amounts of hemolysis. However there still exists sublethal shear effects to red blood cells (RBCs) which may cause any number of serious problems for patients.

The overall goal of this research was to gauge the extent of which sub-hemolytic shear forces affect RBCs and to further determine how these consequences may affect continued normal biological function. Observed changes may also be of value in monitoring the status of patients with medical devices that expose blood to high shear rates. The results of this thesis can be categorized into three general topics.

The first discussed topic is the production of shear-induced erythrocyte microparticles (ErMPs). Microparticles (MPs) are produced by various cells due to a number of different stimuli in the circulatory system. Shear stress has been shown to injure red blood cells resulting in hemolysis or non-reversible sub-hemolytic damage. It is hypothesized that, in the sub-hemolytic shear range, there exist sufficient mechanical stimuli for RBCs to respond with production of ErMPs. RBCs isolated from blood of healthy volunteers were exposed to high shear stress in a microfluidic channel to mimic mechanical trauma similar to that occurring in

ventricular assist devices. In these studies we looked at the concentration of ErMPs after exposure to subhemolytic shear stresses in microfluidic channels. The concentration of shed ErMPs after shear had an upward trend from a control concentration of 5,900 ± 700 ErMP/μL to 64,000 ± 16,000 ErMP/μL after just 15ms exposure of 100,000 s^{-1}. Increasing the shear rate from 50,000s^{-1} to 150,000s^{-1} (exposure time of 10 ms) gave an increase from 9,700±1,100 ErMP/μL to 35,000 ±1,700 ErMP/μL over the control concentration. These results led us to look at other possible responses by RBCs to shear similar to that observed in VAD patients.

RBCs passing through heart pumps, prosthetic heart valves and other cardiovascular devices undergo early senescence attributed to non-physiologic forces. We hypothesized that mechanical trauma accelerates aging by deformation of membrane proteins to cause binding of naturally occurring or native IgG. RBCs isolated from blood of healthy volunteers were exposed to high shear stress in a viscometer or microfluidics channel to mimic mechanical trauma and then incubated with autologous plasma. Increased binding of IgG was observed indicating forces caused conformational or other changes in a membrane protein exposing an epitope(s), likely the senescent cell antigen of band 3. The binding of immunoglobulin suggests it plays a role in the premature sequestration and phagocytosis of mechanically traumatized RBCs in the spleen. Measurement of IgG holds promise as a marker foreshadowing complications in cardiovascular patients and as a means to improve the design of medical devices in which RBCs are susceptible to sublethal trauma. Keeping a view on the concentration of ErMPs as well as IgG positive RBCs could assist in curving further patient complications.

The effects that the ErMPs had on thrombus structure was another area of investigation to examine. Activity of MPs *in vivo* has long been studied and shown to have activity in thrombus promotion and generation. In our study, it was found that ErMPs have the ability to alter the

formation of the fibrin network in a thrombus and further affect clot properties such as hydraulic permeability. The study involved the inspection of flow rates and total lysis times of clots in completely occluded capillary tubes under varying pressure drops. The flow rates through the formed clots with increased ErMP concentrations showed a reduction in flow rate by 46.7% under a pressure gradient of 10mmHg/cm. Reduced flow resulted in the decelerated delivery of fibrinolytic drugs for cleavage of the fibrin network. The decelerated delivery of fibrinolytic drugs corresponded to a time to lysis shift from 5.7 ± 0.7 min to 12.2 ± 1.1 min($p < 0.01$).

Implanted devices cause irreparable damage to blood cells flowing through them. The extent of damage is not fully understood in a capacity below the known threshold for complete hemolysis. The production of microparticles in a sub-hemolytic environment and the comparison of the prior described IgG response to senescent cells and sub-hemolytic forces both introduce an original thought on damage to RBCs before hemolysis. Presented data introduces the idea of using sub-lethal damage as an indication of device integration. Furthermore, if properly utilized the information can spark conversation on broad redesign modifications or reapproach a new design of implanted devices.

Chapter 1 - Introduction

Cardiovascular diseases (CVD) remains the most pressing and largest scale epidemic of the developed world accounting for roughly 80% of lives lost, with over 600,000 deaths a year in the U.S. alone. [1, 2] In addition the current obesity epidemic and its associated diabetes is set to increase the prevalence of cardiovascular diseases throughout the 21st century. There has been a strive to solve or alleviate the problems faced by patients of CVDs for some time now. Patient Louis Washkanskey received the first complete heart transplant in December of 1967 by surgeon, Christian Barnard and still to this day complete heart transplant remains the gold standard for end stage heart disease recovery. Over 45,000 patients annually await a heart transplant due to congestive heart failure; however, only a small fraction of those patients will find a suitable transplant. Total artificial hearts were of curiosity for nearly as long as the complete replacement with a donor heart. Early into their development and first successful implementation, it was determined that complete replacement was unnecessary and only partial heart or ventricular assist was needed to take strain off the heart.

Implantation of ventricular assist devices (VADs) can be used for a number of different reasons; VADs act as a bridge to recovery for patients who only require assistance for tissue repair, a bridge to transplant for patients who are awaiting a donor heart, and as a form of destination therapy. Although VADs are reliable for the treatment of heart disease, as with any implanted device they still cause a number of underlying complications. Integration of synthetic materials into the human biology was among the first of several barriers to overcome.

Operation of VAD pumps introduces supra-physiological flow. The new flow fields create elevated shear stress levels in comparison to usual physiological blood flow. The increased shear stress levels can cause hemolysis, the complete or partial rupture of erythrocytes and release of their contents into the bloodstream. A large concentration of extracellular hemoglobin is toxic to the body, so it's understood that controlling hemolysis caused by implanted devices is of utmost importance. Standard VAD criteria for integration and acceptance for medical trial includes determining an acceptable range of percent hemolysis. Considerable damage to RBC membranes could be sub-hemolytic though, occurring in flow fields classified as below the minimal threshold for hemolysis.

Erythrocytes are of particular interest for blood damage characterization for a number of reasons. Foremost, they account for ~40-45% of the blood volume. Erythrocytes measure in the range of 6-8 μm diameter by 2.2 μm thick. Healthy RBCs also instinctively maintain a biconcave shape. In flow the cells can deform and bend to keep from sustaining any damage to the cell membrane or from blocking flow in the microcirculation. Their deformability is attributed to three main factors: (1) the large surface area-to-volume ratio of the biconcave disc ;(2) the viscosity of the intracellular fluid; and (3) the viscoelastic properties of the cellular membrane. This same essential ability is what allows erythrocytes to maneuver through the small diameter capillaries throughout the body. Erythrocytes travel through every blood vessel within the body, as well as the small diameter capillaries. Therefore, to better understand sub-hemolytic damage, examining the properties of the erythrocytes is required. Like most other cells in the body, erythrocytes are composed of a lipid bilayer of different phospholipids, trans membrane proteins, enzymes, and other molecules. However, due to their simplicity compared to other cells (i.e. their lack of nuclei), erythrocytes can be helpful in determining blood damage.

Human erythrocytes have the ability to undergo large deformations when subjected to stresses, which allows them to pass through capillaries that are narrower than the diameter of a resting RBC. This ability to deform and flow easily through capillaries is limited in damaged and aged erythrocytes. The limitation in deformation also affects the cells ability to flow through the spleen, where blood cells are purposefully filtered for potential removal. Blood flows into the spleen and must be capable of passing though narrow passages within the organ. Healthy erythrocytes readily pass through, while aged or damaged cells may not pass through. These cells may become trapped and are then processed and broken down through a process known as phagocytosis. Measuring a cells ability to deform in varying conditions has long been studied. [3-7] The ability of cells to deform has been measured using many separate techniques including filtration, micropipette aspiration, atomic force microscopy, optical tweezers, and quantitative phase imaging. [3] The micropipette aspiration technique was among the first methods to be used and was first described by Evans in *Blood* and has since been extensively used. [8] Generally there are three moduli used to explain a cells ability to deform: (1) the shear elastic modulus; (2) the area compressibility modulus; and (3) the bending modulus. Each method will give some of the many measurements for cell mechanical properties.

Following decades of innovation and renovation to medical pumps used in blood flow, damage to the cellular components of blood is still a great topic of discussion and concern. Hemolysis is to be kept at a minimum with any in line biomedical device. Additionally, mitigation of the adverse effects caused by non-physiological flow has to be managed. The research presented here is a step in determining how extensive sub-hemolytic shear damage may be and how it may further compromise patients.

Microparticles

One particular cellular reaction due to an outside stimulus, in our case shear, is the presence or production of MPs. From their early detection, MPs were classified as cellular debris not having any particular function. Due to the presence of MPs from numerous cell types and their known presence *in vivo* for both healthy and compromised patients, labs started to research in the possible functions of MPs in blood flow and to the possible causes of MP formation.

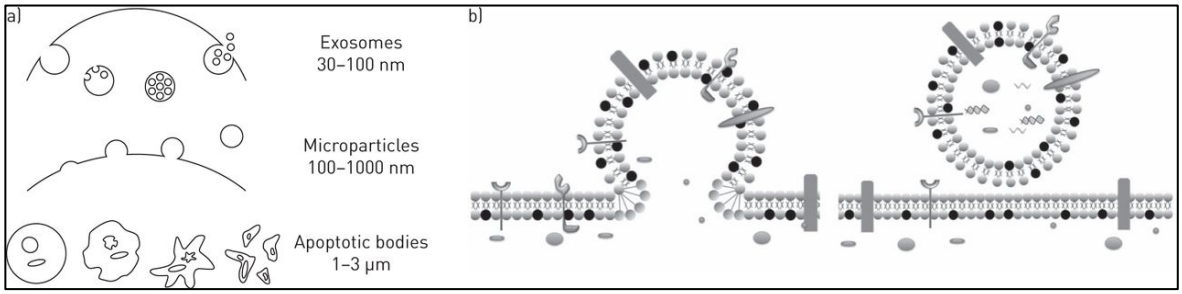

Figure 1-1: Production of Microparticles General Idea

a) Depiction of three different extracellular vesicles b) further detailed view of the production of cellular microparticles[9]

MPs exist in the size range of 0.1 – 1.0 microns and differ from other cell derived vesicles in a number of different ways. The size of the cellular vesicle is important in classifying the type of vesicle. Exosomes exist between 30 to 100 nm and are generally formed by inward budding that are subsequently released after fusing with the cell membrane. Apoptotic bodies are larger in size, between 1 to 3 µm, and form as a result of apoptotic death. Leading up to the death of the cell there is a shrinkage of the cell leaving the membrane amorphous. MPs are generally formed by the outward restructuring of membrane in response to a stimulus. A broad idea of how this restructuring occurs is shown in Figure 1.1 and will be further expanded on moving forward. When MPs are formed the restructuring of the membrane leads to

phosphatidylserine (PS) being more present on the outer layer of the lipid membrane. In most cells the outward expression of PS on a cell is a precursor to apoptosis or programmed cell death and will trigger for the removal of the cell. The use of Annexin V to label apoptotic cells is widely used today and is broadly accepted for most cell types. Conjugated Annexin V will bind to externalized PS allowing for the detection of these "dying" cells in a number of different analytical methods (Figure 1.2). Additionally, the presence of PS on circulating MPs can promote or prompt the coagulation cascade.

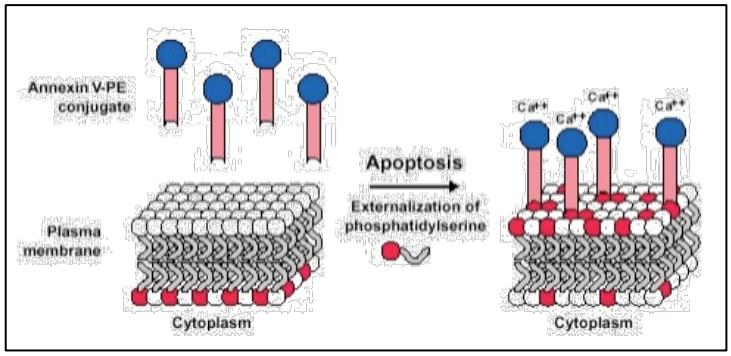

Figure 1-2: Schematic representation of Annexin V binding for apoptosis assays [10]

In an early study by O'Brien, "platelet dust" with platelet like activity was reported.[11] For some time the focus of research regarding MPs was on platelet MPs (PMPs). Along with platelets, all other vascular cells shed MPs, including RBCs, leukocytes, and endothelial cells. Each produced MP will have identifiable characteristics from the mother cell from which they were produced, such as proteins and enclosed cytoplasm.

The production of MPs has been linked to cellular senescence in RBCs.[12, 13] To provide more explanation into how this is applicable, as RBCs age they become less deformable and their ability to flow unhampered through the spleen becomes increasingly diminished. The

senescent RBCs are then removed from flow after being entrapped in the mesh-like network of the spleen. To date RBC senescence has been classified by eryptosis, a form of apoptosis, and a method involving the detection of predisposed cells through Band 3 restructuring or aggregation with subsequent binding of IgG[14, 15]. Both methods contribute to the general idea of increased RBC rigidity.

Thrombosis

The idea of sub-hemolytic shear stresses in VADs which may damage RBCs and severely stunt their lifespan and lead to further patient complications should be a more broadly investigated phenomenon. Several problems for patients experiencing prolonged shear rates exceeding that of physiological conditions has been documented,[4, 16-18] and one effect of increased shear stress conditions are a higher risk of thrombi formation.[19-22] Thrombosis, or the generation of a thrombus, and the structural components of thrombi *in vivo* are greatly dependent on the blood components and concentration of those components involved.

Thrombosis is the end result of the coagulation cascade stemming from either the intrinsic or extrinsic pathways. The extrinsic pathway involves an external trauma causing blood to escape from the vascular system. More relevant to the research in the presented studies is the intrinsic pathway which stems from trauma inside the vascular system. Both pathways are important to hemostasis, or the body's natural ability to maintain a suitable environment. The end result in both cases are thrombin, a naturally occurring enzyme present in plasma, converting fibrinogen into first fibrin monomer then polymer. The fibrin polymer extends trapping platelets as well as other blood components, such as RBCs. Figure 1-3 depicts a general idea of how this process works.

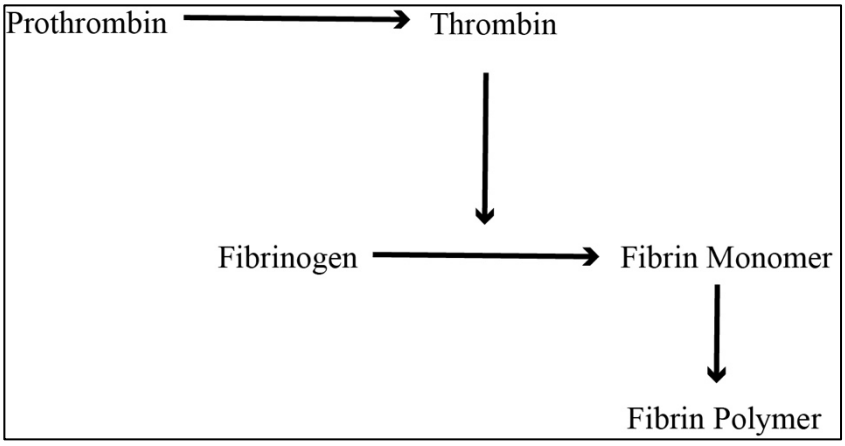

Figure 1-3: Fibrin Thrombus Formation

Thrombosis can cause complete vascular blockage, leading to a lack of oxygen supply to tissues in the body. Depending on the extent of thrombus size and the site of its growth, thrombotic events can cause loss of tissue, organ dysfunction and death. Several CVDs are the direct result of vascular thrombosis: stroke, myocardial infarction, and pulmonary embolism being examples. In most cases a quick response to thrombosis is required to ensure patient safety. The urgency and form of treatment varies by the extent of the thrombus and time of occlusion. Typical treatments include the administration of thrombolytic agents, bypass grafts and angioplasty.

Thrombolytic therapy uses plasminogen activators (PAs) to degrade the fibrin network that provides the structural component of the thrombus. Figure 1-4 summarizes how PAs initiate a cascade of events that result in the dissolution of the blood clot. In summary, PAs convert inactive blood plasminogen to its active form of plasmin, which degrades the fibrin network into soluble fibrin degradation material. As briefly mentioned, the rapid response by PAs is needed to quickly dissolve the clot. Any factors which may stunt the delivery of the PAs and the active plasmin to the face of the clot may have detrimental effects for patients.

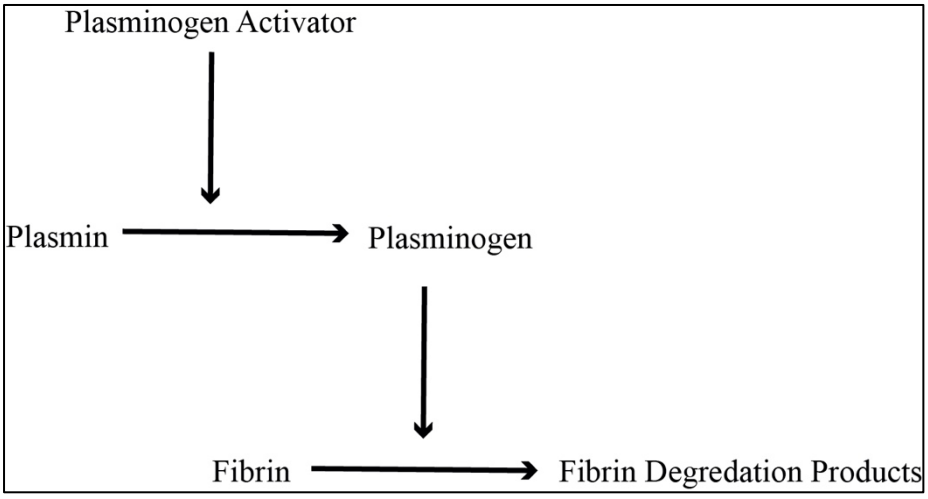

Figure 1-4: Plasminogen Activators

Thrombin concentration amongst other blood components has a direct effect on structural integrity of the clot.[23, 24] The different structural components and fibrin density of the formed thrombus can have drastic effects on permeability.[25, 26] If the flow through the clot is restrained the delivery of the thrombolytic agents used to dissolve the clot would in turn be depressed. Known factors which would decrease the permeability of fibrin networks should be mitigated as best as possible.

The marriage of *in vivo* clinical effects and *in vitro* testing may lend to improvements in several areas of device design and research. Using a controlled shear environment, I sought to divulge the extent of damage sub-hemolytic forces causes on RBCs by implanted devices. The direct effects of shear on RBCs can give insight into the body's natural processes as well. These thoughts and the implications of their results will be discussed more holistically in the following chapters.

Chapter 2 - Production of Erythrocyte Microparticles in a Sub-Hemolytic Environment

For decades, the percent of RBC hemolysis has been used as a measure to facilitate better design and minimize resulting consequences of flow conditions in implanted devices such as heart valves and VADs. Clinical hemolysis levels have continued to decrease with the improvement of devices and their continued evaluation[27]. Though hemolysis levels have dropped significantly as measured by plasma free hemoglobin, shortened RBC lifespans and other indicators of cell injury are still reported in patients with certain implanted cardiovascular devices[28, 29]. Measurement of cellular damage and estimation of the likelihood of premature RBC death with higher accuracy is greatly needed as Olia et al. proposed for sublethal damage to erythrocytes preceding hemolysis[30]. Currently several other factors, including reticulocyte count and lactate dehydrogenase (LDH) tests, are being used to quantify blood trauma in meaningful ways[31].

Sub-hemolytic damage to RBCs has been reported when the RBC membrane is repeatedly stressed beyond normal physiological conditions. The cell's capacity to deform starts to diminish, along with the ability to perform its normal functions[30, 32, 33]. Damage to RBCs has been studied through decreased deformability, increased blood viscosity and RBC aggregation[30, 33-36]. Moreover, much of the physiologic changes that occur to RBCs in flow present similarly in aged or senescent cells[37]. Older red cells isolated by density gradient separation have been shown to be stiffer and smaller in size[38, 39]. The altered rheology of the red cell with mechanical trauma coupled with a recent report of increased binding of IgG

suggests accelerated removal by the spleen[40, 41]. Sub-hemolytic damage has proven detrimental to RBC average lifetime, and has even been related to anemic patients with assistive devices[29, 42]. Thrombosis and inflammatory events without an accompanying measurable hemolysis may be inadvertently prompted by damage to blood and conditions that arise from this damage.

Recently ErMPs have been recognized as greatly contributing to thrombosis, hemostasis and inflammation[43, 44]. In general MPs are vesicles, between 0.1 to 1.0 μm in diameter, shed from the membrane of blood and vascular cells due to the exposure of various stimuli. Initially MPs were classified as cellular debris that served no real function or any biological role. However, their presence in healthy individuals suggested that MPs participated in some biological processes. There have also been some suggestions that vesiculation could also assist RBCs in removing harmful entities[43], such as denatured hemoglobin, band 3 complex aggregates, or damaged membrane [12, 45, 46].

Currently cellular response to membrane damage in RBCs is linked to two separate mechanisms. The first mechanism involves a shift in protein activity resulting in increased PS exposure. Several pathways result in a scrambled membrane including: an increase in cytosolic Ca^{2+} leading to activation of proteases and scramblase causing cytoskeletal damage and an inversion of PS to the outer membrane surface, K^{+} leakage linked to a resultant decrease in transporter activity and increased phospholipid disturbance, and adenosine triphosphate (ATP) depletion again resulting in loss of phospholipid order and ensuing ErMP formation[47, 48]. A second mechanism involves the transmembrane protein band 3 and an autoimmune response triggering for cell removal by macrophages. Oxidatively stressed RBCs are shown to have an increased content of detached band 3 protein, commonly aggregated or degraded in some way,

with increased binding of IgG autoantibodies. Detached band 3 protein is subsequently removed via vesiculation[49-52]. In both proposed methods of ErMP production, some structural alteration of the RBC leads to a beneficial result of loss in membrane, eliminating some harmful RBC characteristic.

Increased production or concentration of ErMPs has been identified in a number of health complications which have an effect on RBCs[53-58]. In patients with pathological conditions including sickle cell disease, thrombosis, and cardiovascular diseases, an increase in MPs is observed. The introduction of implanted devices with higher blood flow rates presents foreign components to the body and, more importantly, high shear conditions that could prompt production of MPs. MP levels have also been shown to fluctuate in patients who have an implanted VAD[19, 44, 59, 60]. The contribution of ErMPs to thrombosis and inflammation is of great concern for these patients. Any increase in ErMPs beyond basal expression levels could have unfavorable results for an already compromised cardiovascular system.

We hypothesized that in the sub-hemolytic shear range there exists enough of a cellular stimulus for RBCs to respond with production of ErMPs. That stimulus could be the mechanical forces themselves or a mechanically induced metabolic pathway. For the latter, known factors such as cytosolic calcium exist to initiate metabolic mechanisms leading to ErMPs[61]. For example, mechanical trauma results in increased intracellular calcium in conjunction with a K^+ efflux[62]. We have examined the production of ErMPs in the subhemolytic regime as a function of shear stress and exposure time. The ability to quantify ErMPs in blood could easily gauge the sub-hemolytic damage caused by flow and possibly predict likelihood of premature RBC removal and the development of anemia.

Figure 2-1: Microfluidic Shear Channel Diagram and Image

a) Shear channel drawing showing dimensions, inlet port and high shear region. b) Microfluidic set-up showing the shear channel with connected tubing and syringe pump visible. c) Post shear microfluidic channel

Materials and Methods

Blood Collection

Venous blood was collected from healthy, adult donors in 3.2% sodium citrate vacutainers (VWR). All blood collection was done following procedures approved by the University of Oklahoma Institutional Review Board. Data was collected from a pool of healthy male and female adult donors, aged 18-64. Donors (n = 10) were informed of the overall goal of the research prior to donations and consent obtained. Blood donations were kept confidential with no identifying documents. Experimental procedures were also performed according to methods approved by the Internal Review Board at the University of Oklahoma. Whole blood was first collected into single centrifuge tubes, then separated at 150 g for 10 minutes. Plasma was then collected for later use. Erythrocytes were isolated with a series of three isotonic saline solution (147.5 mM NaCl) washes, followed by re-suspension in a modified Ringer's Solution (147.5 mM NaCl, 4 mM KCl, 2.25 mM $CaCl_2$, and 10 mM glucose, with 0.05 g/L of Human Serum Albumin). With each isotonic wash, supernatant and buffy coat were removed by Pasteur pipette. After re-suspension in modified Ringer's solution, a Moxi Z Cell Counter (ORFLO) was used to

determine erythrocyte concentration and allowed for adjusting to an overall sample concentration of $5x10^9$ cells/mL (~37% hematocrit).

Microfluidic Shear Channels

Microfluidic channels were used to expose washed RBCs to a single shear exposure under conditions mimicking the high stress, short exposure times exhibited by VADs and prosthetic heart valves. The microfluidic shearing devices contained a constricted region that was designed to expose erythrocytes momentarily (i.e. msec) to high shear conditions [63, 64]. The cross-section of the constricted region was 45 μm wide x 60 μm tall, and the constriction length was varied from 0.7 to 11.6 mm to provide different exposure times to high shear, as is represented in Figure 2-1. Channels were prepared from poly-dimethyl siloxane (PDMS), using a Sylgard® 184 Silicone Elastomer kits (Dow Corning), as previously described [63]. Before running, the channel and tubing were charged with the modified Ringer's solution. Flow through channels was created using an approximately 3 cm segment of tubing (1.57 mm I.D., Silastic® Laboratory) attached to a disposable 1 mL syringe in a KD Scientific syringe pump operated in withdrawal mode. A constant shear environment on the cells was accomplished by maintaining a constant flow rate through the channels. A straight channel microfluidic device (1500 μm wide x 60 μm tall) with no constriction and low shear was used as an additional control.

Flow Cytometry Analysis

Flow cytometry data was collected using a BD Accuri C6 Flow Cytometer (BD Sciences). The detection of events (further expanded upon in Figure 2-1) was done with a series of gates based on forward scatter and side scatter (FSC/SSC) and two separate fluorescent antibodies. The

initial gate for ErMPs was based on fluorescent beads of known size 0.5 and 1.0 μm (Flow Cytometry Sub-Micron Particle Size Reference Kit, Thermo Fisher Sci). RBCs and ErMPs were identified foremost by anti-CD235a-FITC (glycophorin A; eBioscience) binding. In addition to anti-CD235a, a second probe used was a marker for phosphatidylserine (Annexin V Alexa Fluor 647, ThermoFisher Sci), band 3 protein (anti-CD233 FITC, ARP), or bound IgG (anti human IgG Fc Alexa Fluor 647, BioLegend). For tests with the anti-CD233 fluorescent probe, CD235a Alexa Fluor 647 was used so no overlap of fluorescence was seen. Following shear stress, the RBC concentration was adjusted to ~10^6 cells in 0.5 mL Ringer's solution. The RBCs with ErMPs were then labeled with 5 μL fluorescent probes according to manufacturer's protocol. For anti-IgG tests, cellular suspensions were first incubated with previously collected autologous plasma for 30 min. After a 60 min. incubation period with antibodies, cell and microparticle samples in media were then analyzed.

Scanning Electron Microscopy (SEM)

SEM Images were taken at Samuel Roberts Noble Microscopy Laboratory with a ZEISS DSM-960A SEM microscope. Post viscometer shear RBCs were centrifuged and the supernatant was collected. Shear induced ErMPs in the supernatant were then pelleted at 20,000 g for 90 minutes and supernatant was again removed to further concentrate ErMPs. Poly L-Lysine coated glass slides were then used to seed ErMPs before fixing with gluteraldehyde, drying in increasing concentrations of ethanol, critical point drying and sputter coating.

Statistics

In each experiment, significance was assessed using one-way ANOVA with post hoc Tukey's Honest Significant Difference (HSD). Averages were reported as mean ± standard error. Regression analysis with R^2 values were also used to determine fit of data. Significance was defined as $p < 0.05$, and significant data points were symbolized with * in each figure.

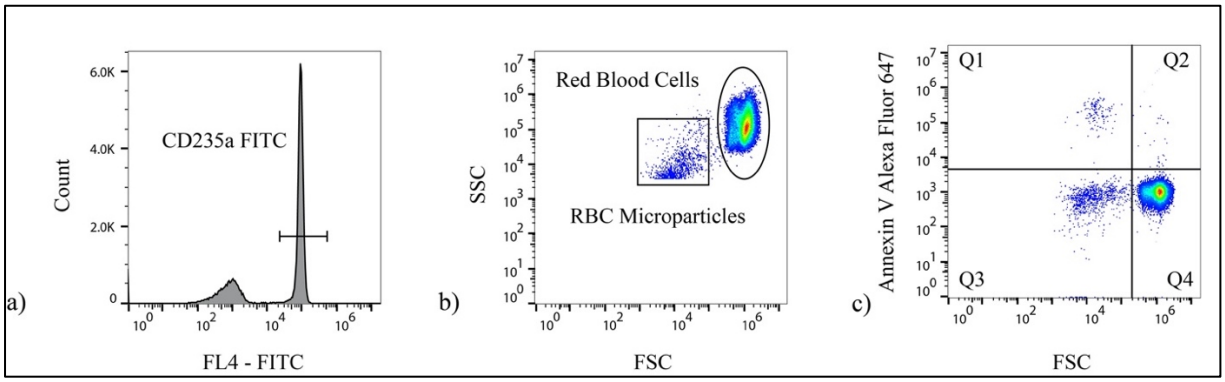

Figure 2-2: Flow Cytometry Methods Used for Detection of ErMPs

Flow cytometry methods for detection and reporting of ErMPs with various antibodies was done using the series of gates shown. a) anti CD235a FITC antibody was used as an initial gate for erythrocyte microparticles. b) Additionally, after the fluorescent gate in the FL1 channel a forward scatter:side scatter (fsc:ssc) gate made on the basis of size was placed around events appearing from ~0.5 and 1.0 μm to quantify ErMPs. The size gate was determined initially using fluorescent beads of known sizes at each 0.5 and 1.0 μm. (c) Alexa fluor 647 labeled Annexin V(shown) or anti-human IgG Fc was then used to determine the ErMPs with externalized PS or IgG presence respectively.

Results

Currently microparticles in blood supernatant are quantified primarily through flow cytometry, due to the ability to quickly and precisely read and analyze cells and particles on several features. The ability to verify MPs based on their mother cell types from which they originated was important for our studies. The data presented was obtained from RBCs and ErMPs collected post shear on washed RBCs. A series of gates were employed, shown in Figure

2-2, to examine the number and average size of shear-induced ErMPs. Initial gating strategies are shown in Figure 2-2a-c. Figure 2-2a depicts a histogram of events as a function of fluorescence intensity while Figure 2-2b shows SSC character versus size as indicated by FSC. Figure 2-2c provides an example of fluorescence intensity versus size for identifying ErMPs. All events have CD235a present and are of correct particle size. Figure 2-3 shows a number of individual runs at varying shear rates and exposure times. Each variation was run n=5 times for an average production of ErMPs. As the exposure time is increased moving from a-c the population of ErMPs, presenting in quadrant Q1, becomes increasingly more dense. Additionally, d-e shows the same increase in Q1 density as the shear rate is increased. The mean percentage shift from Q3 to Q4, reflecting the presence of exposed PS on RBCs, was previously reported on and did not show any significant results[40]. Concentrations reported in Figure 2-4 were found for Annexin V^+ ErMPs (showing in the upper left quadrant, Q1, as in Figure 2-2c). The concentration of shed ErMPs displaying PS after shear had an upward trend from a control concentration of 5,900 ± 700 ErMP/μL to 64,000 ± 16,000 ErMP/μL after just 15ms exposure of 100,000 s^{-1} (Figure 2-4a, $p < 0.001$). Varying the induced shear rate, by manipulating the flowrate in the channels, the same ErMP concentration tests were performed. Increasing the shear rate from 50,000s^{-1} to 150,000s^{-1} (exposure time of 10 ms) gave an increase from 9,700±1,100 ErMP/μL to 35,000 ±1,700 ErMP/μL over the control concentration (Figure 2-4b, $p < 0.001$). Experimental cell velocity and thus shear rate in similar microfluidic channels have been shown to vary, but are generally a fair representative value[65]. Based off of regression analysis on the collected data points (Figure 2-4), the production of microparticles is dependent on both the shear stress and the shear stress exposure time, exhibited by the equation for concentration of ErMP as a function of shear rate, γ, and exposure time, t,: Log_{10} (ErMP /μL) = -

1.45 + 0.46 $Log_{10}(t)$+1.05 $Log_{10}(\gamma)$, R^2=0.74. These results parallel previous ideas with free hemoglobin as a way of measuring blood damage[66, 67]. In our specific study the volume of sample passing through the channel was minimal and did not allow for an accurate measurement of free hemoglobin.

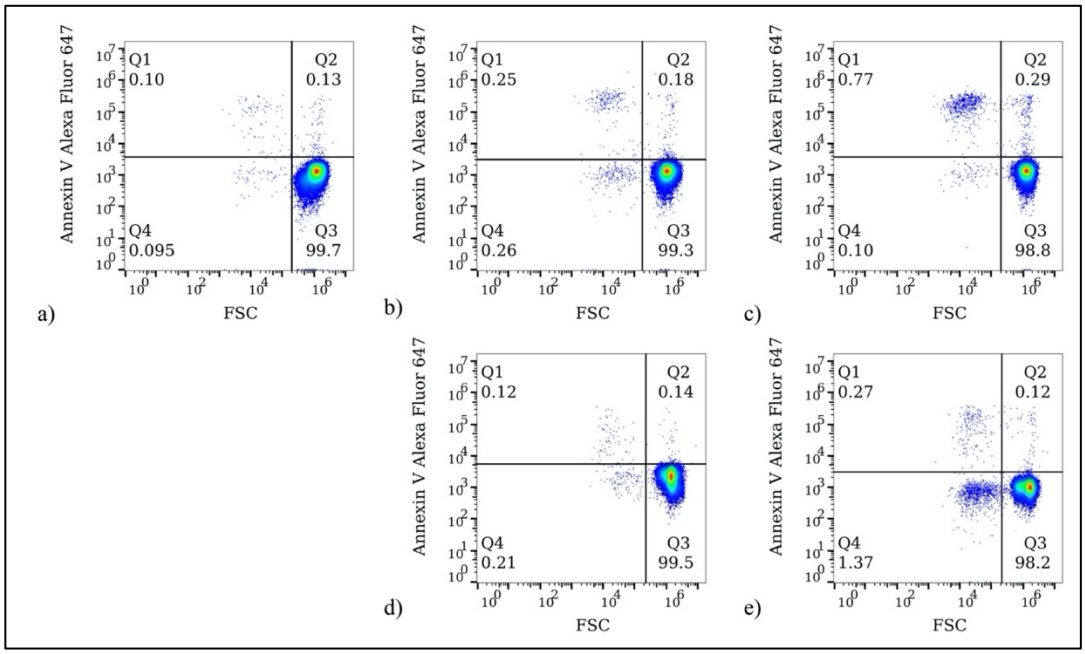

Figure 2-3: Shear Induced ErMP Production for Varied Single Runs

Shown is an increase in ErMP production. Using the same gating strategy presented in Figure 2-1, (a-c) is respectively single runs of control (microfluidic device with no high shear region), 5 ms, and 15 ms shear exposure to 100,000 s^{-1}; as seen from left to right there is a noticeable increase of ErMPs. Similarly (d-e) shows single runs of 50,000 s^{-1} and 150,000 s^{-1} each for 10 ms. X-axis in each represents the FSC or size. Y-axis in each is FL4 showing fluorescence of Annexin V Alexa Fluor 647.

The average shear-induced ErMP recorded by flow cytometry in our studies was approximately 0.64 μm in size, as determined by FSC values. The cutoff seen in Figure 2-5a-c results from our gating strategy of considering events only as low as ~0.45 μm(the lower size limit of the flow cytometer). The observed microparticle size distribution shifts to smaller sizes

on going from a 5 msec exposure to a 15 msec exposure. This trend in ErMP size suggests a higher percentage of ErMPs to be below the flow cytometry size limit (Figure 2-5) across all tests. Additionally, trends show that the mean ErMP size generally decreased as the exposure time was increased (Figure 2-6a) ($p = 0.11$). The cumulative frequency distribution in Figure 2-6b shows the FSC distribution shift of the ErMPs for individual runs in each of the control channel and 5 msec and 10 msec exposure runs at a shear rate of 100,000s^{-1}. The layout gives a straightforward presentation of ErMP size shift. SEM images (Figure 2-7) showed a wide array of particle sizes, most of which were below 100 nm. Those in the range ascribed to MPs (0.1-1.0 μm) were typically below the lower limit of the flow cytometer. The structure of the MPs exhibited irregular shapes with some suggestion of the plastic deformation of the RBC membrane reported by Hochmuth [68].

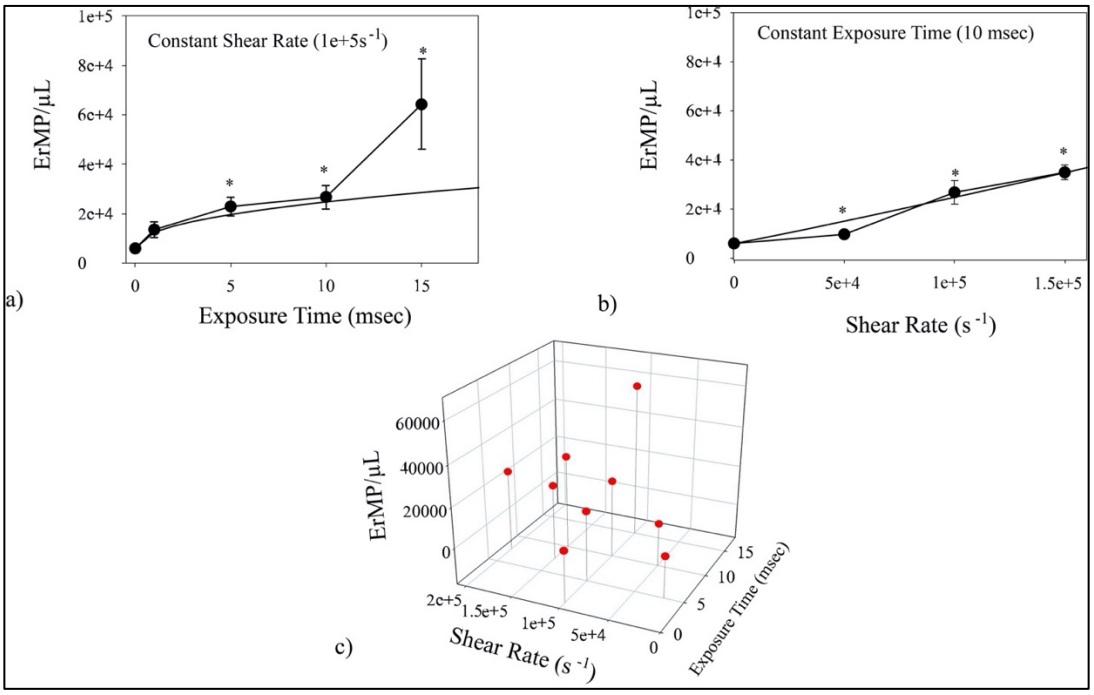

Figure 2-4: Shear Induced ErMP Concentrations from Microfluidic Channel Shear Experiments

Annexin V^+ positive ErMP concentration measured by flow cytometry following shear of washed RBCs in microfluidic devices by varying a) exposure time (100,000s^{-1} shear rate) (n=5, p = 0.001)and b) shear rate (10 ms exposure) (n=5, p < 0.001). Log-log regression analysis, shown as a trend line alongside (R^2=0.75, p = 0.016), was used to determine the ability of predicting the effect shear may have on an RBC suspension. The data points used for regression analysis were plotted in c). The presented data shown as an increase in ErMP over the control concentrations seen from flow cytometry(n=5). *Indicates significance of p<0.05 by Post hoc Tukey HSD.

In addition to exploring the concentration of Annexin V^+ ErMPs after shear in microfluidic channels, similar tests were run viewing the concentration of IgG^+ ErMPs. As previously mentioned, anti-IgG Fc Alexa Fluor 647 antibody was used in combination with anti-CD235a FITC. Results of IgG^+ ErMPs showed similar MP concentrations with a control concentration of 8,800 ± 200 increasing to a concentration of 85,000 ± 22,000 after 15 msec exposure to 100,000 s^{-1} shear. The two antibodies used in conjunction with CD235a were chosen with previously proposed mechanisms of ErMP removal in mind as discussed in the introduction (PS exposure and band 3 aggregation)[69-73].

Detection methods for ErMPs have not yet been standardized. In an attempt to report more inclusive data, consideration for total amount of ErMPs (gating only for anti-CD235a) was considered as well. Removing the secondary fluorescent gate for Annexin V or anti IgG-Fc, the percentage of ErMPs which were negative/positive was obtained (Table 1). As shear stress exposure time was lengthened, the percentage of ErMPs which expressed PS gradually increased. Though the exposure of PS on ErMPs seems highly dependent on the exposure time to increased shear, the magnitude of shear rate had much less of an effect on the determination of lipid orientation on ErMPs with insignificant difference across the varied magnitudes of shear rate tested. These results are enforced by the equation generated for PS^+ ErMP production. ErMPs created from shear stimuli in our studies which showed presence of IgG bound remained fairly consistent across all tests at ~84% of all ErMPs. Though percentage of ErMPs showing

bound IgG remained consistent, the average fluorescence greatly increased with longer exposure times to shear. After 15 msec of shear exposure there was a 50.0 ± 25.9% increase in anti-IgG Fc Alexa Fluor 647 fluorescence as detected by the FL4 channel.

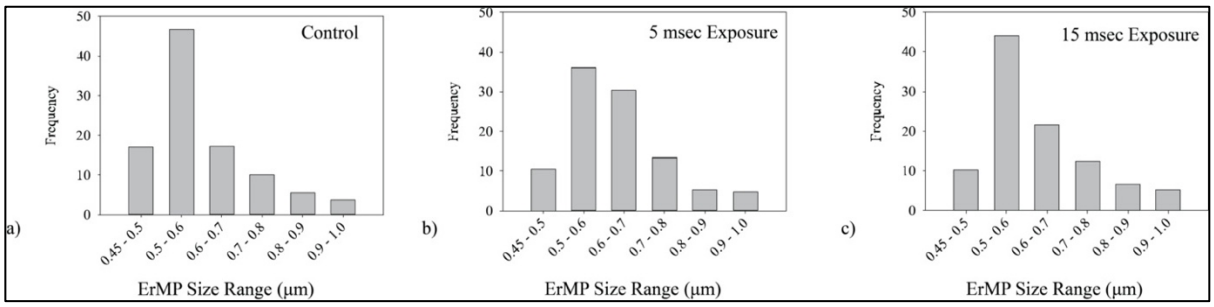

Figure 2-5: ErMP Size Histograms from Flow Cytometry

a) ErMP size histogram comparison for control, 5 msec exposure and 15 msec shear exposure respectively. Data collected for each did not show any significant difference. Flow cytometryshowed an average ErMP size of 0.64 µm.

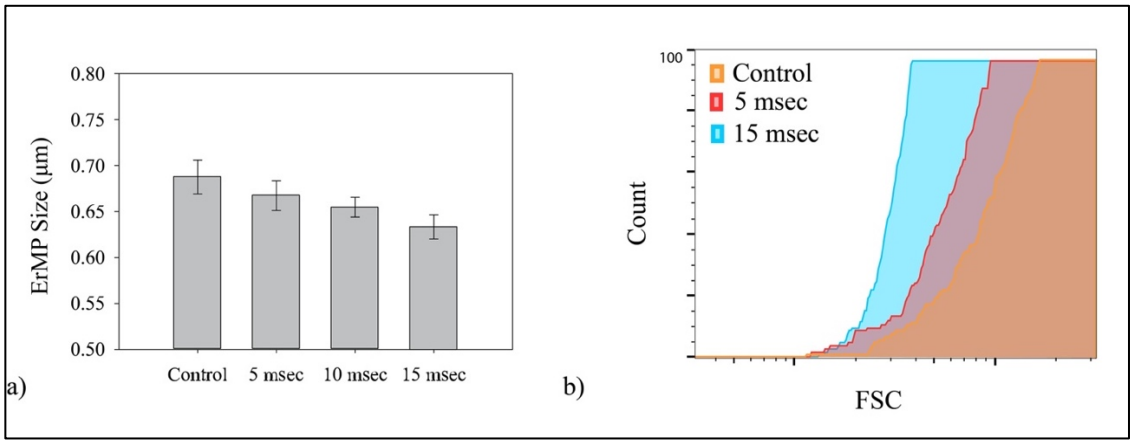

Figure 2-6: Flow Cytometry Mean ErMP Size

a) Using the gating scheme from Figure 2-2, the average FSC value for Annexin V^+ ErMP was averaged across each data point. The FSC were then related to a size through interpolation based on the fluorescent beads of known size, 0.5 and 1.0 µm. (n=5, p=0.11) b) Cumulative Frequency Distribution of three single experiments for control, 5 msec and 15 msec exposure showing FSC differences of ErMPs in each.

Discussion

Experimental tests conducted in the sub-hemolytic range, defined by shear magnitude and duration of shear, show that shear stress injures cells even though it does not cause detectable hemolysis. Apart from extreme cases, hemolysis has been mitigated in many devices to such small levels that the detection methods for damage should not solely rely on the hemoglobin in plasma. Having an easily quantifiable gauge of trauma with low shear would allow for further analysis of certain medical devices involved in blood flow.

One measurement currently shown to have clinical promise in showing blood trauma at low levels is detection of LDH, which has been related to thrombosis in left VAD patients[74, 75]. Results from the current study show that the production of microparticles from washed RBCs has a significant upward trend with both level of shear rate and duration of shear. As represented by the best-fit curve displayed in Figure 2-4a-b, production of ErMPs might also be used in quantifying trauma to RBCs in flow.

Increased MP concentrations have been observed clinically in a number of different pathological conditions affecting RBCs. One such condition is the integration of artificial organs and implants. For patients with implanted VADs, which impart non-physiological, sub-hemolytic flow patterns, ErMP production could foreshadow adverse events[44] like thrombosis or early removal of damaged RBC[76]. While detectable hemolysis levels do occur on occasion, it is typically the result of integration problems and not flow conditions in the devices themselves.

ErMP production may lend to explaining the decreased deformability of RBCs with shear or age. Deformability of RBCs can be attributed to the structural elements of the cytoskeletal proteins, membrane surface-to-volume ratio and the control of ion/water flow across channels.[77] As RBCs age their deformability slowly starts to diminish with a simultaneous

reduction in average erythrocyte size.[78] Similar to the effects of ageing with loss of ErMPs, production or shedding of MPs caused by shear corresponds to the subsequent decrease in size and surface-to-volume ratio concomitant with increased stiffness[7, 39, 43].

PS is an important indicator for the continued regulation of RBC life among an sign of other possible complications. For RBCs, similar to other cells in flow, the externalization of PS is an indicator of apoptosis or programmed cell death. In RBC physiology this is known as eryptosis and warrants quick removal by the spleen. RBCs lipid membrane is constantly monitored by the three different enzymatic transmembrane lipid transporters: flippase, floppase and scramblase. Together they maintain a specific lipid membrane symmetry; however, those proteins are not active in MP leading to a majority of MPs exhibiting PS externally. The loss of membrane symmetry with increased presence of the negatively charged PS on the ErMP outer surface would greatly contribute to procoagulant affects[22, 79]. In several studies MPs have been shown to accelerate coagulation[22, 80-84]. Recent studies have even shown MPs initiate contact pathway coagulation[85, 86]. In our experiments, we found that the longer RBCs are subjected to shear the higher the percentage of ErMPs will show externalized PS presence. In the microfluidic channels, 15 ms of exposure showed a significant increase of ~25% in fraction of EMPs sufficiently showing PS externalization (Table 2-1). The longer RBCs are then subjected to shear the more likely that shed ErMPs would express PS and be likely to promote or initiate coagulation. The studies presented here are also the results of a single exposure to shear in microfluidic devices. *In vivo* RBCs would be exposed to the high shear regions multiple times over their lifetime. Multiple exposures over time may if anything increase the likelihood of ErMP formation and promote coagulation even further. Sinauridze et al. demonstrated that platelet microparticles have 50 to 100 fold higher procoagulant activity than activated platelets

themselves[84]. The large volume fraction of RBCs in comparison to other blood cells presents a possibility for the overproduction of ErMPs when mechanical stimulus is presented.

For patients compromised with CVDs the introduction of ErMPs complicates and already complex system; however, ErMPs may also assist in certain means. In another study looking specifically at ErMPs, Jy et al. determined the prospect of commissioning ErMPs as a potential use as haemostatic agent for treatment of bleeding[87]. Their research indicated that ErMPs greatly reduce bleeding times in both rabbit and rat with low platelets counts. Ex vivo tests were also done on blood from patients with low platelet counts or coagulation defects. In both cases the introduction of ErMPs greatly increased the coagulability of patient blood. Shear stimuli creating ErMP potentially promote thrombotic events and simultaneously inflammatory tendencies; an effect which would greatly affect patients already suffering from cardiovascular diseases, where the control of ErMP concentration as well as senescent RBCs by macrophages is already stressed.

In vivo, the aging of cells and production of MPs would be kept at a physiological concentration with continuous removal. The mechanism or pathway for removing MPs in the body (and more specifically ErMPs once in circulation) has remained an area with little investigation. In general, it is believed that the *in vivo* removal of MPs is accomplished by phagocytic cells within the reticulo-endothelial system (RES) based on some identifying characteristic, such as phosphatidylserine (PS)[69-71, 88]. Willikens et al. showed the preferential removal ErMPs by Kupffer liver cells with an externalization of PS[72]. Briefly, blood cell MPs were collected and labeled with ^{51}Cr then injected through the inferior vena cava. At specified times liver lobules were tied off and the radioactivity was measured to assess uptake.

Table 2-1: Percentage of ErMPs with Various

	PERCENTAGE OF ERMP PRESENTING ANTI -HUMAN IGG FC BINDING	PERCENTAGE OF ERMP PRESENTING ANNEXIN V	AVERAGE ERMP ANTI-HUMAN IGG FC FLUORESCENCE INCREASE
CONTROL	82.7±5.1%	55.8± 5.8%	-
5 MSEC	85.2±5.4%	59.7 ± 7.1%	33.6 ± 33.4%
10 MSEC	85.0±5.8%	*73.9± 14.1%	45.8 ± 35.0%
15 MSEC	83.2±3.8%	*85.2± 4.5%	50.0 ± 25.9%

In addition to the PS preferential phagocytic removal of MPs, an IgG mediated binding and removal was shown by Livtak et al [73]. MPs contain lipid membrane and protein from their mother cell. The removal system for RBCs and ErMPs are likely common or identical. In several studies, autologous IgG was shown to be detected on RBCs, binding to band 3, and prompting them to be removed from circulation, similar to the study by Livtak[89-92]. The band 3 complex, encoded by the gene SLC4A1, plays an important role in both membrane structure as well as the mediating of ions across the membrane. As erythrocytes age, band 3 degrades becoming free from the spectrin network allowing it to clump together[90, 93]. In previously published data we have also shown that erythrocytes present IgG binding, most probably to band 3 complexes, post shear in microfluidic devices similar to those used in these studies[40]. Flow cytometry results, gating for anti-human IgG, showed fairly consistent ErMP concentrations across shear stress exposure similar to PS^+ microparticles. Percentage of ErMPs displaying IgG presence remained fairly consistent at ~84% (Table 1). Our results may in fact support the regulation of ErMP concentration as a combined effect of both band 3 degradation and clustering as well as the detection of PS mediated removal.

The flow cytometric description of blood MPs has great utility in designating MP origin and size; however, limitations of most modern flow cytometers should be taken into consideration. Common flow cytometers are equipped with lasers that have a lower threshold for particle size detection of ~0.5 μm. The sensitivity of the instrument is unpredictable for events with a size lower than such. According to a number of studies the average MP size in normal blood is around 0.25 μm, much smaller than the generally accepted detection limit of conventional flow cytometry, though new more sensitive devices are being introduced[94-96]. The normal physiological concentration of ErMPs in blood is fairly consistent among healthy adults [94]. According to our experiments, concentration of MPs from 0.5 to 1.0 μm drastically increases after only short exposure to an increased shear stress. Effects of blood damage by shear in this study, while shown to be extensive, could be underestimated if only considering events larger than 0.5 μm.

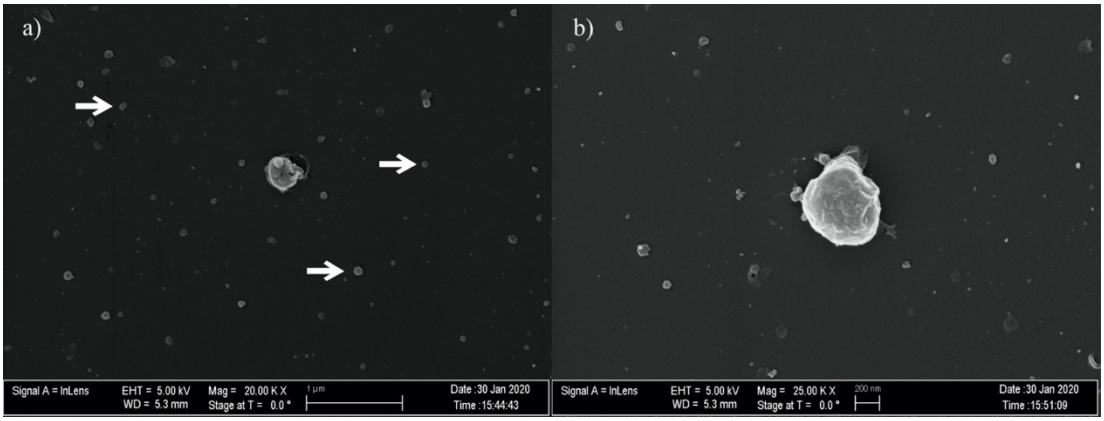

Figure 2-7: ErMP SEM Images

SEM images taken of ErMPs showing general morphology and overall size of ErMPs. a) Arrows point at general size ErMPs seen with SEM technique. b) Higher magnification of ErMPs for closer look of morphology

Design of VADs and other similar medical devices has gradually grown to a point where the clinical hemolysis levels are reduced to near negligible levels. Yet, with the continuing growth of VAD integration and design, patients are still presenting with any number of complications from thrombus formation to gastrointestinal bleeding complications. In light of the natural physiological role that MPs in blood flow play in thrombosis, hemostasis and inflammation, large increases in their concentration could have detrimental effects on cardiology patients with VADs. As such, quantifying sub-hemolytic damage to RBC with MPs should be of interest. The predictability of ErMP production by shear stimulus could provide insight into patient response to VADs as well as provide an indicator to possible complications. This insight into sublethal trauma may further improve the design and operation of medical devices.

This chapter was submitted in part to a peer reviewed journal for publication.

Chapter 3 - A Flow Induced Autoimmune Response and Accelerated Senescence of Red Blood Cells in Cardiovascular Devices

This is a post-peer-review, pre-copyedit version of an article published in Scientific Reports. The final authenticated version is available online at: https://doi.org/10.1038/s41598-019-55924-y

Flow represents an important stimulus of mechanosensing for many fundamental biological processes. That is particularly true for certain functions of the circulatory system. The action of shearing blood flow on vessel walls causes the release of nitric oxide (NO), drives formation of catch bonds during leukocyte rolling, stimulates expression of fibrinolytic trigger tPA, and results in reduced presentation of inflammatory molecules[97-102]. In developmental biology, flow affects gene expression and cell differentiation setting them, for example, on a path to formation of distinct heart chambers[103] and may play an additional role in development by determining arterial or venous cell identity[104]. Through such mechanisms, the physical action of shear stress triggers biochemical responses important to functioning and development of the circulatory system.

Shear stress is also important in the initiation and progression of certain pathologies. In particular, flow has been integral to understanding of atherosclerosis and the localization of plaques. Disturbed flow promotes increased expression of pro-inflammatory species like E-selectin and VCAM-1[105, 106]. Mechanical trauma, a pathology distinctively attributable to flow, occurs when components of blood encounter non-physiologic forces during extracorporeal

circulation with consequences for platelets[107, 108], white cells[109, 110] and von Willebrand Factor, vWF[111, 112] in addition to RBCs.

Once a major concern in mechanical trauma, hemolysis has become less of an issue with design improvements of prosthetic heart valves and heart pumps. A less apparent manifestation of harm is reduced ability of injured RBCs to survive the microcirculation. As early as 1962, sublethal damage was evident in animal studies of extracorporeal circulation by shortened circulatory half-lives and anemia[113]. While flow in contemporary prosthetic heart valves causes little or no hemolysis, the stresses present do reduce cell lifespans by approximately 20%[114]. In similar fashion, the high shear environment in ventricular assist devices (VADs) has been linked to markedly abridged circulatory lifespans for RBCs[115]. This is important because accelerated removal contributes to anemia for an individual and/or means an added metabolic load to replace the lost cells. Loss of RBCs has been attributed to reduced deformability and early capture in the spleen[116]. In vitro experiments by Velker[117] in 1977 first established stiffness of RBCs after shear exposure, a result later confirmed by a number of other groups[4, 118-121].

Sublethal mechanical trauma is in fact known to cause a shortened mean circulatory lifespan for red blood cells. Nanjappa[122] found that the half-life of re-infused Cr^{51}-labelled RBCs in the dog decreased with the length of exposure time by 22-60% after low shear stress ex vivo (~9 Pa). This research observation fits with clinical findings for circulatory lives of RBCs from prosthetic heart valve patients and ventricular assist devices. Compared to controls (122±23 days), patients with biologic heart valves (103±15 days) and mechanical valves (98.8±23 days) have shorter mean RBC lifespans[76]. Likewise, mean RBC lifespans for patients on continuous flow left ventricular assist devices have been reported to be as low as 30 days [115]. This

premature elimination of cells after blood trauma indicates that more subtle, sublethal forms of damage may be involved and hints at underlying mechanisms similar to those affecting removal of the senescent RBC.

Increased rigidity after non-physiological shear is a characteristic shared with senescent red blood cells that contributes to their routine removal after a normal 120 day lifespan[116, 123]. Years ago Kameneva recognized the similarity between cells naturally aged and those exposed to mechanical stress[124]. To our knowledge though, no group has explored links between shear stress and other widely held theories related to senescence. We considered that mechanisms for physiologic elimination of old RBCs might offer insights into the pathology of mechanical trauma.

Rubin has suggested that the two main models of RBC aging are eryptosis, a variation of apoptosis, and band 3 clustering[14]. These theories tend to focus on biochemical aspects that may act in concert with altered deformability[125]. That is, stiff cells will move through the spleen more slowly, affording greater opportunity for recognition of opsonins by macrophages and phagocytosis. One theory for aging involves attachment of methemoglobin to the interior surface of the RBC membrane or other stimulus to promote aggregation of the integral structural transmembrane protein band 3 (SLC4A1, a solute carrier family 4, anion exchanger, member 1) [126, 127]; according to this theory, subsequent binding of naturally occurring antibodies(NAbs) to these band 3 clusters promotes capture of the cell in the spleen[128].

Band 3 contains a senescent antigen, identified by Kay, that has epitopes for NAbs[90, 129]. Since the senescent antigen is present on band 3 in young cells[130], a key step during aging must somehow bring about greater availability. That may occur by aggregation, enzymatic modification or molecular rearrangement. It is conceivable that deformation of a young cell due

to flow will induce accessibility. For example, conformational changes in membrane proteins might expose the senescent antigen[131] as a result of shear. Moreover, it seems plausible that enhanced mobility of membrane proteins during shear could facilitate band 3 clustering and conformational change. By attaching latex beads to the RBC membrane and observing single cells during "tank tread" flow in the rheoscope, Fischer demonstrated relative motion within the surface of the membrane[132]. Such motion should increase the interaction of molecules of band 3 with greater prospects for aggregation and NAbs binding.

We have shown that binding of autologous immunoglobulin G(IgG) to RBCs occurs at exposure times and stress levels found in cardiovascular devices and conclude that it may be a contributing factor to premature removal of red blood cells in patients with these devices. Externalization of phosphatidylserine (PS) on the outer surface of the cell and eryptosis, another prospective basis for removal of senescent RBCs[131, 133, 134], was not found in the present study to be a significant factor.

MATERIALS AND METHODS

Blood Collection

Venous blood was collected from healthy adult donors (n=10), aged 18-64, in 3.2% sodium citrate vacutainers (VWR). All blood collection was done following procedures approved by the University of Oklahoma Institutional Review Board (IRB). Donors were informed of the overall goal of our research prior to donations and informed consent was obtained. Blood donations were kept confidential with no identifying documents. Experimental procedures were also performed according to approved methods set and approved by the IRB at the University of Oklahoma. All RBCs were isolated with a series of three isotonic saline solution (147.5 mM

NaCl) washes, followed by re-suspension in a modified Ringer's Solution (147.5 mM NaCl, 4 mM KCl, 2.25 mM $CaCl_2$, and 10 mM glucose, with 0.05 g/L of Human Serum Albumin). Post initial centrifuge of donor blood, plasma was collected via Pasteur pipette and collected for later use. With each isotonic wash, supernatant and buffy coat were removed by Pasteur pipette. After re-suspension in modified Ringer's solution, a Moxi Z Cell Counter (ORFLO) was used to determine RBC concentration and allowed for adjusting to an overall sample concentration of $5x10^9$ cells/mL (~37% hematocrit).

Shear Methods In Vitro

Two methods were used to expose RBCs to shear in this study—a viscometer and microfluidics channels (Figure 3-1). Both approaches involved shearing cells in a controlled environment for a given period of time. In each case, mechanically traumatized cells were collected for testing following shear with unsheared cells providing a control. The use of a specially designed Hercules Hi-Shear Couette viscometer with R=1.9825 cm, G_1=G_2=0.06 mm and G_3= 0.8 mm (Kaltec Industries) gave initial results. Cone-and-plate and parallel plate end regions of the bob were machined to match the shear stress in the concentric cylinder portion of the sample. Using this method the shear stress was varied while maintaining exposure time at two minutes. Shear stresses tested with the Couette viscometer were over the range of 10 – 130 Pa. Each test used an aliquot of 4.1 mL of the washed RBC suspension prepared as described above.

The second shear method involved the use of microfluidic channels to mimic more closely the flow conditions of high stress, short exposure times exhibited by VADs and prosthetic heart valves. The microfluidic shearing devices contained a constricted region that was designed to expose RBCs transiently (i.e. msec) to high shear conditions [63]. The cross-section

of the constricted region was 45 μm wide x 60 μm tall, and the constriction length was varied from 0.7 to 11.6 mm to provide different high shear exposure times. Channels were prepared from poly-dimethyl siloxane (PDMS), using a Sylgard® 184 Silicone Elastomer kits (Dow Corning), as previously described [63]. Before running, the channel and tubing were charged with the modified Ringers solution. Flow through channels was created using an approximately 3 cm segment of tubing (1.57 mm I.D., Silastic® Laboratory) attached to a 1 mL syringe in a syringe pump. A constant shear environment on the cells is accomplished by maintaining a constant flow rate through the channels. A straight channel microfluidic device (1500 μm wide x 60 μm tall) with no constriction and low shear was used as an additional control.

Flow Cytometry Analysis

Flow cytometry data was collected using a BD Accuri C6 Flow Cytometer (BD Sciences). RBC positive events were identified foremost by anti-CD235a-FITC (glycophorin A; eBioscience) binding.

IgG Binding

Immediately following shear exposure, the cells were collected and suspended to a concentration of 10^6/mL and then incubated for 45 min at 37^{o}C with autologous plasma to permit autoantibody IgG binding to the cell surfaces. Afterwards, cells resuspended at a concentration of 10^6/mL were incubated for an additional 60 min with both 5 μL (0.25 μg)/test mouse anti-CD235a-FITC (eBioscience) and 5 μL/ test mouse anti-IgG Fc Alexa Fluor 647(Biolegend) conjugates before analysis with flow cytometry or fluorescent microscopy. To account for non-

specific contributions, Alexa Fluor 647 Mouse IgG2a, k Isotype Ctrl Antibody (Biolegend) was used, with no apparent binding present in control or experimental tests.

Phosphatidylserine Externalization

In addition to anti-CD235a, a second probe used was a marker for phosphatidylserine, Annexin V Alexa Fluor 647(ThermoFisher Sci). Following shear stress, cells were suspended to 10^6 cells in 0.5 mL Ringers solution. The cellular suspension was then labeled with 5 μL of CD235a-FITC(eBioscience) and 5 μL Annexin V Alexa Fluor® 647 according to company protocol. After a 60 min. incubation period at 37^{o}C, cell and microparticle samples in media were then analyzed by flow cytometry.

Confocal Microscopy

Confocal microscopy images were taken with a Leica SP8 scanning confocal microscope at the Samuel Roberts Noble Microscopy Laboratory. Fresh live cells in media were imaged after labeling as described above for flow cytometry. Images were then processed using FIJI-ImageJ software to remove background noise and conduct further analysis. 50 cells in each of n=3 experiments were evaluated for increased fluorescence above background noise. Cells determined positive for anti-IgG Fc Alexa Fluor 647 were then further evaluated for amount of fluorescence above background by measuring the mean fluorescence.

Statistics

In each experiment, significance was assessed using excel statistical analysis ToolPak one-way ANOVA with further post hoc Tukey honest significant difference (HSD). The Tukey

HSD tests were used to determine specifically how many of the individual tests showed significance when compared directly. Significance was defined as $p < 0.05$. All average values are reported as the mean ± standard error.

RESULTS

IgG Binding to RBC Membrane as a Result of Varying Exposure Time/Shear Stress to Washed RBC

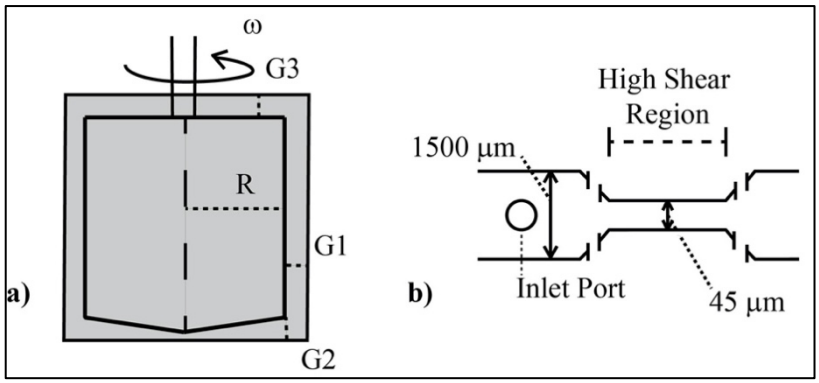

Figure 3-1: Shear Mechanism Diagrams

Two methods of shear generation were used for varying testing conditions. (a) The effect of stress magnitude was examined with a viscometer designed for uniform shear with G_1=G_2, G_3 was machined to give a volume average shear equal to that in the concentric cylinder and cone-and-plate sections. (b) The high shear region in the microfluidic channels were varied in length, from 0.7 to 11.6 mm, to vary time of shear to RBCs at a shear rate of 100,000 s^{-1}. A control for the microfluidic devices with no high shear region was also used.

Nonphysiologic levels of shear produced in vitro, through use of two shear methods (a microfluidics channel and a viscometer, Figure 3-1, described in Materials and Methods), cause autologous IgG to bind to RBCs. Typical findings from flow cytometry (Figure 3-2) indicate a significant increase in IgG-positive RBCs after flow through the microfluidics channel and

subsequent incubation with autologous plasma. Positive events in the upper right quadrant represent RBCs with fluorescently tagged antibody to human IgG. For the specific set of samples in Figure 3-2(c-e) with exposure times to high shear of 0 (control low shear channel), 5 and 15 ms respectively at a wall shear rate of 100,000 s^{-1}, the percent of cells binding are respectively 0.3%, 3.1% and 13.6%, after excluding microparticles and cellular debris by gating specifically for events of size (FSC) and SSC within the range for RBCs. The fraction of cells binding IgG rises steadily in a statistically significant way ($p<0.001$) as the exposure time is increased (Figure 3-2f). Average percentage of cells with antibody increases from a control value of 1.0% up to a value of 15.9% at the maximum exposure time tested, across the combined average of all individual tests. This control represents testing of washed RBCs, not run through a channel. Values for the straight channel lacking a high shear region are similar at 1.6±0.5%. Flow cytometry results are also suggestive ($p=0.07$) of greater damage to IgG-positive cells with higher average fluorescence occurring as exposure time increased (Figure 3-3a). Confocal microscopy(Figure 3-3b) of cells incubated with the same probes for CD235a and IgG confirmed the presence of immunoglobulin on RBCs after shear. 50 cells in each experiment(n=3), control and shear samples (10 ms exposure to 100,000 s^{-1}), were analyzed using FIJI ImageJ software and RBCs with detectable fluorescence above the background were recorded. Analysis of fluorescence in confocal microscopy also supported flow cytometry results, yielding a higher average fluorescence intensity of positive cells recorded after 10 ms shear at 100,000 s^{-1} (Figure 3-3c). Fluorescence intensity of anti-IgG Fc Alexa Fluor 647 positive sheared cells is much higher than that for anti-IgG positive control cells, approximately 3 times greater according to confocal microscopy images.

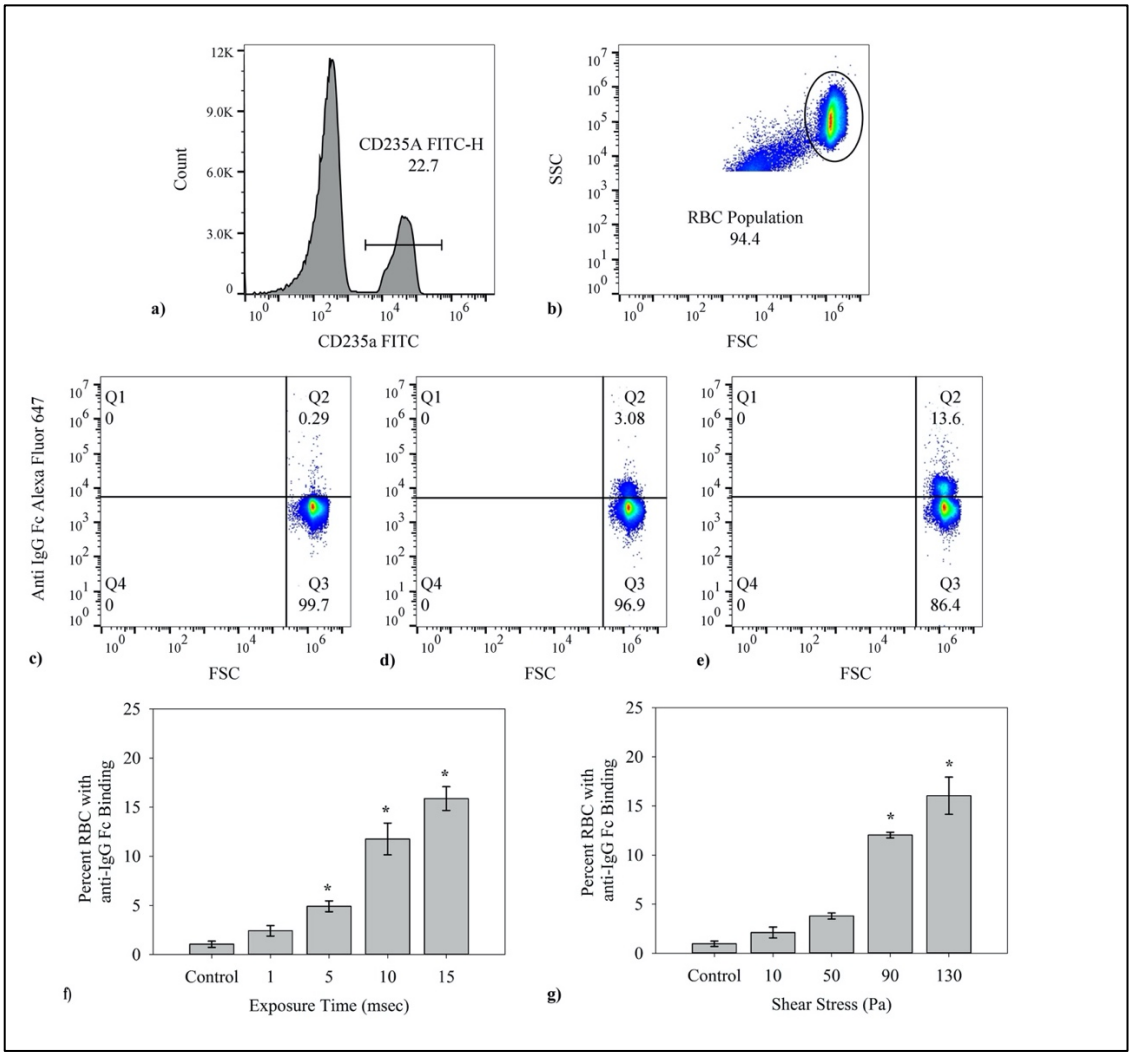

Figure 3-2: Percent Cell anti-IgG Fc Flow Cytometry Results

The general flow cytometry methods used in determining percent of cells which were fluorescent is shown. Flow cytometry results were collected via the BD Accuri C6 flow cytometer then further analyzed using FlowJo software. (a) In every case the events were first gated for presence of CD235a (FITC conjugated), (b) then additionally gated according to FSC-SSC to exclude any cellular debris or microparticles. (c-e) Representative output from the BD Accuri C6 Flow Cytometer for RBCs in a control, 5 ms and 15 ms high shear exposure time samples, respectively from left to right. Each y-axis corresponds to fluorescence intensity from the FL4-anti-IgG Alexa Fluor 647 conjugate and the x-axis shows FSC, relating to event size. Each individual test was run for 75,000 total RBCs. (f) The percent of CD235a+ RBCs with IgG attached grew with duration of shear after a single exposure in a microfluidics channel at 100,000 s^{-1} ($n=5$, $p<0.001$). (g) The fraction of CD235a+ RBCs binding IgG increased with the magnitude of the stress in the viscometer for 2 min. ($n=5$, $p < 0.001$) Data presented in (f-g) is the average ±standard error, with * representing significance according to post hoc Tukey HSD. Additional tests for Alexa Fluor 647 Mouse IgG2a, k Isotype Ctrl Antibody to account for the possibility of non-specific binding was omitted in (f-g), having on average 0 ± 0.1% average binding across all tests.

In general, the effects of mechanical trauma on blood cells have been found to depend on both shear stress and exposure time. We carried out experiments with a viscometer to investigate immunoglobulin attachment as a function of shear stress over the range of 0-130 Pa. Binding of IgG also depends on magnitude of shear stress(Figure 3-2g). The results for unsheared control sample shows on average 1.1% cells testing positive for IgG, similar to the value for the zero shear control in the exposure time experiments. Extent of binding increases with shear stress starting at 0 Pa with a value of 1.1% for a 2 min exposure and rising to 16.0% at 130 Pa.

Phosphatidylserine Exposure on RBCs After Exposure to Shear Stress

For the red blood cell, externalized PS marks the cell for eryptosis[133]. Eryptosis potentially offers an alternative mechanism to explain elimination of mechanically traumatized cells. Fluorescently labelled Annexin V was used with flow cytometry to investigate the presence of externalized PS on cells and microparticles.

Only a small fraction of cells(1-3%) bound Annexin V and the concentration does not increase over the control level with exposure time(Figure 3-4b). While the number of RBCs expressing PS does not increase, those that do are susceptible to greater exposure of PS with shear over the range of 0-15 ms(Figure 3-4c). Results shown are the fluorescence increase, relative to the control average. Cells which expressed Annexin V fluorescence had on average 3.0 times greater FL4 (Alexa Fluor 647) values after 15 ms exposure in microfluidic channels than the control.

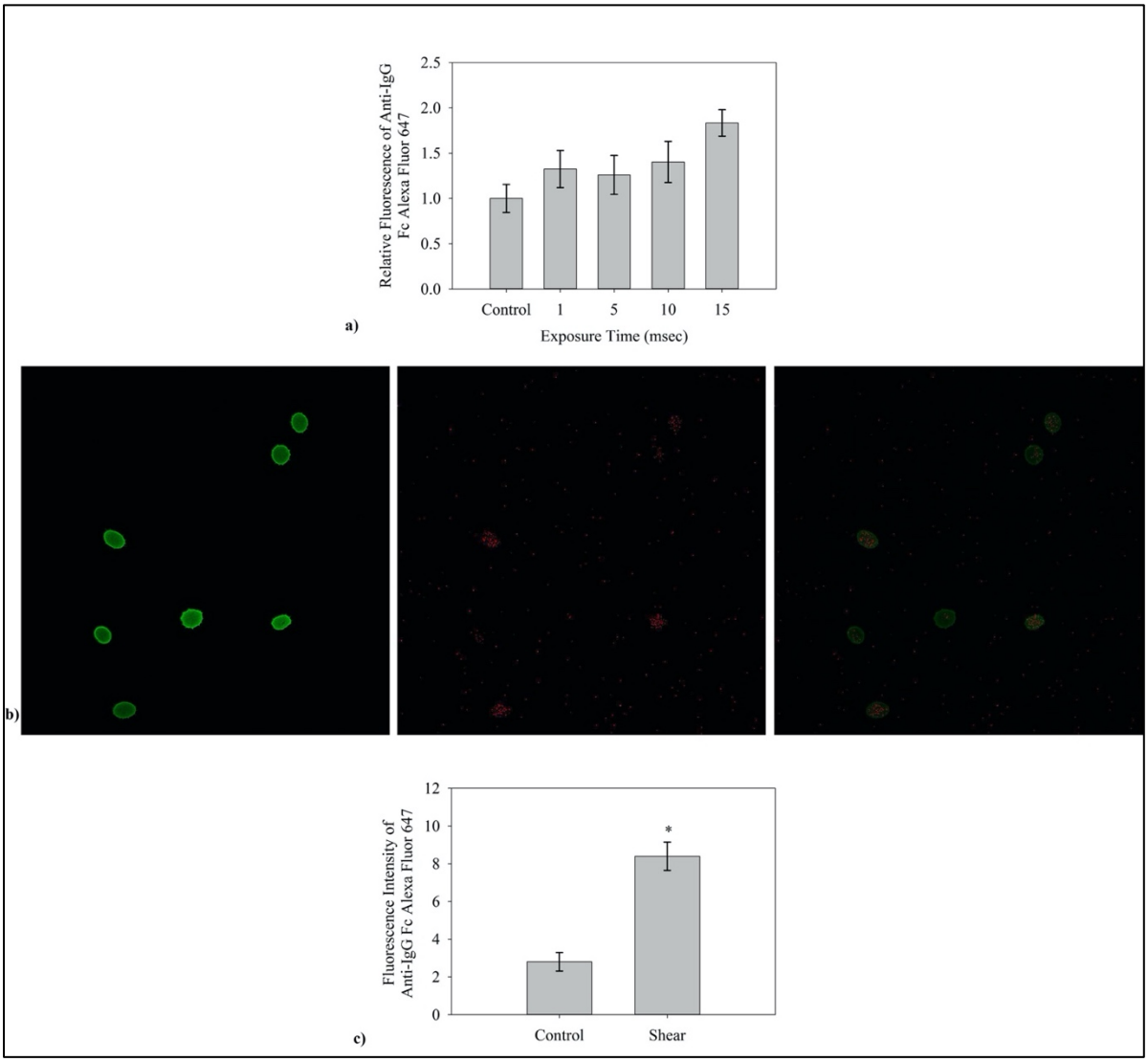

Figure 3-3: Anti-IgG FC Antibody Confocal Microscopy Results

An average increase in fluorescence of RBCs which presented anti-IgG Fc Alexa Fluor 647 fluorescence was presented by data collected via flow cytometry and in collected confocal microscopy images of live cells in media. (a) The average fluorescence of the control flow cytometry results was found. That value was then taken as a reference for the relative increase in fluorescence recorded by flow cytometry(n=5). (b) Confocal microscopy images shown are from left to right accordingly, anti-CD235a fluorescence, anti-IgG Fc fluorescence, and an overlay of the two images to show binding presence across the RBC. (c) Confocal microscope images were further analyzed by measuring the average intensity above background noise. Fluorescent intensity is presented as mean fluorescence above the background of the image.

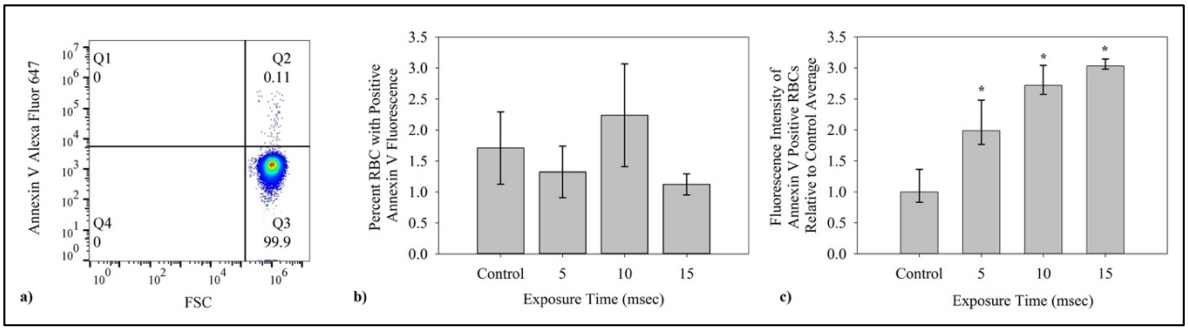

Figure 3-4: Percent Cell Annexin V Binding Flow Cytometry Results

Average percent of cells which bind Annexin V Alexa fluor 647 was also studied for microfluidic channels. (a) Similar to the FC detection of IgG presence, presence of PS on RBCs was determined using first gates for CD235a FITC fluorescence and on event size by FSC-SSC. (b) The fraction of red blood cells with externalized PS as determined by binding of fluorescently labeled Annexin V was small and did not increase with duration of shear (n=5). (c) The average fluorescence of the control flow cytometry results was found. That value was then taken as a reference for the relative increase in fluorescence recorded by flow cytometry. The amount of PS fluorescence in the positive subpopulation did increase significantly with exposure time(n=5, p = 0.01).

DISCUSSION

The importance of mechanical forces on cells to aspects of the immune system has recently been reviewed[102]. In this study, immunoglobulin binding increased with the magnitude of the stress and length of exposure (Figures 3-2f and 3-2g). The results of this sublethal damage follow well-known trends for hemolysis. Findings provide evidence for a unique autoimmune response to shear forces and a new insight to RBC removal after mechanical trauma. The binding of IgG to the membrane mirrors that for senescent RBCs. Old RBCs have high levels of immunoglobulin G which serves as an opsonin, marking the cells for erythrophagocytosis by macrophages and neutrophils in the spleen[135]. The level of bound antibodies increases markedly as the cell ages. Franco found that biotinylated RBCs, though present in a low concentration, had significantly higher levels of IgG after 126 days in the human[136]. Similar experiments in the dog with biotinylated RBCs showed a seven fold

increase in bound naturally occurring antibodies (NAbs)[137]. NAbs binding to band 3 in the RBC is known and has been proven to promote phagocytosis of the cell[138]. To explain the underlying process determining the effect of aging, Low proposed that the formation and attachment of methemoglobin to the interior surface of the cell membrane promoted IgG binding via aggregation of transmembrane protein band 3[126]. We hypothesize that deformation of the cell by shear results in conformational or translational motion of band 3 to expose epitopes for NAbs and an autoimmune response similar to that from senescence. The concept is illustrated in Figure 3-5.

The effects of shear on RBCs found in this research might also be compared to autoimmune hemolytic anemias, characterized by the attachment of immunoglobulin IgG and/or IgM[139]. Binding of immunoglobulins G and/or M to RBCs is the hallmark of autoimmune hemolytic anemia, “not an uncommon” clinical condition according to Chaudhary, with ultimate loss of RBCs by complement activation and the reticuloendothelial system. IgG, a relatively poor activator of the complement system[139], leads primarily to removal of RBCs in the spleen[140]. With loss of RBCs and putative IgG binding, the cardiovascular patients groups mentioned above can be said to have a mechanically induced auto-immune hemolytic anemia.

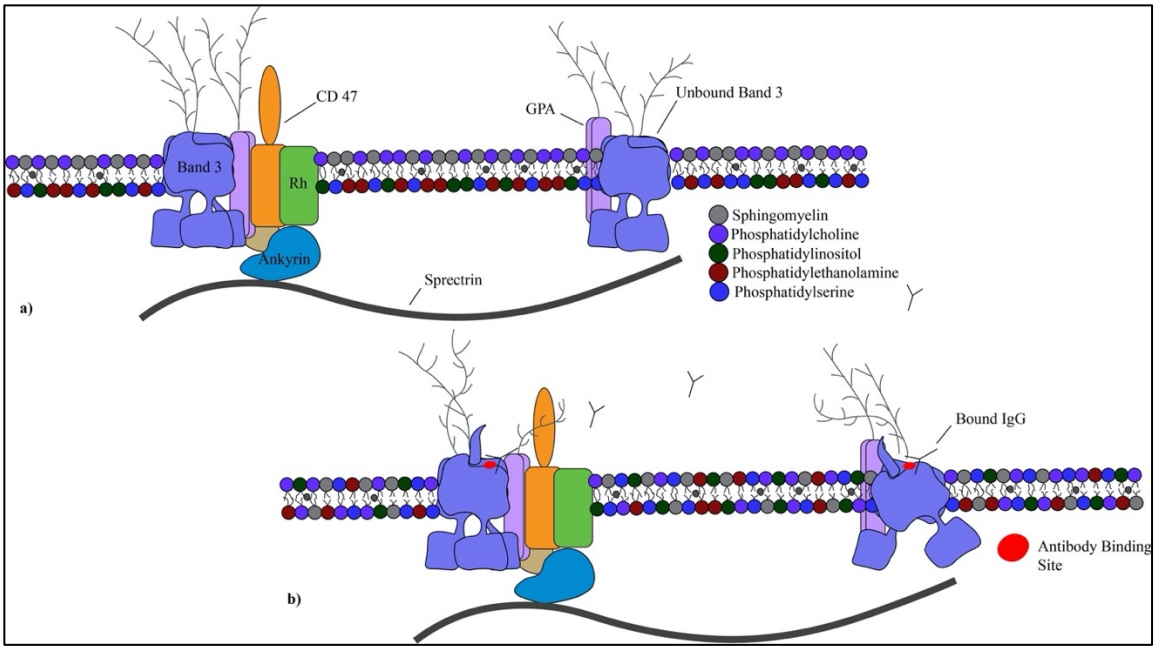

Figure 3-5: RBC Membrane Visualization Pre/Post Shear

A visualization of the RBC membrane and the proposed response to shear stress by some change in Band 3 with IgG. Glycophorin A (GPA), Rhesus (Rh) protein, CD47, and ankyrin included as relevance to their inclusion in the Band 3 complex and anchoring to the RBC spectrin network. Lipids sphingomyelin, phosphatidylcholine, phosphatidylinositol, phosphatidylethanolamine and PS shown to demonstrate lipid bilayer asymmetry. (a) Healthy RBC membranes exhibit a continuous sorting of phospholipids to maintain consistency and peak performing proteins. The Band 3 protein exists commonly as a tetramer within a protein complex tied into the spectrin network through the protein ankyrin. Band 3 also exists as a free moving dimer. (b) Postulated conformational changes of Band 3 after shear exposes the senescent cell antigen and leads to binding of naturally occurring antibodies.

With the prospect of an immune component to RBC removal, the relative importance of RBC deformability and IgG opsonization remains an open question. Poor RBC deformability has long been recognized for both senescent and mechanically traumatized RBCs. Working independently, Sutera and Shiga observed the flow of density separated, older cells in the rheoscope and reported increased stiffness[141, 142] and many groups have found decreased deformability after non-physiologic shear of a non-segregated population of RBCs. Stiff red blood cells are challenged by the small dimensions of the trabeculated surfaces in the spleen.

Notably, perfusion of an isolated rabbit spleen ex vivo with a mixture of sheared (<10 N/m^2) and unsheared RBCs in sera demonstrated selective removal of the traumatized cells[143]. Some clinical work supports the significance of altered rheology. Abridged RBC lifespans noted above for prosthetic heart valve patients correspond to reports of increased rigidity of red blood cells[144, 145]. Moreover, decreasing filterability of RBCs isolated from valve patients has been correlated with lower whole blood hematocrit[145], a result possibly due to bound proteins [146]. Another aspect of the RBC survival in the circulation is opsonization and phagocytosis in the spleen[135]. While reduced RBC deformability will slow passage through the spleen and thereby facilitate recognition of opsonins, it does not, at least in vitro, promote phagocytosis[125]. In studying diamide treated RBCs, Safeukui concluded splenic sequestration did not depend on reduced membrane deformability and suggested aggregation of membrane proteins such as band 3 led to splenic entrapment[123]. Thus, rheology and immunology seemingly act together to set circulatory lifespan of senescent and traumatized RBCs.

Some have suggested exposure of phosphatidylserine and apoptosis-like processes, eryptosis, as a mechanism for senescence, although this view no longer seems to be held generally[133, 147] and, in fact, PS levels are not high in aged RBCs[136]. Likewise, at 1-2%, only a very small fraction of RBCs displayed phosphatidylserine after shear (Figure 3-4b), even at the longest exposure. However, the extent of PS exposed in this subpopulation did grow with exposure time (Figure 3-4c). The nature of this group of RBCs is unclear, and while they are affected by shear, they do not appear to be a result of mechanical trauma since the fraction of PS positive cells did not increase with exposure time (Figure 3-4b).

As RBCs age, they also lose membrane and hemoglobin by shedding vesicles or microparticles, which has been suggested as a mechanism to rid the cell of harmful species[148].

Older cells are known to be smaller. Unsheared control cells binding IgG were smaller than other cells in the sample and presumably represented a senescent subpopulation. Interestingly, those sheared cells binding IgG were also a smaller size sub-population. Thus, senescent and mechanically traumatized cells share displayed increased IgG binding, reduced deformability, smaller size and microparticle shedding.

While ventricular assist devices and prosthetic heart valves extend the lives of many patients who suffer with cardiovascular problems, they operate with regions of flow where blood experiences high shear stresses[149] similar to conditions yielding the results of Figure 3-2f. The stresses can damage cells leading to complications like anemia and thrombosis so that the discovery of increased IgG binding to RBCs after shear may have important clinical applications. Currently, a good indicator of sublethal damage is not available, though assays for bound IgG or possibly another chemical marker of senescence[130] may meet that need. IgG should be feasible since its measurement on RBCs is already important to monitoring of patients with autoimmune hemolytic anemia[102]. Thus, it could prove to be an effective method for assessing how well patients adapt to medical devices with extracorporeal flow and for anticipating which individuals are more likely to suffer a complication like stroke, thrombosis or gastrointestingal bleeding.

An ongoing challenge is to translate flow characteristics from computer simulations into predictions of measurable blood damage. IgG binding should be valuable to engineers as a guide to further improvements in device design to reduce stress well below levels discernible by hemolysis. Linking flow history of blood to an experimental measure of the cell damage could facilitate making further improvements in design and operating conditions. In particular,

assessing the level of sublethal damage to cells is essential to progress in addressing abbreviated RBC lifespans.

Chapter 4 - Shear Stimulated Red Blood Cell Microparticles: Effect on Clot Structure and Fibrinolysis

MPs are released portions of plasma membrane from stimulated or apoptotic cells. These small particles are heterogeneous in size and composition and exist in a range of ~0.1 – 1.0 μm and typically display proteins from the mother cell which shed them. An increase in MP concentration has been linked to several clinical conditions, including immune-mediated pathologies, vascular and infectious diseases.[59, 61, 150, 151] Higher levels of MPs have also been observed in patients on ventricular assist devices where formation may be attributed to mechanical trauma.[44] In a healthy individual the most common MPs stem from platelets while in a diseased state any cell may increase release of MPs.[152] An increase in MP concentration above the physiological range can trigger several issues. One great threat is the procoagulant activity linked to the presence of MPs.[21, 153] MPs show presence of two procoagulant entities, tissue factor (TF) and the negatively charged membrane phospholipid phosphatidylserine (PS).[154-156] Tissue factor in combination with Factor VII initiates coagulation while exposed PS serves as a site for formation of prothrombinase and generation of thrombin.[157, 158] Thrombus formation due to MP involvement could have life threatening implications.

Clot structure, permeability and lysis are affected by and dependent on the composition of cellular components present.[25, 26] Platelet involvement in the fibrin (FB) network structural integrity is well-known and its effect on permeability has been shown in several studies.[159, 160] At the molecular level, platelet integrin αIIbβ3 reacts with arginine-glycine-aspartic

acid(RGD) sites on fibrin providing a means of retracting the FB mesh.[161] Less well appreciated is the ability of RBCs to bind to clots through formation of covalent bonds.[162-164]

With membrane proteins from the parent cells, MPs of both platelets and red cells can be integral components as well. In a study by Zubairova et al. the incorporation of MPs directly into the FB network within clots was demonstrated by scanning electron microscopy.[165] There it was shown that platelet derived microparticles (PMPs) have a direct effect on the FB network. Specifically, FB networks formed in the presence of MPs had a less porous structure with thinner fibers. Additional studies have shown that PMPs play a role in FB clot permeability and resistance to lysis.[166, 167] Conversely to the role PMPs possess, Levin et al. showed that ErMPs displayed a prominent fibrinolytic activity.[168] In their study, they utilized euglobulin lysis times of samples prepared with added ErMPs from both washed and unwashed stored RBCs. Thus the source and methods of MP production have seemed to differentiate the possible effects that they have on hemostasis. This holds true for all MP types in blood.

Due to the crucial role PMPs can play in the initiation and formation of a thrombus, the contributions that other MPs make merit investigation. In a study by Sansone et al. looking at the overall linked role of microparticles in vascular function, it was seen that ErMP numbers increased significantly becoming the highest concentration of MPs present in left ventricular assist device (LVAD) patients and appearing to play a dominant role in NO scavenging. [169] Each specific MP displays proteins from the mother cell. Different surface proteins for the various MPs, such as the greater presence of TF on PMPs, will affect their role in coagulation and clot structure.[156] The ability of MPs to bind or associate with the FB network by the same mechanism as the source cell is what bestows their ability to truly affect clot structure and

properties. In LVAD patient groups, the increased presence of ErMPs becomes a focal point for examination.

A natural coagulation process requires the presence of minimal blood flow and shear stresses,[170, 171] though an increase past the normal physiological range caused by ventricular assist devices (VADs) and other medical devices has been shown to have extensive effects on the body.[44] Non-physiological shear effects provide the foundation for continued thrombotic complications in already compromised patients. Mitigation of shear effects by device design modifications and concurrent drug administration has been evolving progressively over time. In particular, the variation of velocity gradient directly affects the clotting time and structural uniformity of formed clots.[172-174] Increasing shear rate on whole blood has the ability to increase the amount of platelet activation and increase aggregation.[175] Knowing the effects that shear has on platelets in blood flow and its interaction with fibrin clots warrants investigation of other direct shear stress consequences. One shear stress consequence yet to be thoroughly studied is the production of shear induced ErMPs.

We hypothesized that the increase in shear induced ErMPs has a significant effect on the structural integrity of a clot with implications for fibrinolysis. The FB structure has extensive repercussions on the transport of plasminogen activator and thus on the rate of fibrinolysis.[176-179] The effect of MPs on clot formation and fibrinolysis remains an open question. Antithrombin activity by ErMPs and faster lysis times in clots formed with ErMPs have been reported by one group.[180, 181] Our studies looked to examine how the presence of ErMPs would affect the FB structure and fibrinolytic degradation of clots under an imposed controlled pressure drop and permeation with a thrombolytic agent.

Materials and Methods

Blood Collection and Preparation

Venous blood was collected from healthy, adult donors in 3.2% sodium citrate vacutainers (VWR). Data was collected from a pool of healthy male and female adult donors, aged 18-64. Donors (n = 12) were informed of the nature and overall goal of the research prior to donations and consent obtained. Blood collection and experimental procedures were approved by the University of Oklahoma Institutional Review Board.

Whole blood was first collected into single centrifuge tubes then separated at 150 g for 10 minutes. Plasma was pipetted off and collected for further processing and use. Erythrocytes were isolated with a series of three isotonic saline solution (147.5 mM NaCl) washes, followed by re-suspension in platelet-free plasma (PFP). With each isotonic wash, supernatant and buffy coat were removed by Pasteur pipette. After the final re-suspension, a Moxi Z Cell Counter (ORFLO) was used to determine erythrocyte concentration and allowed for adjusting to an overall sample concentration of $5x10^9$ cells/mL (~37% hematocrit). The washed, resuspended erythrocytes were designated PFP/RBC. Platelet-poor plasma (PPP; ~$2\pm0.5E10^4$/ μL) and platelet-free plasmas (PFP) were obtained by centrifugation at 150g for 10 min and an additional 6000g for 20 min [182], respectively.

Shear Method

The use of a specially designed Hercules Hi-Shear Couette viscometer (Kaltec Industries) was used to shear blood. Cone-and-plate and parallel plate end regions of the bob were machined to match the shear stress in the concentric cylinder portion of the sample. Using this method the shear stress was varied while maintaining exposure time at two minutes. Shear stresses tested

with the Couette viscometer were kept in the sub-hemolytic range at both 90 and 130 Pa. Each test used an aliquot of 4.1 mL of the PFP/RBC suspension prepared as described above or of whole blood.

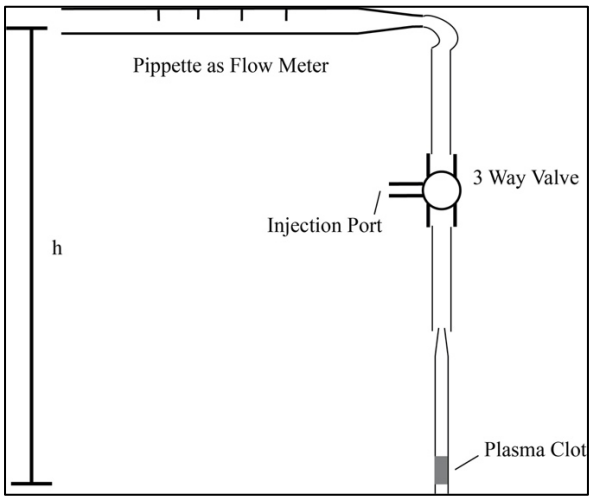

Figure 4-1: Experimental Apparatus for Clot Lysis and Flow

The experimental configuration used to test flow rate and thrombolytic times. A three-way valve was used to backfill lysing solution. Height, h, determines the applied pressure drop.

Clot Lysis and Flow

Fibrinogen (FG) from human plasma, 0.1mg FG/mL Ringers solution (147.5 mM NaCl, 4 mM KCl, 2.25 mM $CaCl_2$, and 10 mM glucose, with 0.05 g/L of Human Serum Albumin), was prepared and frozen in small aliquots at -20 °C until use. Natelson blood capillary tubes (0.2 cm inner diameter) were primed for clot adherence by etching with a dilute solution of hydrofluoric acid and coating the interior surface with a thin layer of FG as previously described.[176, 183]

Plasma clots devoid of RBCs were selected to minimize the fibrinolytic limitations related to the structural composition of the clots by competing elements. Clots for the lysis and flow measurements were formed from an unsheared PFP control and two sheared samples: (1)

PFP isolated from PFP/RBC after shear and (2) PFP from anticoagulated whole blood after shear. Coagulation was initiated by the addition of 16 μL of 0.25 M $CaCl_2$ to a mixture containing 50 μL PPP and 50 μL of either control or sample PFP. Seventy microliters of the mixture was injected into a capillary tube and allowed to gel for 2 h at 37 °C to form a ~1.25-cm long clot. Clots that formed with visible structural deformities discernable by the unaided eye such as interior void volumes or incomplete adherence to the tube wall were excluded from the study. The experimental configuration for permeation studies of clot lysis was adapted from Wu et al. (Figure 4-1).[176] Occluded capillary tubes were connected to rubber tubing and a glass pipette (as a flowmeter) filled with a solution of 5 mL Ringers solution, 2 mL autologous PFP (as a source of plasminogen), and 2500 IU streptokinase (SK) (Sigma Aldrich) as the fibrinolytic study agent. Fibrinolysis of plasma clots by 2500 IU SK was investigated at room temperature under varying pressure gradients of 5 and 10 mmHg/cm..

Flow Cytometry

Flow cytometry data was collected using a BD Accuri C6 Flow Cytometer (BD Sciences) to find MP concentrations in the size range of 0.45-1.0 μm. The detection of events (further expanded upon in Figure 4-2) was done with a series of gates based on forward scatter and side scatter(FSC/SSC) and two separate fluorescent antibodies. The initial gate for ErMPs was based on fluorescent beads of known size 0.5 and 1.0 μm (Flow Cytometry Sub-Micron Particle Size Reference Kit, Thermo Fisher Sci). ErMPs were identified foremost by anti-CD235a-FITC (glycophorin A; eBioscience) binding. In addition to anti-CD235a, a second probe for phosphatidylserine(Annexin V Alexa Fluor 647,ThermoFisher Sci) was used. Following shear stress, the RBC concentration was adjusted to ~10^6 cells in 0.5 mL Ringer's solution. The RBCs

with ErMPs were then labeled with 5 µL fluorescent probes according to protocol provided by the supplier.

Confocal Microscopy

Thin (~200 µm) chambers were prepared by affixing three layers of double-sided tape to a microscope slide to form three sides of a ~1 × 2 cm rectangle. A #1.5 coverslip was placed over the tape to form the chamber that was then filled with sample and sealed with grease. Clot media was prepared by mixing 50 µL PFP, 40 µL PPP, 10 µL FG, labeled with Alexa Fluor 647 (Sigma) and then clotting was initiated using 16 µL of 0.25 M $CaCl_2$ solution before being injected into the thin chamber. After an incubation period of 2 hrs at 37 °C the slides were viewed on the Leica SP8 confocal microscope at the Samuel Roberts Noble Microscopy Lab at the University of Oklahoma. Collected images were then processed using Otsu's method for threshold in Fiji: ImageJ software. The total percent coverage was determined in each individual image and recorded for data analysis.

Data Analysis

Each experiment was assessed using one-way ANOVA with further post hoc t-tests. Significance was defined as $p < 0.05$. All average values are reported as the mean ± standard error.

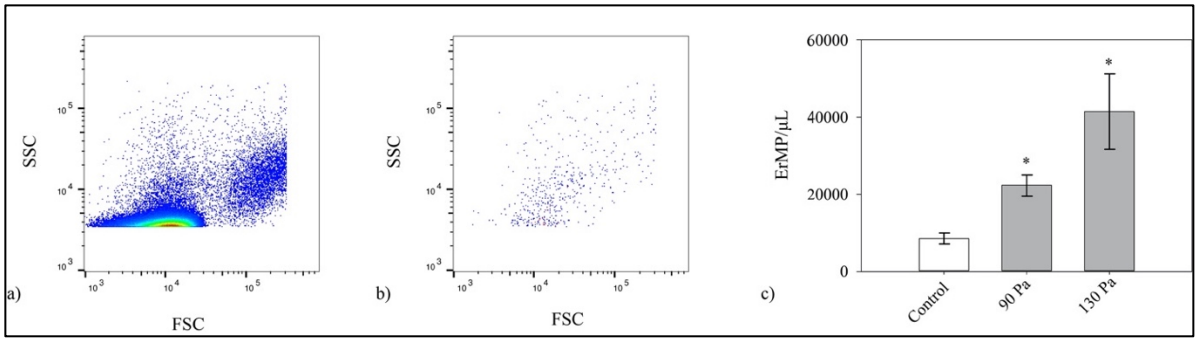

Figure 4-2: ErMP Concentration Determined by Flow Cytometry

Flow cytometry was used to determine the average concentration of ErMPs added into the clots. Mean concentration was determined by events based on gating for both size from 0.5 – 1.0 µm and fluorescent tags, anti-CD235a and AnnexinV. a) Shown is a FSC-SSC for a single experiment with no gating b) as well as after gating for the anti-CD235a and Annexin V to ensure relevancy of results and each event is a true ErMP. c) Average ErMP concentrations for each of the control, 90 Pa and 130 Pa are shown as means ± std error. (n=5)

Results

In past studies by Lawrie et al., endogenous thrombin potential was shown to be greatly affected by microparticles in fresh frozen plasma.[184]. Less documented is the effect MPs, particularly ErMPs, have on the clot structure and how these structural changes to the FB network may affect performance of fibrinolytic drugs. To shed light on how ErMP concentration levels influence clot properties, flow through an occluded capillary tube (Figure 4-1) was examined. Base level of anti-CD235a^{+}/Annexin V^{+} ErMPs in the control plasma had a concentration of 8,500 ± 1,500 ErMP/µL in the size range 0.45-1.0 µm. PFP/RBC samples sheared at 90 Pa for 2 minutes had an increase in concentration to 22,300 ± 3,200 ErMP/µL and finally the 130 Pa sheared sample showed 41,500 ± 11,200 ErMP/µL.

As seen in Figure 4-3, flow through the plasma clots generally decreased relative to control after shear although the difference for a pressure gradient of 5 mmHg/cm was not significant for the 90 Pa samples. Flow rate varied inversely with the concentration of MPs found for the PFP/RBC samples. As might be expected, plasma clots formed from sheared whole

blood reduced the flow rate more than the PFP/RBCs plasma clots, as the platelet free plasma component from the sheared whole blood included additional MPs produced by other blood cell types. The difference between the two times doesn't differ greatly, suggesting that ErMPs significantly contribute to the change in hydraulic permeability.

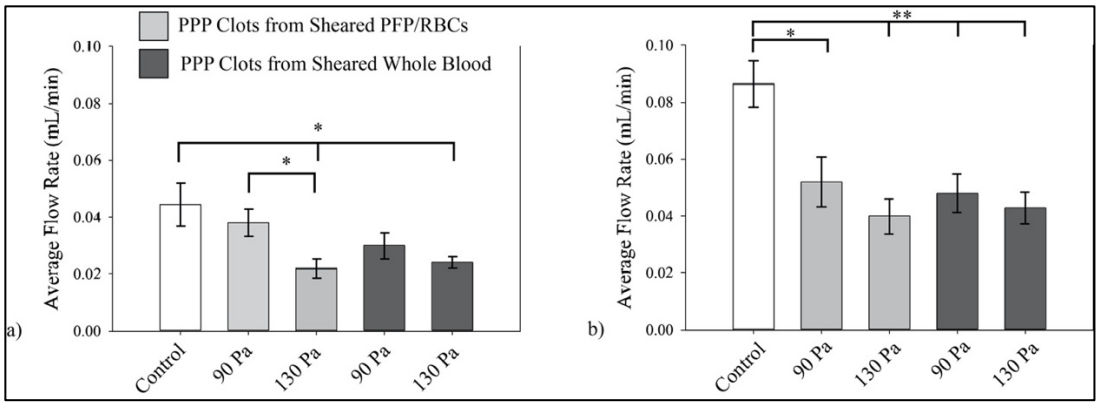

Figure 4-3: Average Flow Through ErMP Clots with Varied Conditions

Average clot lysis times at varied pressure gradients and shear induced ErMP concentration additions according to shear stress on specified components. Results of imposed pressure gradient of a) 5 mmHg/cm for PFP clots from sheared PFP/RBC ($p = 0.13$) and PFP from sheared whole blood (p 0.003) and b) 10 mmHg/cm for PFP from sheared PFP/RBC ($p = 0.01$) and from sheared whole blood ($p = 0.001$) as well. Shown are means ± std error for each. (n=5) * $p<0.05$; ** $p < 0.01$

The change in flow through the clot due to introduction of ErMPs also has a significant effect on the clot lysis time (Figure 4-4). Lysis times generally increased after shear, though again the 5 mmHg/cm pressure gradient was not as discerning. With a shear of 90 Pa, a pressure gradient of 10 mmHg/cm, and a corresponding introduction of 22,300 ± 3,200 ErMPs/μL plasma, the clot lysis time is extended from a value of 5.7 ± 0.7 min for the control to 7.2 ± 0.7 min ($p = 0.07$). Increasing the shear stress to 130 Pa under the same pressure gradient of 10 mmHg/cm-clot further increased the clot lysis time to 12.2 ± 1.1 min ($p < 0.01$). Compared

to controls, the clot lysis time was extended to 13.3 ± 2.1 min and 13.7 ± 1.2 min ($p < 0.01$) when clots were made with plasma isolated from sheared whole blood at 90 Pa and 130 Pa respectively. The minimal increase comparing these ErMP concentrations at 10mmHg/cm-clot may be indicative of competing interaction by other shear induced entities, i.e. PMPs. At a pressure gradient of 5 mmHg/cm, the difference in lysis times between 90 and 130 Pa sheared samples is less, but still statistically significant ($p < 0.01$).

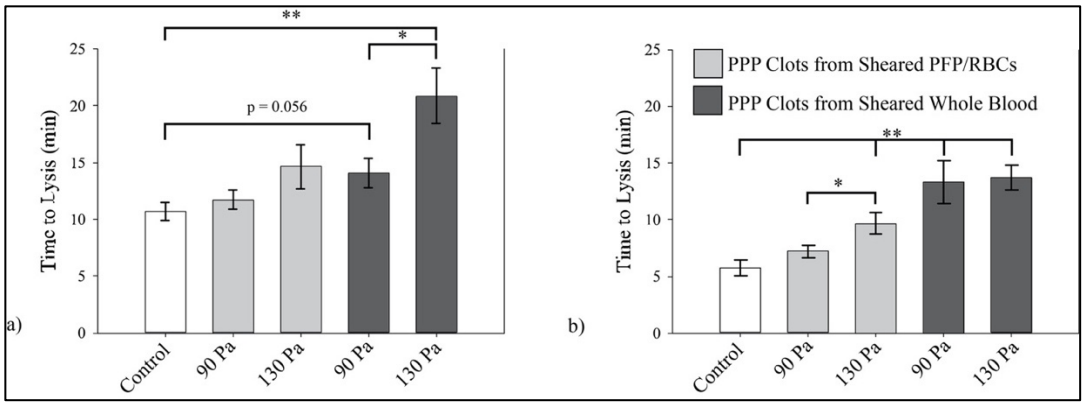

Figure 4-4: Average Clot Lysis Times of ErMP Clots with Varied Conditions

Average clot lysis times at varied pressure gradients and shear induced ErMP concentration additions according to shear stress on specified components. Results of imposed pressure gradient of a) 5 mmHg/cm for PFP clots from sheared PFP/RBC ($p = 0.13$) and PFP from sheared whole blood (p 0.003) and b) 10 mmHg/cm for PFP from sheared PFP/RBC ($p = 0.01$) and from sheared whole blood ($p = 0.001$) as well. Shown are means ± std error for each. (n=5) * $p<0.05$; ** $p < 0.01$

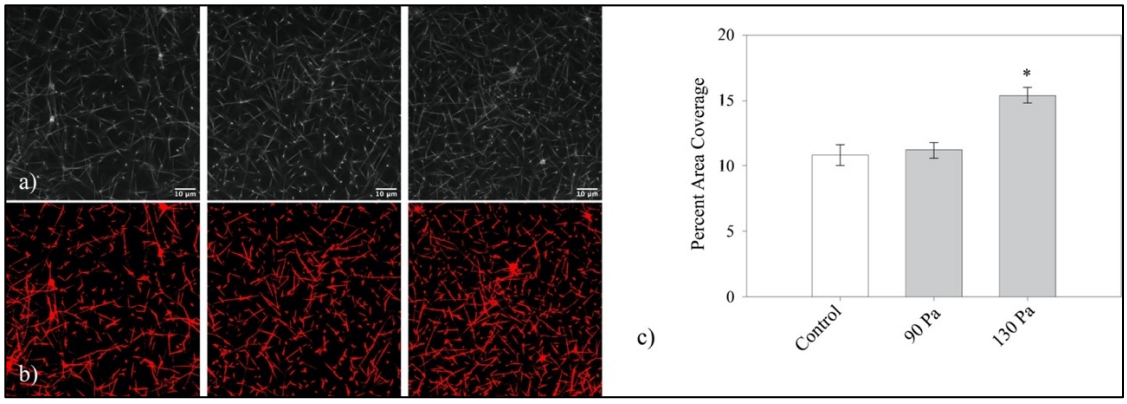

Figure 4-5: Confocal Microscopy Images and Coverage Results

a) Control clot image of fluorescent fibrin chains show very little binding with large gaps in area. Unlike the results of the flow experiments, samples prepared for confocal microscopy with plasma from PFP/RBC after shear at 90 Pa failed to show a discernable difference. After 130 Pa the fibrin clots showed a marked increase in binding and the percent of coverage. b) Highlighted fibrin chains using Otsu's method of threshold for each of the control, 90 Pa and 130 Pa. c) Confocal microscopy results for images based on clot formed post shear of RBCs resuspended in PDP. Results from images processed using Otsu's method of threshold then analyzed for percent area coverage on a single z-axis, ($p < 0.001$). (n=3)

Confocal microscopy was used to better understand how the introduction of MPs affects the clot structure. Visual changes in the clot structure with shear can be seen in Figure 4-5 with an increasing in FB chain contact points, as well as a larger percent area coverage. Using Otsu's method of threshold processing image analysis, the average percent area of FB coverage was determined for each of the experimental values tested and the control. While no clearly discernible difference from control was observed for the 90 Pa sheared sample, a comparison of the control images to the clots formed with plasma from the 130 Pa shear PFP/RBC saw a 41% increase in percent area coverage by FB (Figure 4-5).

The flow of the media through the clots was also used to determine the shift in clot permeability according to the Darcy Equation:

$$K_s = Q\mu L/A\Delta P \quad \text{Equation 4-1}$$

With Q = media flow rate (m^3s^{-1}), μ = media viscosity(kg $m^{-1}s^{-1}$), L = length of clot(m), A = cross sectional area of the capillary tube containing the clot (m^2) and ΔP = induced differential pressure (kg $m^{-1}s^{-2}$) on the clot length.[185] In Figure 4-6, the average values for permeability K_s recorded show that from the control a definite shift is seen at both shear stresses tested and for both plasma clot variations.

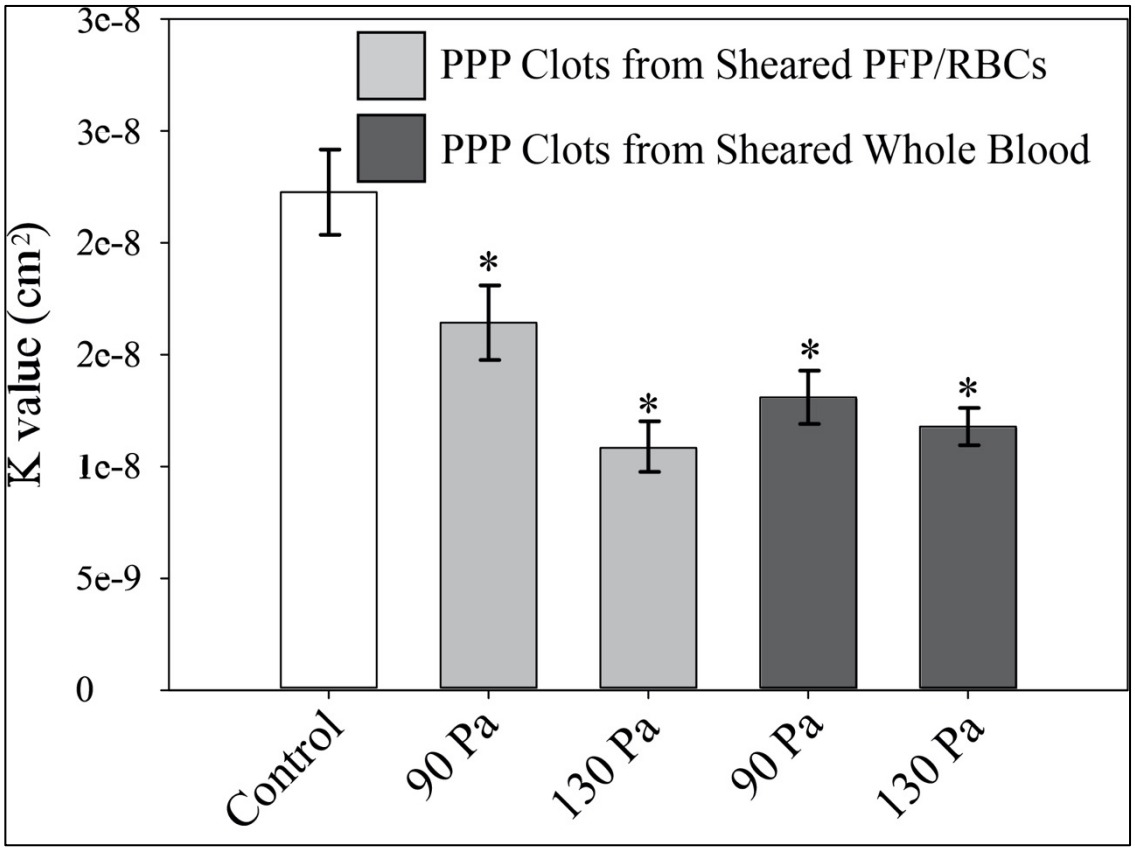

Figure 4-6: Mean Values of Permeability Constant Ks

Mean Values of Permeability K_s Using Darcey's Equation taken from the average flow rate through the produced plasma clots in glass capillary tubes with varied amount of shear induced ErMP additions. (n=10) Visible is a discernable decrease in the mean permeability for clots with increased presence of ErMPs.

In supplementation to the *in vitro* testing, simulations were made to visualize the effects the ErMPs had on the FB clot structure. A cellular automata based model was created to

simulate FB polymerization in the presence of differing ErMP concentrations. Models of this nature are commonly used to simulate both polymer migration [186] and biological processes such as clot formation [187, 188], tumor growth [187], and infection control for medical implants [189]. The model roughly mimicked the general outcome from our experimental tests, showing an increase in coverage and branch points. Additional information and the general model outcome is described more extensively in the appendices for reference.

Discussion

Adverse effects of increased shear stresses on blood flow in VADs and other implanted devices has been a topic of discussion for some time. Our study looked to focus on what effects shear stress induced ErMPs have on clot structure and properties related to the clot structure. The results of the investigation can be used to gain a better understanding of shear related complications seen in patients with an implanted cardiac assist device. A number of problems for patients experiencing prolonged shear rates exceeding that of physiological conditions has been documented.[4, 16-18] In several studies, adverse effects post implementation were related to the presence of MPs in patients.[44, 59, 190] Normal physiological concentrations of MPs assist in intercellular communication, regulation of cell proliferation and coagulation homeostasis, and immune function.[191] While physiological MP concentrations provide biological function, studies have shown increased MP concentrations are indicative of higher risk of thrombi formation, decreased PT and an increase of inflammation.[19-22] The principal reason for the pro-coagulation capabilities of ErMPs is the presence of externalized PS. Negatively charged PS serves as a procoagulant entity promoting the initiation of thrombus formation.[192] Our goal in this study was to relate how shear induced PS exposed ErMPs particularly would affect the fibrin clot structure. The production of PS exposed ErMPs is not singular to shear stress and has been

common in multiple other diseases.[55, 150, 151, 190] The findings reported here are much further reaching than with just VAD and implanted device patients.

In previous studies, the presence of or variance in concentration of certain components in blood and formed clots has been shown to impact the structure of the fibrin network and clot properties.[159, 185] An article by Gersh et al. showed incorporation of RBCs has extensive effects on the mechanical properties of the formed thrombus.[185] Fibrin diameter was affected by varying RBC concentrations though no resulting change in permeability was seen. Further, they reported that incorporation of RBCs accelerated the lysis of clots. In contrast to Gersh, others have shown that platelet rich clots (PRCs) are extremely resistant to lysis. [193, 194] Our data showed an increased resistance to flow with the incorporation of shear induced ErMPs (Figure 4-3). This resistance to flow corresponded to a further resistance to lysis similar to what was seen with PRC. Comparing the clots formed from plasma taken post shear of resuspended RBCs in PFP to the equivalent control at a pressure gradient of 10mmHg/cm, a restriction in flow rates of 38.9% ($p=0.02$) and 53.3% ($p=0.002$) for shear stresses of 90 and 130 Pa respectively was seen.

The increase in density of the fibrin network seen in the confocal microscopy images of our research is consistent with the effects seen in flow rate through the clots. Figure 4-5 a-b visually conveys the increase in clot density and suggests how a more tortuous path caused by ErMP concentration can limit transport of a thrombolytic agent. The extent of flow reduction was determined by comparing the permeability of the clots, K_s. There was a definitive restriction on flow when comparing clots from sheared PFP/RBC($p<0.001$) and PFP($P<0.001$) of sheared whole blood to the control clots, as represented by the calculated K_s values(Figure 4-6). Permeability dropped by as much as ½ with the increased number of MPs. Such reductions in

flow through the clot reduce the accessibility of thrombolytic therapy drugs commonly used to dissolve acute occlusions. Lysing of fibrin clots is directly affected by the transport of the thrombolytic agent leading to efforts to improve their delivery to clots in several studies.[176-179] As mentioned earlier, Levin et al. analyzed the influence that ErMPs produced during storage of blood has on fibrinolysis.[168] Overall, their findings, unlike ours, showed an accelerated euglobulin clot lysis time of donor plasma. The methods involved in their study differed from ours, in that the ErMPs were collected from stored blood or in the addition of ionophore, not collected post shear of freshly drawn venous blood. Their method of testing clot lysis utilized an optical method with streptokinase and chromogenic substrate components as well as a coagulometer. In this method the ErMPs will not have a similar effect on clot lysis that we saw, as there is no induced pressure gradient acting on the clot for delivery of streptokinase.

A comparison of the two types of clots produced in this study may shed light on the ErMP contributions to clot structure in relation to other MPs. There was minimal difference in the measured flow rates between clots prepared with plasma from the resuspended RBCs and with clots prepared with plasma from sheared whole blood where additional shear induced PMP may be present. This suggests that shear stimulated ErMPs have a significant effect on the fibrin network and its ability to stunt flow. The difference in protein presence on ErMPs and their ability to interact with the fibrin network of thrombi in various ways may be a contributing factor to these effects. In a number of studies, certain variable characteristics of blood have been shown to affect fibrin clot permeability.[185, 195] The most reasonable factor for ErMPs effect on fibrin structure arrangement is the exposed PS on their external side. However other characteristics of ErMPs cannot be ruled out. For example Band 3, a transmembrane protein on RBCs, has shown to aggregate into protein rafts [90, 92] and was shown to be present on a high

percentage of shear induced ErMPs.[196] The large aggregation rafts of Band 3 on RBCs, may promote ErMP formation and affect properties of the MP.[15, 197] Susceptibility to the production of MPs in the regulation by Band 3 could then lead to a larger effect on the arrangement of the fibrin clots.

Several investigators have looked to model the permeability and void fraction within the complex fibrin clots. Past studies for modeling permeability in a fibrous clot have generally followed the form:

$$\frac{k_f}{{a_f}^2} = f(\phi_f)$$ Equation 4-2

where k_f is the permeability, a_f is the fiber radius and ϕ_f is the fiber volume fraction. This heavily relies on the structural components of the fibers in the clots. [159, 198-200] Each specific study utilizes a different model and approach to explain the void and fiber volume fractions. One commonly used equation for estimating fibrin gel and blood clot permeability is the Davies equation (Equation 4-3).[201-203]

$$\frac{k_f}{a_f^2} = \left[16\phi_f^{1.5}(1 + 56\phi_f^3)\right]^{-1}$$ Equation 4-3

Using the experimental values from the capillary tube tests and the average fibrin diameter from the confocal images we solved for the fiber volume fraction ϕ_f. For each of the control, 90 Pa and 130 Pa clots formed from resuspended RBCs in PPP the corresponding fiber volume fractions were 0.039, 0.047 and 0.061. Though a small shift, the resultant flow rates in the clots were greatly affected. The fiber volume fractions calculated generally followed what was seen in confocal imaging as well, further verifying how ErMPs affect the fibrin network. Moreover, our studies were done with a Ringers/PPP solution. *In vivo*, the viscous effects that blood and its components have on the flow through the clots would be even more extensive, leading to an

extremely stunted delivery of thrombolytic agents. The shift in flow attributed to the growth in the fibrin network was further verified by computer aided simulations done in another study.

Furthermore, in both the experimental setup and the computer simulations the production of fibrin clot structures were done in a static environment where *in vivo* there would be a flow characteristic aligning the polymer chains. An alignment of polymer chains would cause less diverse connection points seen in confocal microscopy. Keeping the limitations in mind, the research still shows that increasing ErMP concentrations does result in denser FB networks.

Sublethal shear damage to RBCs and their further ability to function at full capacity has been a topic of discussion for years.[30, 32] Effects on circulation extending past immediate damage to RBCs due to prolonged exposure of sub-hemolytic shear has only recently started to shift the focus of discussion. One product of shear stimulus in implanted devices has been the increased presence of MPs from various cell types, notably those from RBCs. In our study it was shown that ErMPs influence the fibrin network of thrombi *in vitro*. With the sustained use of VADs for patients suffering from cardiac diseases, an environment harboring the ability to promote ErMP production is likely. Thrombus produced in the presence of shear induced ErMPs are more densely packed with less permeability. These thrombi will not only limit permeability and flow through the clots but hinder lytic agents from functioning to their complete potential. The ability of these shear stimulated ErMPs to both initiate thrombus formation and affect the structural components of the fibrin network shows that further consideration should be taken to mitigate their production.

This chapter was submitted in part to a peer reviewed journal for publication.

Chapter 5 – Conclusions and Future Implications

Implanted medical devices have evolved over the past decades to allow patients a more fulfilled life by minimizing adverse effects and broadening patient independence with device integration and size. Prolonged use of these medical devices, specifically VADs, still requires continued research and development. In several studies the extended use of VADs has been attributed to an increased risk of adverse effects.[44, 75, 115] The findings reported here support the premise that the sub-hemolytic environment created by medical promote the premature removal of RBCs, a proliferation of ErMPs, and further support an environment for a more complex fibrin network in thrombi.

Chapter 2 Conclusions

In Chapter 2, the measurement of ErMP concentrations using flow cytometry was determined post shear in a microfluidic device. ErMP concentration was shown to increase with increasing shear stress and the exposure time of shear stress. This outcome from a sub-hemolytic shear environment supports the thought that damage to RBCs occurs under a threshold for complete hemolysis. The measurable increase in ErMP concentration in a clinical setting could lend to development of design in medical devices as well as give insight into the extent of device integration. Continued monitoring of ErMP concentration can help determine a patient's likelihood of having an adverse event.

- ErMP concertation increases with increasing shear stress and/or an increase in shear stress exposure time

- Results indicate that measuring the levels of clinical ErMPs may have merit in determining the degree of integration of VADs and other implanted devices with their continued use
- Knowing the shear limits on the production of ErMPs may contribute to design considerations of implanted devices moving forward

Chapter 3 Conclusions

Chapter 3 outlines a novel autoimmune response to target damaged RBCs by the body. In previous research, autologous response by IgG binding to Band 3 has been shown to increase the likelihood of phagocytic removal. My research shows that this same method of detection is not limited to biological aging but is also presented in RBCs damaged by shear *in vitro*. The revelation that sub-hemolytic shear damage existes which primes cells toward premature removal promotes the further investigation of direct medical and *in vivo* testing. Further, it could prove to be an effective method for assessing how well patients adapt to medical devices and a valuable tool to engineers as a guide to further improve device design to reduce stress well below hemolysis levels.

- A number of similarities between RBC senescence and cells exposed to mechanical trauma exist (Ref. Table 2.1)
- Autologous IgG binding increases with shear exposure in both a Couette Viscometer and microfluidic channels
- After shear the presence of PS did not increase on RBCs, except for a small side population, possibly predisposed to shear damage

- Accelerated aging could lead to premature clearance of RBCs from the circulatory system and enhanced thrombotic activity with ErMPs

Chapter 4 Conclusions

The extent of ErMP involvement in fibrin structure and its effects on clot permeability and lysis was analyzed in Chapter 4. In past studies MP presence has shown to promote thrombus generation and a decrease in prothrombin time. Post sub-hemolytic shear damage clot lysis times increased and permeability constants calculated according to flow in our experimental apparatus decreased as the ErMP concentrations increased. Decreasing the permeability of clots *in vivo* would greatly limit the response time of thrombolytic medicines. This outcome promotes continued monitoring of ErMPs in patients with implanted devices.

- ErMPs produced in a sub-hemolytic environment were shown to affect the fibrin network as viewed with confocal microscopy
- As the concentration of ErMPs in an occluded capillary tube increased, the flow rate through the clot decreased and subsequently led to an increase in clot lysis time
- Fiber volume fraction according to Davies equation aligns with the confocal microscopy images

Future Work

The results from the studies presented here further promote the ongoing need to investigate how a sub-hemolytic environment affects RBCs and blood flow in a whole. The presented studies have a controlled environment with precise shear stress and exposure times.

Moving forward the responses of RBCs to sub-hemolytic shear in various models of VADs should be investigated. This will complexify the stimuli seen by the blood cells, but in return give a more closely related response to what is seen in patients that have these long term implanted VADs. The data taken from these devices in response to sub-hemolytic forces can be extensive. Using whole blood in these devices we can look not only at the produced ErMPs but other cellular MPs as well, such as PMPs. Additionally, looking at the amount of fluorescence from Annexin V (from externalized PS) on both ErMPs and PMPs it would be possible to see how much effect the two may have.

Another area in which we have started work is the idea that certain cells are predisposed to damage. Aged RBCs are known to slowly lose membrane and become denser and more spherical in shape. Utilizing this fact, it is possible to differentiate cell age based on density centrifugation. Testing for IgG binding post shear of younger/older cells we can determine if the autoimmune system we described in Chapter 3 has a preference to cells already at the end of their determined life span. If proven to be a factor, the use of stored blood for blood transfusions in patients with implanted devices would be a problem. Work has been initiated in using a percoll density gradient to selectively collect aged cells or younger cells and has been included in the appendices.

Building from the idea of RBCs predisposed to damage, designing microfluidic devices that introduce multiple shear channels may lend further insight into the mechanisms explained in the studies here. The current microfluidic channel design simulates the flow fields of VADs; however, the idea of blood cell recirculation hasn't been deeply examined in my research. Blood cells in circulation on average travel the body and make it back to the heart every 30 seconds.[204] A microfluidic system similar to the current high shear region/low shear region

with multiple high shear regions could introduce an idea of recirculation. Figure 5-1 briefly shows how that may be accomplished.

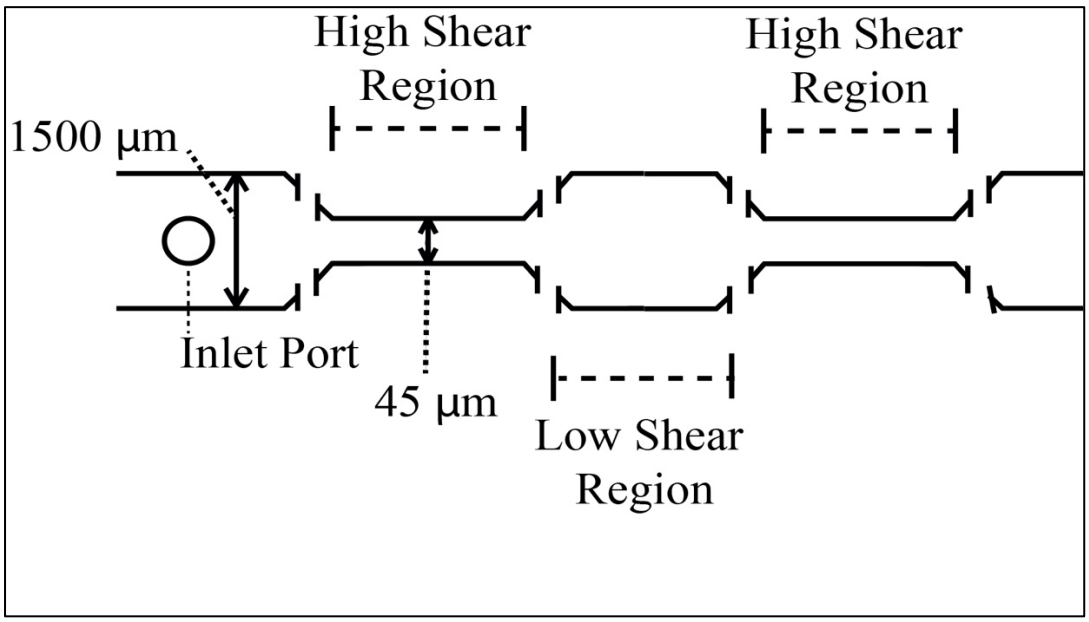

Figure 5-1: Proposed Multiple High Shear Region Microfluidics

The experiments examined in this research focused on RBCs and a response to sub-hemolytic trauma. Moving forward, there may be a great deal of benefit in seeing differences and/or similarities in MPs and their effects on complicating patient life and *in vivo* responses. The continued review of trauma in VADs is important to the continued betterment of patient life and understanding of how to mitigate damage done by forces uncommon to physiological flow. The groundwork laid out by the research presented in the previous studies can be utilized in several ongoing designs to better understand cellular responses by RBCs as well as other cells in blood flow.

References

1. WHO, *Diabetes.* 2016.
2. Writing Group, M., et al., *Heart Disease and Stroke Statistics-2016 Update: A Report From the American Heart Association.* Circulation, 2016. **133**(4): p. e38-360.
3. Kim, J., H. Lee, and S. Shin, *Advances in the measurement of red blood cell deformability: A brief review.* Journal of Cellular Biotechnology, 2015. **1**(1): p. 63-79.
4. Simmonds, M.J., et al., *Erythrocyte deformability responses to intermittent and continuous subhemolytic shear stress.* Biorheology, 2014. **51**(2-3): p. 171-85.
5. Meram, E., et al., *Shear stress-induced improvement of red blood cell deformability.* Biorheology, 2013. **50**(3-4): p. 165-76.
6. M., H.R., *Micropipette Aspiration of Living Cells.* Journal of Biomechanics, 2000. **33**: p. 15-22.
7. Shiga T, M.N., Kon K., *Erythrocyte Rheology.* Critical Reviews in Oncology/Hematology, 1990. **10**: p. 9-48.
8. Evans E. A., L.C.P.L., *Intrinsic Material Properties of the Erythrocyte Membrane Indicated by Mechanical Analysis of Deformation.* Blood, 1975. **43**: p. 27-30.
9. Nieri, D., et al., *Cell-derived microparticles and the lung*. 2016, European Respiratory Review. p. 266-277.
10. *Theory of Cancer Biology: A view through my thesis*. eukaryoticgeneexpression.weebly.com.
11. O'Brien, J.R., *The platelet-like activity of serum*. 1955, British Journal of Haematology. p. 223-228.

12. Rubin, O., et al., *Red Blood Cell Microparticles: Clinical Relevance.* Transfusion Medicine and Hemotherapy, 2012. **39**: p. 342-347.

13. Bosman, G.J., et al., *Erythrocyte ageing in vivo and in vitro: structural aspects and implications for transfusion.* Transfus Med, 2008. **18**(6): p. 335-47.

14. Rubin, O., et al., *Red blood cell microparticles: clinical relevance.* Transfus Med Hemother, 2012. **39**(5): p. 342-7.

15. Low, P.S., et al., *The role of hemoglobin denaturation and band 3 clustering in red blood cell aging.* Science, 1985. **227**(4686): p. 531-533.

16. Kameneva, M.V., et al., *Decrease in red blood cell deformability caused by hypothermia, hemodilution, and mechanical stress: factors related to cardiopulmonary bypass*. 1999, ASAIO Journal.

17. Simon, M.A., et al., *Current and future considerations in the use of mechanical circulatory support devices: an update, 2008-2018*. 2019, Annu Rev Biomed Eng. p. 33-60.

18. Han, J.J., M.A. Acker, and P. Atluri, *Left ventricular assist devices: synergistic model between technology and medicine*. 2018, Circulation. p. 2841-2851.

19. Burnier, L., et al., *Cell-derived microparticles in haemostasis and vascular medicine.* Thrombosis and Haemostasis, 2009.

20. Diamant, M., et al., *Cellular microparticles: new players in the field of vascular disease?* European Journal of Clinical Investigation, 2004. **34**(6): p. 392-401.

21. Fischer, D., et al., *Microparticles from stored red blood cells enhance procoagulant and pro inflammatory activity*. 2017, Transfusion. p. 2701-2711.

22. Zubairova, L.D., et al., *Circulating Microparticles Alter Formation, Structure, and Properties of Fibrin Clots.* Sci Rep, 2015. **5**: p. 17611.

23. Wolberg, A.S. and R.A. Campbell, *Thrombin generation, fibrin clot formation and hemostasis*. 2008, Transfus Apher Sci. p. 15-23.

24. Ryan, E.A., et al., *Structural origins of fibrin clot rheology*. 1999: Biophysical Journal. p. 2813-2826.

25. Staessens, S., et al., *Structural analysis of ischemic stroke thrombi: histological indications for therapy resistance*. 2020: Haematologica. p. 498-507.

26. Jang, I.-K., et al., *Differential sensitivity of erythrocyte-rich and platelet-rich arterial thrombi to lysis with recombinant tissue-type plasminogen activator*. 1989: Circulation. p. 920-928.

27. Mecozzi, G., et al., *Intravascular hemolysis in patients with new-generation prosthetic heart valves: a prospective study.* J Thorac Cardiovasc Surg, 2002. **123**(3): p. 550-6.

28. Mitlyng, B.L., et al., *Use of Breath Carbon Monoxide to Measure the Influence of Prosthetic Heart Valves on Erythrocyte Survival.* The American Journal of Cardiology, 2006. **97**(9): p. 1374-1376.

29. Taimeh, Z., et al., *Erythrocyte aging as a mechanism of anemia and a biomarker of device thrombosis in continuous-flow left ventricular assist devices.* The Journal of Heart and Lung Transplantation, 2017. **36**(6): p. 625-632.

30. Olia, S.E., et al., *Mechanical blood trauma in assisted circulation: sublethal RBC damage preceding hemolysis.* Int J Artif Organs, 2016. **39**(4): p. 150-9.

31. Barcellini, W. and B. Fattizzo, *Clinical Applications of Hemolytic Markers in the Differential Diagnosis and Management of Hemolytic Anemia.* Dis Markers, 2015. **2015**: p. 635670.

32. Dao, K.M., et al., *Sensitivity of the erythrocyte membrane bilayer to subhemolytic mechanical trauma as detected by fluorescence anisotropy.* Biorheology, 1994. **31**(1): p. 69-76.

33. Kameneva, M.V., et al., *Mechanisms of red blood cell trauma in assisted circulation. Rheologic similarities of red blood cell transformations due to natural aging and mechanical stress.* Blood Trauma In Assisted Circulation, 1995: p. 457-460.

34. Kameneva, M.V., et al., *Decrease in red blood cell deformability caused by hypothermia, hemodilution, and mechanical stress: factors related to cardiopulmonary bypass. .* ASAIO J, 1999. **45**(4): p. 307-310.

35. Simmonds, M.J., et al., *Erythrocyte deformability responses to intermittent and continuous subhemolytic shear stress.* Biorheology, 2014. **51**(2-3): p. 171-185.

36. O'Rear, E.A., et al., *Reduced erythrocyte deformability associated with calcium accumulation.* Biochimica et Biophysica Acta, 1982: p. 274-280.

37. Sutera, S.P., *Flow-induced trauma to blood cells.* Circulation Research, 1977. **41**(1).

38. Shiga, T., et al., *Cell age-dependent changes in deformability and calcium accumulation of human erythrocytes.* Biochimica et Biophysica Acta, 1985: p. 289-299.

39. Sutera, S.P., et al., *Age-Related Changes in Deformability of Human Erythrocytes.* Blood, 1985. **65**(2): p. 275-282.

40. Buerck, J.P., et al., *A Flow Induced Autoimmune Response and Accelerated Senescence of Red Blood Cells in Cardiovascular Devices.* Sci Rep, 2019. **9**(1): p. 19443.

41. Sandza, J.G., et al., *Subhemolytic trauma of erythrocytes: recognition and sequestration by the spleen as a function of shear.* Transactions American Society for Artificial Internal Organs, 1974. **B 20**: p. 457-462.

42. Alaarg, A., et al., *Red blood cell vesiculation in hereditary hemolytic anemia.* Front Physiol, 2013. **4**: p. 365.

43. Willekens, F.L., et al., *Erythrocyte vesiculation: a self-protective mechanism?* Br J Haematol, 2008. **141**(4): p. 549-56.

44. Nascimbene, A., et al., *Association between cell-derived microparticles and adverse events in patients with nonpulsatile left ventricular assist devices.* J Heart Lung Transplant, 2014. **33**(5): p. 470-7.

45. Kay, M.M.B., et al., *Senescent cell antigen is immunologically related to band 3.* Cell Biology, 1983. **80**: p. 1631-1635.

46. Low, P.S., et al., *Contribution of the Band 3-Ankyrin Interaction to Erythrocyte Membrane Mechanical Stability.* Blood, 1991. **77**(7): p. 1581-1586.

47. Burger, P., et al., *Potassium leakage primes stored erythrocytes for phosphatidylserine exposure and shedding of pro-coagulant vesicles.* Br J Haematol, 2013. **160**(3): p. 377-86.

48. Edouard M. Bevers, P.C., David W.C. Dekers, Robert F.A. Zwaal, *Lipid translocation across the plasma membrane of mammalian cells.* Biochimica et Biophysica Acta, 1999: p. 317-330.

49. Koshiar, R.L., et al., *Erythrocyte-derived microparticles supporting activated protein C-mediated regulation of blood coagulation.* PLoS One, 2014. **9**(8): p. e104200.

50. Greenwalt, T.J., D.J. Byran, and U.J. Dumaswala, *Erythrocyte membrane vesiculation and changes in membrane composition during storage in citrate-phosphate-dextrose-adenine-1.* Vox Sang, 1984. **47**(4): p. 261-270.

51. U.J. Dumaswala, T.J.G., *Human Erythrocytes Shed Exocytic Vesicles in Vivo.* Transfusion, 1984. **24**: p. 490-492.

52. Lutz, H.U., S.-C. Liu, and J. Palek, *Release of spectrin-free vesicles from human erythrocytes during ATP depletion.* 1977.

53. Badimon, L., et al., *Diet, microparticles and atherothrombosis.* Frontiers in Bioscience, 2018. **23**: p. 432-457.

54. Suades, R., et al., *Growing thrombi release increased levels of CD235a(+) microparticles and decreased levels of activated platelet-derived microparticles. Validation in ST-elevation myocardial infarction patients.* J Thromb Haemost, 2015. **13**(10): p. 1776-86.

55. Chiva-Blanch, G., et al., *Microparticle Shedding by Erythrocytes, Monocytes and Vascular Smooth Muscular Cells Is Reduced by Aspirin in Diabetic Patients.* Rev Esp Cardiol (Engl Ed), 2016. **69**(7): p. 672-80.

56. Badimon, L., et al., *Microvesicles in Atherosclerosis and Angiogenesis: From Bench to Bedside and Reverse.* Front Cardiovasc Med, 2017. **4**: p. 77.

57. Hugel, B.n.d., et al., *Elevated Levels of Circulating Procoagulant Microparticles in Patients With Paroxysmal Nocturnal Hemoglobinuria and Aplastic Anemia.* Hemostasis, Thrombosis, and Vascular Biology, 1999. **93**(10): p. 3451-3456.

58. van Beers, E.J., et al., *Circulating erythrocyte-derived microparticles are associated with coagulation activation in sickle cell disease.* Haematologica, 2009. **94**(11): p. 1513-9.

59. Jeske, W.P., et al., *Blood Cell Microparticles as Biomarkers of Hemostatic Abnormalities in Patients with Implanted Cardiac Assist Devices.* Biomarkers in Medicine, 2016. **10**(10): p. 1095-1104.

60. Vion, A.C., et al., *Shear stress regulates endothelial microparticle release.* Circ Res, 2013. **112**(10): p. 1323-33.

61. Westerman, M. and J.B. Porter, *Red blood cell-derived Microparticles: An overview*. 2016: Blood Cells, Molecules and Diseases. p. 134-139.

62. O'Rear, E.A., et al., *Increased intracellular calcium and decreased deformability of erythrocytes from prosthetic heart valve patients.* Clinical Hemorheology, 1984. **4**(5): p. 461-471.

63. Alsmadi, N.Z., et al., *Constricted microfluidic devices to study the effects of transient high shear exposure on platelets.* Biomicrofluidics, 2017. **11**(6).

64. Son, Y., *Determination of shear viscosity and shear rate from pressure drop and flow rate relationship in a rectangular channel.* Polymer, 2007. **48**: p. 632-637.

65. Lewis, C.S., et al., *Effects of Transient Exposure to High Shear on Neutrophil Rolling Behavior*. 2018, Cellular and Molecular Bioengineering. p. 279-290.

66. Zhang, T., et al., *Study of flow-induced hemolysis using novel Couette-type blood-shearing devices.* Artif Organs, 2011. **35**(12): p. 1180-6.

67. Toninato, R., G. Fadda, and F.M. Susin, *A red blood cell model to estimate the hemolysis fingerprint of cardiovascular devices*. 2018, Artificial Organs. p. 58-67.

68. Hochmuth, R.M., E.A. Evans, and D.F. Colvard, *Viscosity of human red cell membrane in plastic flow*. 1976: Microvascular Research. p. 155-159.

69. Distler, J.H.W., et al., *The release of microparticles by apoptotic cells and their effects on macrophages.* Apoptosis, 2005. **10**: p. 731-741.

70. Burger, D., et al., *Microparticles: biomarkers and beyond.* Clin Sci (Lond), 2013. **124**(7): p. 423-41.

71. Terrisse, A.D., et al., *Internalization of microparticles by endothelial cells promotes platelet/endothelial cell interaction under flow.* Journal of Thrombosis and Haemostasis, 2010. **8**(12): p. 2810-2819.

72. Willekens, F.L., et al., *Liver Kupffer cells rapidly remove red blood cell-derived vesicles from the circulation by scavenger receptors.* Blood, 2005. **105**(5): p. 2141-5.

73. Litvack, M.L., M. Post, and N. Palaniyar, *IgM promotes the clearance of small particles and apoptotic microparticles by macrophages.* PLoS One, 2011. **6**(3): p. e17223.

74. Shah, P., et al., *Lactate Dehydrogenase Is Superior to Serum Free Hemoglobin as a Marker of Pump Thrombosis in Left Ventricular Assist Devices.* The Journal of Heart and Lung Transplantation, 2013. **32**(4).

75. Bartoli, C.R., et al., *Clinical and In Vitro Evidence That Subclinical Hemolysis Contributes to LVAD Thrombosis.* Annals of Thoracic Surgery, 2018. **105**(3): p. 807-814.

76. Mitlyng, B.L., et al., *Use of breath carbon monoxide to measure the influence of prosthetic heart valves on erythrocyte survival.* American Journal of Cardiology, 2006. **97**(9): p. 1374-1376.

77. O'Rear, E.A., et al., *Use of a Rheological Technique to Evaluate Erythrocyte Membrane Alterations.* Journal of Rheology, 1979. **23**(6): p. 721-733.

78. Guo, Q., et al., *Microfluidic analysis of red blood cell deformability.* J Biomech, 2014. **47**(8): p. 1767-76.

79. Waugh, R.E., et al., *Rheologic properties of senescent erythrocytes: loss of surface area and volume with red blood cell age.* Blood, 1992. **79**: p. 1351-1358.

80. Nomura, S. and M. Shimizu, *Clinical significance of procoagulant microparticles.* J Intensive Care, 2015. **3**(1): p. 2.

81. Berckmans, R.N., R; Boing, AN; Romijn, FPHTM; Hack, CE; Sturk, A, *Cell-derived microparticles circulate in healthy humans and support low grade thrombin generation.* Thrombosis and Haemostasis, 2001. **85**(4): p. 639-646.

82. Ziad Mallat, M., et al., *Shed Membrane Microparticles With Procoagulant Potential in Human Atherosclerotic Plaques: A Role for Apoptosis in Plaque Thrombogenicity.* Circulation, 1999: p. 348-353.

83. Biró, E., et al., *Human Cell-Derived Microparticles Promote Thrombus Formation In Vivo In a Tissue Factor-Dependent Manner.* Journal of Thrombosis and Haemostasis, 2003. **12**: p. 2561-2568.

84. Sinauridze, E.I., et al., *Platelet microparticle membranes have 50- to 100-fold higher specific procoagulant activity than activated platelets.* Thrombosis and Haemostasis, 2007. **97**(3): p. 425-434.

85. Lipets, E., et al., *Circulating contact-pathway-activating microparticles together with factors IXa and XIa induce spontaneous clotting in plasma of hematology and cardiologic patients.* PLoS One, 2014. **9**(1): p. e87692.

86. Van Der Meijden, P.E., et al., *Platelet- and erythrocyte-derived microparticles trigger thrombin generation via factor XIIa.* J Thromb Haemost, 2012. **10**(7): p. 1355-62.

87. Jy, W., et al., *Red cell-derived microparticles (RMP) as haemostatic agent.* Thromb Haemost, 2013. **110**(4): p. 751-60.

88. Nauta, A.J., et al., *Direct binding of C1q to apoptotic cells and cells blebs induces complement activation.* Eur J Immunology, 2002. **32**: p. 1726-1736.

89. Kay, M.M.B., *Mechanism of removal of-senescent cells by human macrophages in situ.* Proc. Nat. Acad. Sci, 1975. **72**(9): p. 3521-3525.

90. Kay, M., *Immunoregulation of cellular life span.* Ann N Y Acad Sci, 2005. **1057**: p. 85-111.

91. Turrini, F., et al., *Clustering of Integral Membrane Proteins of the Human Erythrocyte Membrane Stimulates Autologous IgG Binding, Complement Deposition, and Phogocytosis.* The Journal of Biological Chemistry, 1991. **266**(35): p. 23611-23617.

92. Lutz, H.U. and A. Bogdanova, *Mechanisms tagging senescent red blood cells for clearance in healthy humans.* Front Physiol, 2013. **4**: p. 387.

93. Czerwinski, M., et al., *Degradation of the human erythrocyte membrane band 3 studied with the monoclonal antibody directed against an epitope on the cytoplasmic fragment of band 3.* Eur. J. Biochem, 1988. **174**: p. 647-654.

94. Grisendi, G., et al., *Detection of microparticles from human red blood cells by multiparametric flow cytometry.* Blood Transfus, 2015. **13**(2): p. 274-80.

95. Chandler, W.L., *Measurement of microvesicle levels in human blood using flow cytometry.* Cytometry B Clin Cytom, 2016. **90**(4): p. 326-36.

96. Orozco, A.F. and D.E. Lewis, *Flow cytometric analysis of circulating microparticles in plasma.* Cytometry A, 2010. **77**(6): p. 502-14.

97. Korenaga, R., et al., *Laminar-Flow Stimulates Atp- and Shear Stress-Dependent Nitric-Oxide Production in Cultured Bovine Endothelial-Cells.* Biochemical and Biophysical Research Communications, 1994. **198**(1): p. 213-219.

98. Kuchan, M.J. and J.A. Frangos, *Role of Calcium and Calmodulin in Flow-Induced Nitric-Oxide Production in Endothelial-Cells.* American Journal of Physiology, 1994. **266**(3): p. C628-C636.

99. Diamond, S.L., S.G. Eskin, and L.V. Mcintire, *Fluid-Flow Stimulates Tissue Plasminogen-Activator Secretion by Cultured Human-Endothelial Cells.* Science, 1989. **243**(4897): p. 1483-1485.

100. Ando, J. and K. Yamamoto, *Vascular Mechanobiology - Endothelial Cell Responses to Fluid Shear Stress -.* Circulation Journal, 2009. **73**(11): p. 1983-1992.

101. Ando, J., et al., *Shear-Stress Inhibits Adhesion of Cultured Mouse Endothelial-Cells to Lymphocytes by down-Regulating Vcam-1 Expression.* American Journal of Physiology, 1994. **267**(3): p. C679-C687.

102. Huse, M., *Mechanical forces in the immune system.* Nature Reviews Immunology, 2017. **17**(11): p. 679-690.

103. Poelmann, R.E., A.C.G.D. Groot, and B.P. Hierck, *The development of the heart and microcirculation: role of shear stress.* Medical & Biological Engineering & Computing, 2008. **46**(5): p. 479-484.

104. le Noble, F., et al., *Flow regulates arterial-venous differentiation in the chick embryo yolk sac.* Development, 2004. **131**(2): p. 361-75.

105. Brown, A.J., et al., *Role of biomechanical forces in the natural history of coronary atherosclerosis.* Nature Reviews Cardiology, 2016. **13**(4): p. 210-220.

106. Tarbell, J.M., et al., *Fluid Mechanics, Arterial Disease, and Gene Expression.* Annual Review of Fluid Mechanics, Vol 46, 2014. **46**: p. 591-614.

107. Bluestein, D., K.B. Chandran, and K.B. Manning, *Towards non-thrombogenic performance of blood recirculating devices.* Ann Biomed Eng, 2010. **38**(3): p. 1236-56.

108. Slepian, M.J., et al., *Shear-mediated platelet activation in the free flow: Perspectives on the emerging spectrum of cell mechanobiological mechanisms mediating cardiovascular implant thrombosis.* J Biomech, 2017. **50**: p. 20-25.

109. Carter, J., et al., *Short exposure time sensitivity of white cells to shear stress.* Asaio Journal, 2003. **49**(6): p. 687-691.

110. Lewis, C.S., et al., *Effects of Transient Exposure to High Shear on Neutrophil Rolling Behavior.* Cellular and Molecular Bioengineering, 2018. **11**(4): p. 279-290.

111. Jilma-Stohlawetz, P., et al., *Acquired von Willebrand factor deficiency caused by LVAD is ADAMTS-13 and platelet dependent.* Thrombosis Research, 2016. **137**: p. 196-201.

112. Nascimbene, A., et al., *von Willebrand factor proteolysis by ADAMTS-13 in patients on left ventricular assist device support.* J Heart Lung Transplant, 2017. **36**(4): p. 477-479.

113. Brinsfield, D.E., et al., *Hematological Changes in Long-Term Perfusion.* Journal of Applied Physiology, 1962. **17**(3): p. 531-534.

114. Shapira, Y., M. Vaturi, and A. Sagie, *Hemolysis Associated With Prosthetic Heart Valves A Review.* Cardiology in Review, 2009. **17**(3): p. 121-124.

115. Taimeh, Z., et al., *Erythrocyte aging as a mechanism of anemia and a biomarker of device thrombosis in continuous-flow left ventricular assist devices.* Journal of Heart and Lung Transplantation, 2017. **36**(6): p. 625-632.

116. Barrett KE, B.M., Scott B, Heddwen LB, *Ganong's Review of Medical Physiology*. 25th ed. 2016, New York: McGraw-Hill Education.

117. Velker, J.A., L.V. Mcintire, and E.C. Lynch, *Alteration of Erythrocyte Deformability Due to Shear-Stress as Assessed by Nuclepore Filters.* Transactions American Society for Artificial Internal Organs, 1977. **23**: p. 732-735.

118. O'Rear, E.A., et al., *Reduced erythrocyte deformability associated with calcium accumulation.* Biochim Biophys Acta, 1982. **691**(2): p. 274-80.

119. Lee, S.S., et al., *Shear induced damage of red blood cells monitored by the decrease of their deformability.* Korea-Australia Rheology Journal, 2004. **16**(3): p. 141-146.

120. Lee, S.S., et al., *Strain hardening of red blood cells by accumulated cyclic supraphysiological stress.* Artificial Organs, 2007. **31**(1): p. 80-86.

121. Watanabe, N., et al., *Deformability of human red blood cells exposed to a uniform shear stress as measured by a cyclically reversing shear flow generator.* Physiological Measurement, 2007. **28**(5): p. 531-545.

122. Nanjappa, B.N., H.K. Chang, and C.A. Glomski, *Trauma of the erythrocyte membrane associated with low shear stress.* Biophys J, 1973. **13**(11): p. 1212-22.

123. Safeukui, I., et al., *Sensing of red blood cells with decreased membrane deformability by the human spleen.* Blood Adv, 2018. **2**(20): p. 2581-2587.

124. Kameneva, M.V., et al., *Mechanisms of red blood cell trauma in assisted circulation. Rheologic similarities of red blood cell transformations due to natural aging and mechanical stress.* ASAIO J, 1995. **41**(3): p. M457-60.

125. Baerlocher, G.M., et al., *Erythrocyte deformability has no influence on the rate of erythrophagocytosis in vitro by autologous human monocytes/macrophages.* Br J Haematol, 1994. **86**(3): p. 629-34.

126. Low, P.S., et al., *The Role of Hemoglobin Denaturation and Band-3 Clustering in Red Blood-Cell Aging.* Science, 1985. **227**(4686): p. 531-533.

127. Schluter, K. and D. Drenckhahn, *Co-Clustering of Denatured Hemoglobin with Band-3 - Its Role in Binding of Autoantibodies against Band-3 to Abnormal and Aged Erythrocytes.* Proceedings of the National Academy of Sciences of the United States of America, 1986. **83**(16): p. 6137-6141.

128. Hornig, R. and H.U. Lutz, *Band 3 protein clustering on human erythrocytes promotes binding of naturally occurring anti-band 3 and anti-spectrin antibodies.* Exp Gerontol, 2000. **35**(8): p. 1025-44.

129. Kay, M.M.B., *Role of Physiologic Autoantibody in the Removal of Senescent Human Red-Cells.* Journal of Supramolecular Structure, 1978. **9**(4): p. 555-567.

130. Lutz, H.U. and A. Bogdanova, *Mechanisms tagging senescent red blood cells for clearance in healthy humans.* Frontiers in Physiology, 2013. **4**.

131. Bosman, G.J.C.G.M., et al., *Erythrocyte ageing in vivo and in vitro: structural aspects and implications for transfusion.* Transfusion Medicine, 2008. **18**(6): p. 335-347.

132. Fischer, T.M., *On the Energy-Dissipation in a Tank-Treading Human Red-Blood-Cell.* Biophysical Journal, 1980. **32**(2): p. 863-868.

133. Qadri, S.M., et al., *Eryptosis in health and disease: A paradigm shift towards understanding the (patho)physiological implications of programmed cell death of erythrocytes.* Blood Reviews, 2017. **31**(6): p. 349-361.

134. Ghashghaeinia, M., et al., *The impact of erythrocyte age on eryptosis.* British Journal of Haematology, 2012. **157**(5): p. 606-614.

135. Meinderts, S.M., et al., *Human and murine splenic neutrophils are potent phagocytes of IgG-opsonized red blood cells.* Blood Advances, 2017. **1**(14): p. 875-886.

136. Franco, R.S., et al., *Changes in the properties of normal human red blood cells during in vivo aging.* American Journal of Hematology, 2013. **88**(1): p. 44-51.

137. Rettig, M.P., et al., *Evaluation of biochemical changes during in vivo erythrocyte senescence in the dog.* Blood, 1999. **93**(1): p. 376-384.

138. Simak, J. and M.P. Gelderman, *Cell membrane microparticles in blood and blood products: Potentially pathogenic agents and diagnostic markers.* Transfusion Medicine Reviews, 2006. **20**(1): p. 1-26.

139. Chaudhary, R.K. and S.S. Das, *Autoimmune hemolytic anemia: From lab to bedside.* Asian J Transfus Sci, 2014. **8**(1): p. 5-12.

140. Strobel, E., *Hemolytic Transfusion Reactions.* Transfus Med Hemother, 2008. **35**(5): p. 346-353.

141. Sutera, S.P., et al., *Age-Related-Changes in Deformability of Human-Erythrocytes.* Blood, 1985. **65**(2): p. 275-282.

142. Shiga, T., et al., *Cell Age-Dependent Changes in Deformability and Calcium Accumulation of Human-Erythrocytes.* Biochimica Et Biophysica Acta, 1985. **814**(2): p. 289-299.

143. Sandza, J.G., et al., *Subhemolytic Trauma of Erythrocytes - Recognition and Sequestration by Spleen as a Function of Shear.* Transactions American Society for Artificial Internal Organs, 1974. **B 20**: p. 457-462.

144. Johnsson, R., P.T. Harjola, and P. Siltanen, *Effect of Pentoxifylline on Red-Cell Flexibility in Arterio-Sclerotic Patients and in Patients with Heart-Valve Prosthesis.* Scandinavian Journal of Clinical & Laboratory Investigation, 1981. **41**: p. 297-300.

145. Orear, E.A., et al., *Increased Intracellular Calcium and Decreased Deformability of Erythrocytes from Prosthetic Heart-Valve Patients.* Clinical Hemorheology, 1984. **4**(5): p. 461-471.

146. Koyama, T. and Y. Kikuchi, *Reduced Red-Cell Filterability Due to Red-Cell Plasma-Protein Interactions.* Biorheology, 1982. **19**(4): p. 579-585.

147. Chung, S.M., et al., *Lysophosphatidic acid induces thrombogenic activity through phosphatidylserine exposure and procoagulant microvesicle generation in human erythrocytes.* Arterioscler Thromb Vasc Biol, 2007. **27**(2): p. 414-21.

148. Ratajczak, M.Z., *Microvesicles: from "dust to crown".* Blood, 2006. **108**(9): p. 2885-2886.

149. Quinlan, N.J. and P.N. Dooley, *Models of flow-induced loading on blood cells in laminar and turbulent flow, with application to cardiovascular device flow.* Annals of Biomedical Engineering, 2007. **35**(8): p. 1347-1356.

150. Badimon, L., et al., *Microvesicles in atherosclerosis and angiogenesis: from bench to bedside and reverse*. 2017, Frontiers in Cardiovascular Medicine.

151. van Beers, E.J., et al., *Circulating erythrocyte-derived Microparticles are associated with coagulation activation in sickle cell disease*. 2009, Haemotologica. p. 1513-1519.

152. Mause, S.F. and C. Weber, *Microparticles: Protagonists of novel communication network for intercellular information exchange*. 2010, Circulation Research. p. 1047-1057.

153. Koshiar, R.L., et al., *Erythrocyte-derived microparticles supporting activated C-mediated regulation of blood coagulation*. 2014, PLoS ONE.

154. Morel, O., et al., *Procoagulant Microparticles disrupting the vascular homeostasis equation?* 2006, Arterioscler Thromb Vasc Biol. p. 2594-2604.

155. Nomura, S. and M. Shimizu, *Clinical significance of procoagulant Microparticles*. 2015, Journal of Intensive Care.

156. Biró, É., et al., *Human cell-derived microparticles promote thrombus formation in vivo in a tissue factor-dependent manner*. 2003, Journal of Thrombosis and Haemostastis. p. 2561-2568.

157. Kalafatis, M., et al., *Platelets and prothrombin*. 2005, Humana Press: Platelet Function. p. 283-300.

158. Reddy, E.C. and M.L. Rand, *Procoagulant phosphatidylserine-exposing platelets in vitro and in vivo*. 2020, Frontiers in Cardiovascular Medicine.

159. Wufsus, A.R., N.E. Macera, and K.B. Neeves, *The hydraulic permeability of blood clots as a function of fibrin and platelet density*. 2013, Biophysical Journal. p. 1812-1823.

160. Hunter, P.J., *Platelet-Rich blood clots*. 2013, Biophysical Journal. p. 1641.

161. Litvinov, R.I., et al., *The platelet intern αIIbβ3 differentially interacts with fibrin versus fibrinogen*. 2016, Journal of Biological Chemistry. p. 7858-7867.

162. Byrnes, J.R., et al., *Factor XIIIa-dependent retention of red blood cells in clots is mediated by fibrin a-chain cross linking*. 2015: Blood.

163. Litvinov, R.I. and J.W. Weisel, *Role of red blood cells in haemostasis and thrombosis*. 2017, ISBT Sci Ser. p. 176-183.

164. Weisel, J.W. and R.I. Litvinov, *Red blood cells: the forgotten player in hemostasis and thrombosis*. 2019, Journal of Thrombosis and Haemostasis. p. 271-282.

165. Zubairova, L.D., et al., *Circulating microparticles alter formation, structure and properties of fibrin clots*. 2015, Scientific Reports.

166. Tehrani, S., et al., *Atorvastatin has antithrombotic effects in patients with type 1 diabetes and dyslipidemia*. 2010, Thrombosis Research.

167. Cunningham, M.T., B.A. Citron, and T.A.W. Koerner, *Evidence of a phospholipid binding species within human fibrinogen preparations*. 2004. p. 325-334.

168. Levin, G., E. Sukhareva, and A. Lavrentieva, *Impact of Microparticles derived from erythrocytes on fibrinolysis*. 2016, J Thromb Thrombolysis. p. 452-458.

169. Sansone, R., et al., *Macrovascular and microvascular function after implantation of left ventricular assist devices in end-stage heart failure: Role of Microparticles*. 2015, The Journal of Heart and Lung Transplantation.

170. Bark, D.L.J., A.N. Para, and D.N. Ku, *Correlation of thrombosis growth rate to pathological wall shear rate during platelet accumulation*. 2012, Biotechnology and Bioengineering. p. 2642-2650.

171. Casa, L.D.C., D.H. Deaton, and D.N. Ku, *Role of high shear rate in thrombosis*. 2015, Journal of Vascular Surgery. p. 1068-1080.

172. Hathcock, J.J., *Flow effects on coagulation and thrombosis*. 2006, Arteriosclerosis, Thrombosis, and Vascular Biology. p. 1729-1737.

173. Dintenfass, L., *Effect of velocity gradient on the clotting time of blood and on the consistency of clots formed in Vitro*. 1966, Circulation Research.

174. Ranucci, M., et al., *Blood viscosity during coagulation at different shear rates*. 2014, Physiological Reports.

175. Nobili, M., et al., *Platelet activation due to hemodynamic shear stresses: damage accumulation model and comparison to In Vitro measurements*. 2008, ASAIO J. p. 64-72.

176. JH, W., S. K, and D. SL, *Transport phenomena and clot dissolving therapy: an experimental investigation of diffusion-controlled and permeation-enhanced fibrinolysis.* Thrombosis and Haemostasis, 1994: p. 105-112.

177. Piebalgs, A., B. Gu, and D. Roi, *Computational simulations of thrombolytic therapy in acute ischemic stroke*. 2018, Scientific Reports.

178. Bannish, B.E., I.N. Chernysh, and J.P. Keener, *Molecular and physical mechanisms of fibrinolysis and thrombolysis from mathematical modeling and experiments*. 2017, Scientific Reports.

179. Leach, J.K., E. Patterson, and E.A. O'Rear, *Distributed intraclot thrombolysis: mechanisms of accelerated thrombolysis with encapsulated plasminogen activators*. 2004, Journal of Thrombosis and Haemostasis. p. 1548-1555.

180. Levin, G.Y. and E. Sukhareva, *Antithrombin activity in microvesicles derived from stored red blood cells*. 2015: Blood Transfusions. p. 688-689.

181. Levin, G.Y. and E.G. Sukhareva, *Antithrombin activity of erythrocyte microparticles*. 2017, Bull Exp Diol Med. p. 718-721.

182. Lacroix, R., et al., *Impact of pre-analytical parameters on the measurement of circulating microparticles: towards standardization of protocol*. 2012: Journal of Thrombosis and Haemostastis. p. 437-446.

183. Nguyen, H.X. and E.A. O'Rear, *An In Vitro thrombolysis study using a mixture of fast-acting and slower release microspheres*. 2016: Pharmaceutical Research. p. 1552-1563.

184. Lawrie, A.S., et al., *The characterization and impact of microparticles on haemostastis within fresh-frozen plasma*. 2008, The International Journal of Transfustion Medicine. p. 197-204.

185. Gersh, K.C., C. Nagaswami, and J.W. Weisel, *Fibrin network structure and clot mechanical properties are altered by incorporation of erythrocytes*. 2009, Thromb Haemost. p. 1169-1175.

186. Smith, M., et al., *Cellular Automaton Simulation of Polymers.* MRS Proceedings, 1991. **248**.

187. Chopard, B., et al., *Lattice-Gas Cellular Automaton Models for Biology: From Fluids to Cells.* Acta Biotheoretica, 2010. **58**(4): p. 329-340.

188. Xu, Z., et al., *Computational approaches to studying thrombus development.* Arterioscler Thromb Vasc Biol, 2011. **31**(3): p. 500-5.

189. Prieto-Langarica, A., et al., *A Cellular Automata Model of Infection Control on Medical Implants.* Applications and applied mathematics : an international journal, 2011. **6**(1): p. 1-10.

190. Hugel, B., et al., *Elevated levels of circulating procoagulant Microparticles in patients with paroxysmal nocturnal hemoglobinuria and aplastic anemia*. 1999, Blood. p. 3451-3456.

191. Augustine, D., et al., *Dynamic release and clearance of circulating microparticles during cardiac stress.* Circ Res, 2014. **114**(1): p. 109-13.

192. Owens, A.P., 3rd and N. Mackman, *Microparticles in hemostasis and thrombosis.* Circ Res, 2011. **108**(10): p. 1284-97.

193. Jang, I.-K., et al., *Differential sensitivity of erythrocyte-rich and platelet-rich arterial thrombi to lysis with recombinant tissue-type plasminogen activator*. 1989: Circulation.

194. Tomkins, A.J., et al., *Platelet rich clots are resistant to lysis by thrombolytic therapy in a rat Madeleines of embolic stroke*. 2015, Experimental & Translational Stroke Medicine.

195. Undas, A., et al., *Plasma homocysteine affects fibrin clot permeability and resistance to lysis in human subjects*. 2006, Arterioscler Thrombosis Vasc Biol. p. 1397-1404.

196. Buerck, J.P., et al., *A flow induced autoimmune response and accelerated senescence of red blood cells in cardiovascular devices*. 2019: Scientific Reports.

197. Wang, D.N., *Band 3 protein: structure, flexibility and function*. 1994, FEBS Letters. p. 26-31.

198. Higdon, J. and G. Ford, *Permeability of three-dimensional models of fibrous porous media*. 1996, J. Fluid Mech. p. 341-361.

199. Clague, D. and R. Phillips, *A numerical calculation of the hydraulic permeability of three-dimensional disordered fibrous media*. 1997: Phys. Fluids. p. 1562-1572.

200. Mattern, K.J. and W.M. Deen, *"Mixing rules" for estimating the hydraulic permeability of fiber mixtures*. 2008: AIChE J. p. 32-41.

201. Blomback, B., et al., *Native fibrin gel networks observed by 3D microscopy, permeation and turbidity*. 1989, Biochimica et Biophysica Acta - Protein Structure and Molecular Enzymology. p. 96-110.

202. Davies, C.N., *The separation of airborne dust and particulates.* 1952, Mech. Eng. p. 185-213.

203. Diamond, S.L. and S. Anand, *Inner clot diffusion and permeation during fibrinolysis*. 1993, Biophysical Journal. p. 2622-2643.

204. *The circulatory system; Part II: The heart and circulation of blood*.

Appendices

Shear Calculations

Hercules High Shear Viscometer

High shear viscometer was used as an initial and unique shear device on sub-hemolytic shear testing on blood. The following equations were used to determine the necessary theoretical torque and RPM required to maintain the shear stress desired.

$$\tau = \mu\gamma = \mu\frac{dV_\theta}{dr} = \mu\frac{\Delta V}{h}$$

$$\tau = \mu\frac{\omega R_{bob}}{h} = \mu\frac{2\pi(RPM)R_{bob}}{h}$$

$$h = R_{cup} - R_{bob}$$

$$F = \tau A = \tau(2\pi R_{bob}L)$$

$$T = r_{perpendicular}F$$

$$T = R_{cup}(2\pi R_{bob}L)\mu\frac{2\pi(RPM)R_{bob}}{h}$$

Where: τ = shear stress
μ = viscosity
V = volume
r = radius
h = gap length
ω = angular momentum
RPM = Rotations per minute
L = length bob
A = surface area bob
T = torque

PDMS Microfluidic Channels

Shear rate in the microfluidic channels was determined using Navier–Stokes equation in steady-state flow in a straight channel, also known as Poiseuille flow. In microfluidic channel design,

the fluid is driven through a long, straight channel. Keeping the no-slip boundary conditions at the wall in mind and a constant pressure gradient we arrive at the following equation for a rectangular channel. (Governing Equations in Microfluidics)

$$v_x(y,z) = \frac{4h^2\Delta p}{\pi^3 \eta L}\sum_{n,odd}^{\infty}\frac{1}{n^3}\left[1-\frac{\cosh n\pi\frac{y}{h}}{\cosh n\pi\frac{w}{2h}}\right]\sin(n\pi\frac{z}{h})$$

Son et al. further verified the ability to test the apparent shear rate in a rectangular microfluidic system with H comparable to H. It was shown that for an aspect ratio near one the error in calculations is minimal and can be used as evaluated by the following equations.

$$\frac{\partial \rho}{\partial t}+\frac{\partial}{\partial x}(\rho v_x)+\frac{\partial}{\partial y}(\rho v_y)+\frac{\partial}{\partial z}(\rho v_z)=0$$

$$\rho\left(\frac{\partial v_x}{\partial t}+v_x\frac{\partial v_x}{\partial}+v_y\frac{v_x}{\partial}+v_z\frac{\partial v_x}{\partial}\right)=-\frac{\partial P}{\partial x}+\mu\left(\frac{\partial^2 v_x}{\partial x^2}+\frac{\partial^2 v_x}{\partial y^2}+\frac{\partial^2 v_x}{\partial z^2}\right)+\rho g_x$$

These two equations can be simplified by assuming incompressible fluid and fluid flow only in the x-direction to find the following equation for the shear stress:

$$-\frac{\partial P}{\partial x}-\left(\frac{\partial}{\partial y}(\rho\tau_{yx})+\frac{\partial}{\partial z}(\rho\tau_{zx})\right)=0$$

$$-\frac{\partial P}{\partial x}+\mu\left(\frac{\partial^2 v_x}{\partial y^2}+\frac{\partial^2 v_x}{\partial z^2}\right)=0$$

$$v_x=\frac{\frac{1}{2}\Delta P}{\mu L}(z^2-b^2)+\sum_{n=0}^{\infty}A_n cos(\frac{(2n+1)\pi z}{2b})\cosh(\frac{(2n+1)\pi y}{2b})$$

$$A_n=16b^2\left(\frac{\Delta P}{\mu L}\right)(-1)^n/((2n+1)\pi)^3\cosh(\frac{(2n+1)\pi a}{2b}$$

The shear rate, γ_a, is then calculated from the flow rate, the channel dimensions and a value f* which is shown following and can be found in the paper by Son et al.[64]

$$\gamma_a=\frac{6Q}{WH^2}\left(1+\frac{H}{W}\right)f(\frac{H}{W})$$

$$f(x) = \left[\left(1 + \frac{1}{x}\right)^2 \left(1 - \frac{192}{\pi^5 x} \sum_{i=1,3,5}^{\infty} \frac{\tanh\left(\frac{\pi}{2} ix\right)}{i^5}\right)\right]$$

Microfluidic Channel Preparation

PDMS Channels

1. Mix curing agent and base in 1:10 ratio in weigh boat (mix well, so that bubbles form)
2. Pour into petri dish on top of mold created on silicon wafer
3. Place in desiccator under vacuum for 30 minutes, until bubbles disappear completely
4. Add elbow ports for exits, ensuring no bubbles are trapped below
5. Place in drying oven for at least an hour at ~75 °C

Slide Preparation

Slides must first be cleaned in HNO_3, then treated with Aquasil to reduce leaking

HNO3 treatment:

1. 1. Mix stock (70%) nitric acid with nanopure H2O to create solution of 28.9% HNO3
2. Place slides in rack to keep them from touching and submerge in HNO3 for 1 hour
3. Remove from acid promptly and rinse in nanopure H2O for 5 minutes.
4. Place slides in oven to dry under vacuum at ~80°C
5. Remove when dry and allow to cool

Aquasil Treatment

1. 1. Filter stock Aquasil solution into 350 mL of nanopure water to create 1% Aquasil solution
2. Place slides in rack to keep them from touching and submerge in Aquasil solution for 15 seconds.
3. Dip in nanopure H2O to rinse.
    a. Slides should now be hydrophobic. If water sticks to them, rather than beading, the Aquasil treatment did not work properly
4. Place in oven under vacuum to dry at ~80°C
5. Remove from oven when dry and allow to cool for later use

Flow Experiments

1. Clean PDMS channel bottom with tape to remove any large dust or dirt particles
2. Place glass slide and PDMS channel in plasma cleaner for one minute on high power
3. Seal PDMS channel to slide, pressing out any visible air bubbles
4. Charge channels and tubing with 1% HSA in Ringers (without calcium)
5. Allow to sit for 30 minutes for blocking purposes
6. Rinse channels with Ringers if needed(using 1 mL syringe)
7. Place 150 uL of Ringers in wells, and pull through at appropriate flow rate using syringe pump
8. Once the wells are nearly empty, add blood or cellular suspension and continue to pull through until sufficient effluent is collected
9. Test on flow cytometry

Accuri C6 Cytometer

Prior to running BD Accuri C6 Flow Cytometer:

1. Check fluid levels in all bottles, ensuring that the Waste is empty (should have small amount of DI water with bleach) and the Sheath, Cleaner and Decontamination bottles are full

2. Gently push the sample stage back, remove and discard the SIP cover and place a tube containing at least 2 mL of 0.22 µm filtered, DI water on the SIP

3. Firmly press the power button on the front of the unit to turn on the cytometer. During start up, the BD Accuri C6 Software Traffic Light turns yellow and the cytometer pumps start to run. When powered on, the cytometer automatically flushes the fluidics lines with sheath. This process takes approximately five minutes. (Should be done at least 30 minutes prior to use)

4. When the BD Accuri C6 Software Traffic Light turns green and BD Accuri C6 Software displays the message C6 is connected and ready, run 0.22 µm filtered, DI water for at least 5 minutes on fast flow before processing samples

Prior to running each 'new' sample:

1. When the BD Accuri C6 Software Traffic Light turns green and BD Accuri C6 Software displays the message C6 is connected and ready, run purge or backflush

2. When the BD Accuri C6 Software Traffic Light turns green and BD Accuri C6 Software displays the message C6 is connected and ready, run 0.22 µm filtered, DI water for 15 seconds before processing samples

Running a sample:

1. When the BD Accuri C6 Software Traffic Light turns green and BD Accuri C6 Software displays the message C6 is connected and ready, place sample on SIP and pull table under so sample is resting securely

2. Ensure the flow is set to slow and the gating is set correctly for your sample, then select run

Annexin V Experimental Run and Labeling

1. Blood collection at Goddard Student Health Center
    a. Ensure informed consent, questionnaire, gift card and ethnicity forms are filled out completely
    b. 6 blue cap tubes, 3.5 mL 3.2% sodium citrate anticoagulant
    c. First tube is discarded, remaining 5 are kept for daily experiments
2. Confining blood to single 15 mL tube
    a. Ensure each collection blue top tube is well mixed
    b. With pipette remove 3 mL from each tube and add to single 15 mL tube
    c. Again mix blood in 15 mL tube by gently turning back and forth
    d. Mark top of blood on tube with sharpie for future use
3. Finding Pre wash Hematocrit
    a. Take microhematocrit tube and set in 15 mL tube with blood at an angle to allow blood to run up tube ~80%
    b. Immediately remove from blood and cap with putty
    c. Repeat for second hematocrit tube
    d. Place in microhematocrit centrifuge opposite each other and spin for 3 minutes
    e. Check and record hematocrit from both tubes
4. Take 15 mL tube and place in centrifuge with another 15 mL counter balance tube and centrifuge for 10 minutes
5. Remove carefully and take to biosafety hood
6. With Pasteur pipette carefully remove top of supernatant (~3 mL) and place in additional tube for later use
7. Remove rest of supernatant and buffy coat with Pasteur pipette and discard into waste
8. Refill tube to marker line with isotonic solution and mix gently by rotating tube back and forth
9. Repeat steps 4-6, without need for removing early supernatant, for a total of 3 washes
10. After third wash and centrifuging remove supernatant and replace with Ringers solution, again to marked line
11. Before centrifuging, hematocrit and cell count taken

a. For cell count ORFLO Moxi Mini Automated Cell Counter is used with Type S Moxi Z Cassette
b. In tube add 3 mL isotonic solution and 1 μL of cell suspension for 3000:1 dilution
c. Two cell counts should be averaged for consistency

12. Remove supernatant for a final concentration of $5 * 10^9$ RBC/mL
13. Shear environment protocol run
    a. Couette Viscometer
    b. Microfluidic Shear Channel
14. Post shear cells collected and a final concentration of $1 *10^6$ is pipetted into a microcentrifuge tube for each shear level/exposure time tested as well as a control
15. The cells are then labeled with 5 μL of cd235a FITC conjugate and Annexin V Alexa fluor 647 (ThermoFisher Sci)*
16. After further incubation with antibody for ~1 hr on hematology mixer, cells are run with BD Accuri C6 flow cytometer

*Fluorescent conjugates were chosen based on the excitation and detection to ensure little overlap and the requirement of color compensation to not be needed. Reference to each conjugate can be found in Molecular Probes Handbook: A Guide to Fluorescent Probes and Labeling Technologies 11^{th} Edition, 2010. (Alexa Fluor 647 absorption 650nm and emission 668nm; FITC absorption 494nm and emission 518nm)

IgG Fc Experimental Run and Labeling

1. Blood collection at Goddard Student Health Center
    a. Ensure informed consent, questionnaire, gift card and ethnicity forms are filled out completely
    b. 6 blue cap tubes, 3.5 mL 3.2% sodium citrate anticoagulant
    c. First tube is discarded, remaining 5 are kept for daily experiments
2. Confining blood to single 15 mL tube
    a. Ensure each collection blue top tube is well mixed
    b. With pipette remove 3 mL from each tube and add to single 15 mL tube
    c. Again mix blood in 15 mL tube by gently turning back and forth
    d. Mark top of blood on tube with sharpie for future use
3. Finding Pre wash Hematocrit
    a. Take microhematocrit tube and set in 15 mL tube with blood at an angle to allow blood to run up tube ~80%
    b. Immediately remove from blood and cap with putty
    c. Repeat for second hematocrit tube
    d. Place in microhematocrit centrifuge opposite each other and spin for 3 minutes
    e. Check and record hematocrit from both tubes
4. Take 15 mL tube and place in centrifuge with another 15 mL counter balance tube and centrifuge for 10 minutes
5. Remove carefully and take to biosafety hood
6. With Pasteur pipette carefully remove top of supernatant (~3 mL) and place in additional tube for later use
7. Remove rest of supernatant and buffy coat with Pasteur pipette and discard into waste
8. Refill tube to marker line with isotonic solution and mix gently by rotating tube back and forth
9. Repeat steps 4-6, without need for removing early supernatant, for a total of 3 washes
10. After third wash and centrifuging remove supernatant and replace with Ringers solution, again to marked line
11. Before centrifuging, hematocrit and cell count taken

a. For cell count ORFLO Moxi Mini Automated Cell Counter is used with Type S Moxi Z Cassette
b. In tube add 3 mL isotonic solution and 1 μL of cell suspension for 3000:1 dilution
c. Two cell counts should be averaged for consistency

12. Remove supernatant for a final concentration of $5 * 10^9$ RBC/mL
13. Shear environment protocol run
    a. Couette Viscometer
    b. Microfluidic Shear Channel
14. Post shear cells collected and a final concentration of $1 *10^6$ is pipetted into a microcentrifuge tube for each shear level/exposure time tested as well as a control
15. Immediately following the cells are allowed to incubate at 37°C with 5 μL of the collected supernatant from earlier for 30 min
16. After the incubation period of 30 min, the cells are then labeled with 5 μL of cd235a FITC conjugate and Alexa fluor 647 anti-human IgG Fc (BioLegend)
17. After further incubation with antibody for ~1 hr on hematology mixer, cells are run with BD Accuri C6 flow cytometer

*Fluorescent conjugates were chosen based on the excitation and detection to ensure little overlap and the requirement of color compensation to not be needed. Reference to each conjugate can be found in Molecular Probes Handbook: A Guide to Fluorescent Probes and Labeling Technologies 11^{th} Edition, 2010. (Alexa Fluor 647 absorption 650nm and emission 668nm; FITC absorption 494nm and emission 518nm)

Clot Procedures

1. Blood collection at Goddard Student Health Center
2. Confining blood to single 15 mL tube
3. Centrifuging blood
    a. For collection of washed cells same procedures as previously used
    b. Collect plasma and run additional centrifuge step at 6000g for 20 min to pellet platelets for PFP
    c. This plasma is used in final wash step to resuspend RBCs in PFP
4. Run Couette Viscometer shear step at required shear stress for study
5. Post shear centrifuge blood to collect MP rich plasma for clot production
6. Caraway capillary tube treatment
    a. Tubes first treated with clot adherence by etching with a dilute solution of hydrofluoric acid
    b. Tubes then treated with fibrinogen solution to ensure adherence
7. Clots are created from 16 µL of 0.25 M $CaCl_2$ to a mixture containing 50 µL PPP and 50 µL of either control or sample PFP
8. 70 µL of the mixture was injected into capillary tube and allowed to gel for 2 h at 37 °C to form a ~1.25-cm long clot
9. Any clots with visible structural deformities should be discarded

Percoll Density Gradient Procedures

1. Percoll and isotonic saline mixed to produce two solution with desired density according to the manufacture (Equation listed below)
2. 2 mL of sheared and non-sheared RBCs were layered separately onto the two Percoll solutions in 2.5. mL vials
3. Vials then centrifuged for 15 minutes at 150g.
4. RBCs pulled into the Percoll solution were removed and placed into separate 1.5 mL microcentrifuge tubes.
5. Approximately 1 mL of ringer solution added into the microcentrifuge tubes and centrifuged at 6000 rpm for 10 minutes
6. After the first wash, the Percoll/ringer solution was removed and replaced with fresh ringer solution.
7. The samples were centrifuged again for 10 minutes at 6000 rpm, and the above procedure was repeated once more to ensure percoll removal

$$\rho_i = \frac{v_o\rho_o + v_x\rho_{10}}{v_x + v_o}$$

Where: v_x = volume of diluting medium
v_o = volume of undiluted percoll
ρ_o = density of percoll
ρ_x = density of diluting solution (typically saline
ρ_i = density of produced solution

Chapter 2 - Figure 4 Data:

Following data was the raw collected data used for each figure in prospective figures.

Figure 3a:

	Control	5	10	15
	4140	26305	30185	34780
	6880	11260	17900	119130
	7215	19040	21710	63310
	7414.5	24718.5	19600	16575
	4063	33155	44245	87550
Mean	5943	22896	26728	64269
Std Error	757	3677	4862	18299

Figure 3b:

	Control	50,000 s^{-1}	100,000s^{-1}	150,000s^{-1}
	4140	13082	30185	40667
	6880	11459	17900	30733
	7215	78667	21710	33212
	7414.5	8533	19600	36,201
	4063	7480	44245	33,656
Mean	5943	9684	26728	34894
Std Error	757	1100	4862	1684

Chapter 3 - Figure 2 Data:

Following data was the raw collected data used for each figure in prospective figures.

Figure 2 f:
Percent cells for anti-IgG Fc alexa fluor 647 fluorescence as detected by the FL4 channel for varying exposure times to high shear in microfluidic channels.

	St Channel	1 msec	5 msec	10 msec	15 msec	Control
	1.68	2.47	4.77	10.68	15.97	1.98
	0.61	1.88	4.08	10.94	19.73	0.45
	1.12	1.00	7.00	16.82	12.11	2.31
	0.10	2.48	4.77	13.40	15.97	0.67
	1.72	4.25	3.94	7.00	15.64	2.42
Mean	1.05	2.42	4.91	11.77	15.88	1.56
Std Error	0.31	0.53	0.55	1.62	1.21	0.42

*Values shown are percent

Figure 2g:
Percent cells for anti-IgG Fc alexa fluor 647 fluorescence as detected by the FL4 channel for varying shear stresses in Couette Viscometer.

	Control	100 dyn/cm2	500 dyn/cm2	900 dyn/cm2	1300 dyn/cm2
	0.85	1.75	4.63	12.77	12.90
	0.89	1.96	3.53	12.69	21.24
	0.04	1.60	2.89	11.40	19.62
	1.44	1.00	4.32	11.57	15.00
	1.59	4.25	3.58	11.75	11.44
Mean	0.96	2.11	3.79	12.04	16.04
Std Error	0.27	0.56	0.31	0.29	1.90

*Values shown are percent

Chapter 3 - Figure 3 Data:

Following data was the raw collected data used for each figure in prospective figures.

Figure 3c:
Relative increase in fluorescence values from FL4 channel relating to the anti-IgG Fc alexa fluor 647 fluorescence.

	Control	1 msec	5 msec	10 msec	15 msec
	1.08	1.46	1.43	1.20	1.45
	1.08	0.73	2.01	1.89	1.57
	1.50	1.04	1.15	1.99	1.88
	0.64	1.93	0.87	0.83	2.25
	0.70	1.46	0.84	1.11	2.03
Mean	1.00	1.33	1.26	1.40	1.83
Std Error	0.16	0.21	0.21	0.23	0.15

*Values are relative to average from control values.

Chapter 3 - Figure 4 Data:

Following data was the raw collected data used for each figure in prospective figures.

Figure 4b:
Percent cells for Annexin V alexa fluor 647 fluorescence as detected by the FL4 channel for varying exposure times to high shear in microfluidic channels.

	Control	5 msec	10 msec	15 msec
	2.07	1.23	0.65	0.65
	0.19	0.80	4.32	0.77
	3.66	0.38	4.19	1.38
	0.95	2.83	1.23	1.47
	1.68	1.38	0.80	1.34
Mean	1.71	1.32	2.24	1.12
Std Error	0.58	0.42	0.83	0.17

*Values shown are percents

Figure 4c:
Relative increase in fluorescence values from FL4 channel relating to the Annexin V alexa fluor 647 fluorescence.

	Control	5 msec	10 msec	15 msec
	1.48	1.45	2.67	3.20
	0.80	1.60	2.24	3.02
	0.74	2.47	3.14	2.91
	0.67	1.89	2.78	2.95
	1.30	2.53	2.77	3.08
Mean	1.00	1.99	2.72	3.03
Std Error	0.16	0.22	0.14	0.05

*Values are relative to average from control values.

Chapter 4 - Figure 3 Data

Following data was the raw collected data used for each figure in prospective figures.

Pressure Drop 10mmHg/cm			
	Plasma		
	Control	90 Pa	130 Pa
	4.77	5.25	8.67
	5.23	8.53	7.2
	5.17	7.68	8.7
	8.38	8.00	11.55
	5.13	6.55	12.17
Average	5.74	7.20	9.66
Std Dev	1.49	1.31	2.11
Std Err	0.67	0.66	1.06

Pressure Drop 5mmHg/cm			
	Plasma		
	Control	90 Pa	130 Pa
	12.42	13.75	12.75
	10.33	10.42	8.7
	12.37	9.08	18.92
	8.28	12.75	19.00
	10.08	12.63	13.92
Average	10.70	11.73	14.65
Std Dev	1.74	1.91	4.37
Std Err	0.78	0.86	1.95

Pressure Drop 10mmHg/cm			
	Whole Blood		
	Control	90 Pa	130 Pa
	4.77	8.72	9.75
	5.23	10.27	15.53
	5.17	18.97	13.37
	8.38	15.72	15.15
	5.13	12.92	14.75
Average	5.74	13.32	13.71
Std Dev	1.49	4.13	2.36
Std Err	0.67	2.07	1.18

Pressure Drop 5mmHg/cm			
	Whole Blood		
	Control	90 Pa	130 Pa
	12.42	9.80	15.15
	10.33	13.75	15.8
	12.37	17.33	20.7
	8.28	13.42	27.08
	10.08	15.92	25.55
Average	10.70	14.04	20.86
Std Dev	1.74	2.86	5.45
Std Err	0.78	1.28	2.44

Chapter 4 - Figure 4 Data

Following data was the raw collected data used for each figure in prospective figures.

Pressure Drop 10mmHg/cm			
	Plasma		
	Control	90 Pa	130 Pa
	0.082	0.07	0.031
	0.09	0.06	0.028
	0.06	0.02	0.063
	0.11	0.06	0.036
	0.09	0.05	0.041
Average	0.085	0.052	0.040
Std Dev	0.0171	0.0180	0.0136
Std Err	0.008	0.008	0.006

Pressure Drop 5mmHg/cm			
	Plasma		
	Control	90 Pa	130 Pa
	0.042	0.03	0.029
	0.03	0.05	0.025
	0.03	0.03	0.013
	0.07	0.05	0.028
	0.05	0.03	0.014
Average	0.043	0.037	0.022
Std Dev	0.015	0.009	0.008
Std Err	0.007	0.004	0.003

Pressure Drop 10mmHg/cm			
	Whole Blood		
	Control	90 Pa	130 Pa
	0.082	0.07	0.053
	0.09	0.04	0.059
	0.06	0.05	0.034
	0.11	0.05	0.033
	0.09	0.03	0.036
Average	0.085	0.047	0.043
Std Dev	0.017	0.013	0.012
Std Err	0.008	0.006	0.005

Pressure Drop 5mmHg/cm			
	Whole Blood		
	Control	90 Pa	130 Pa
	0.042	0.04	0.027
	0.03	0.03	0.026
	0.03	0.02	0.028
	0.07	0.04	0.021
	0.05	0.020	0.018
Average	0.043	0.027	0.024
Std Dev	0.015	0.008	0.005
Std Err	0.0068	0.004	0.002

Chapter 4 - Figure 5 Data

Following data was the raw collected data used for each figure in prospective figures.

	Control	90 Pa	130 Pa
	12.7	14.6	14.4
	16.1	12.5	13.5
	12.9	12.6	15.1
	16.3	13.1	14.1
	14.9	12.9	16.0
	8.6	9.2	13.5
	8.4	7.7	15.2
	7.9	7.8	12.0
	6.7	8.9	14.3
	9.2	7.9	13.5
	10.2	12.6	15.5
	8.9	12.2	16.6
	9.6	12.6	16.6
	10.6	11.1	19.8
	9.8	12.5	20.6
Average	10.9	11.1	15.0

Phenylhydrazine Data

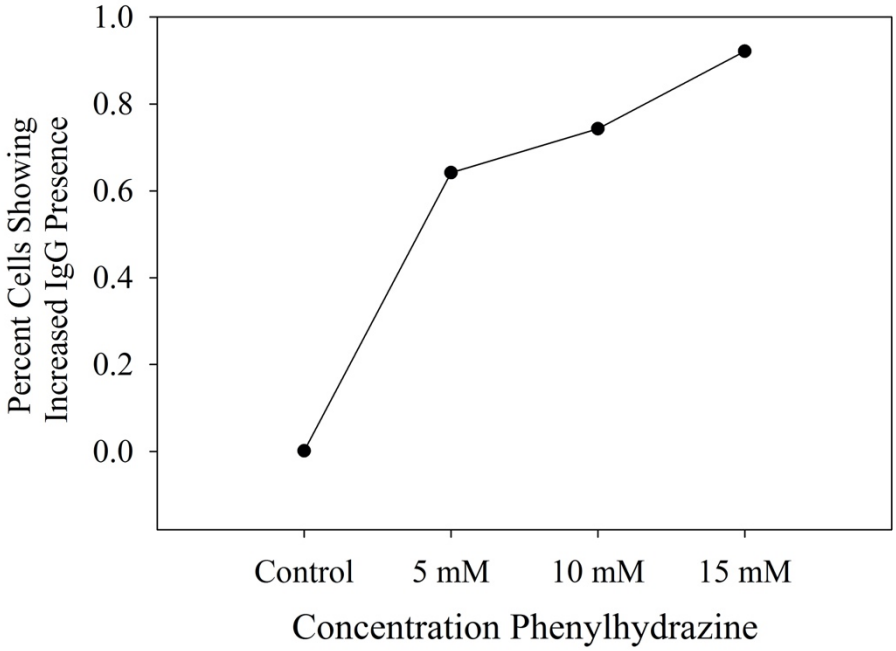

*Shown is 0 – 100% where 1.0 relates to 100%

Dynamic Light Scattering Data

The Brookhaven NanoBrook Omni (scattering angle 173º) was used to find average ErMP size for its ability to size in high salt concentration solutions, similar to the Ringers solution used in our experiments. To accomplish concentrations of ErMPs large enough for detection, a Couette Viscometer was used to shear 4.2mL washed RBCs, for 2 min at 900 dyn/cm^2. Post shear, blood was collected and centrifuged at 150g for 10 min, and the ErMP containing supernatant was removed for further processing. Before DLS measurements were taken, two - 8 hour dialysis steps were done with a MWCO of 100 kD to remove any free hemoglobin present in suspension.

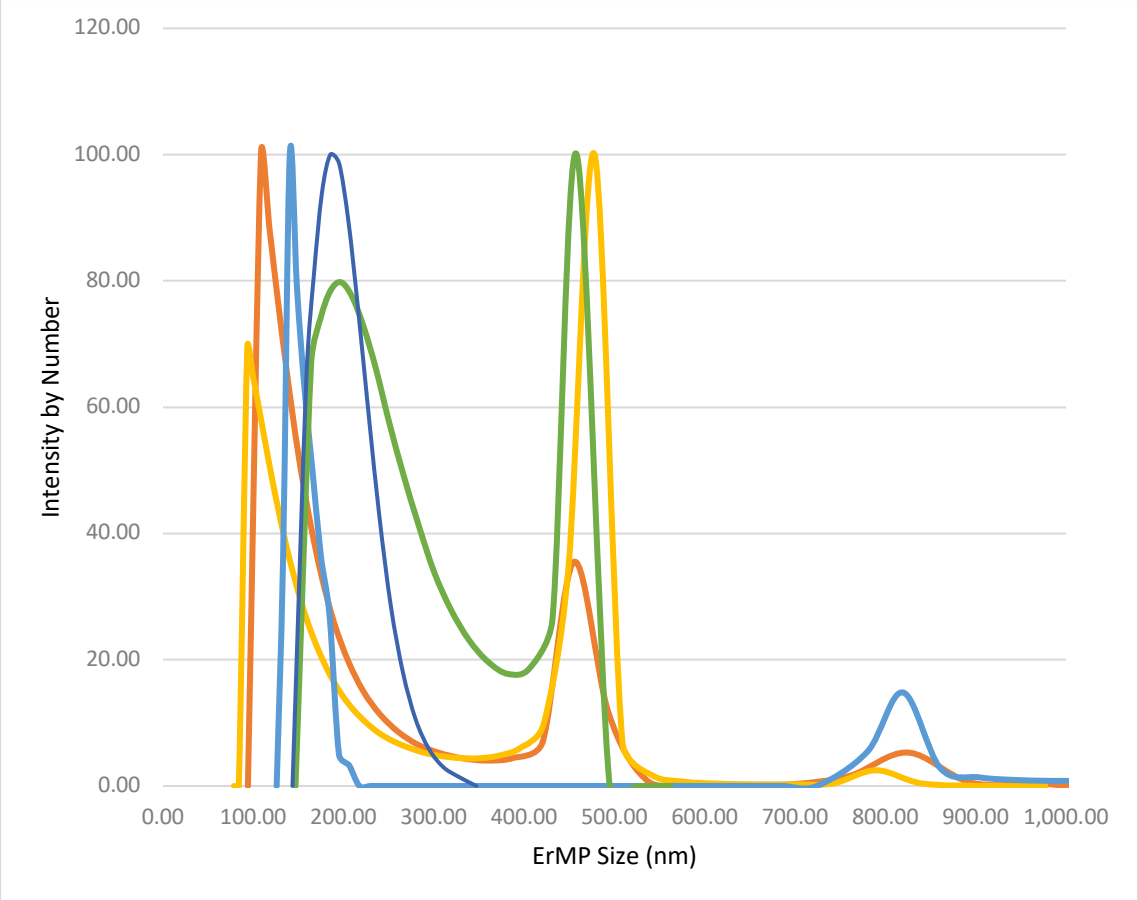

ErMP Clot Model Simulations

A clot simulation model was created using Visual Basic for Applications (VBA) in Microsoft Excel. The program allowed inputs for the size of the lattice, ErMP concentration, FG concentration, reactivity parameter, and number of timesteps to execute. In the grid, each cell represents one of four possible states: empty, ErMP (red), FG (blue), or FB (green). The ErMPs serve as catalyst that initiate the conversion of FG to FB. All simulations ran for 2500 timesteps at a grid size of 26x52 cells (rows x columns). Data collection occurred every 100 timesteps and included calculating FB coverage and number of connection points. A range from 5-15% of starting FG concentrations were tested to choose a concentration for later simulations testing different ErMP concentrations, and also verify the model behaves as expected. For the ErMP studies, an FG starting concentration of 10% was chosen because the lower concentrations result in grids that do not visually look clotted within a reasonable number of timesteps, and the larger values were not used because physiological normal levels of FG are not large. Two ErMP concentrations were tested, 0.5% and 1%, and were selected to mimic the increase in ErMPs seen *in vitro*.

The model uses different rules to dictate the movements and interactions of each component for each timestep. A timestep is defined as a raster across the grid where each component is allowed the opportunity to move or interact with other components. Movement of each cell was determined randomly through a random number generator, generating a number from 1 to 1000. For each case, the cell would attempt to migrate to one of its 8 neighbors based on the generated random number (i.e. 1-125 results in a move to neighbor 1). All elements (ErMP, FG, and FB) in the lattice randomly migrate during the simulation. In the scenario that a ErMP, FG, or FB try to move to an occupied cell, resulting in a collision of the two elements,

there may be an interaction with that cell. Interactions only occur amongst FGs and ErMPs, or between two FBs. In the case that FB moves to collide with an ErMP or FG cell, no interaction takes place. In the case that an interaction is possible, an additional reactivity parameter must also be met. The reactivity parameter was set at 0.5 and a random number generator was used to see if the criteria was met (random number less than 500). If the reaction parameter criteria is not met, they do not interact and no conversion or bond formation takes place. In the instance that an FG attempts to move to a cell containing an ErMP, or vice versa, and the reactivity parameter is satisfied, the cell originally containing the FG is converted to FB, and the MP remains in its respective cell. If an FB monomer encounters another FB monomer, and the reactivity parameter is satisfied, then the two will form a dimer. Similar to actual clot structure, the formed fibrin polymers are linear. As the polymers grow, FB monomers are added onto the end of an FB polymer, or two FB polymers can combine if their ends interact, so long as the addition maintains the linear nature of the polymer. The only FB cells allowed to migrate are monomers and those in a dimer, so long as the dimer does not break. If those in a longer polymer could move the linear nature of that polymer would be compromised. If the random number generator chooses a move that is not allowed for the FB ‘mer, no move occurs. This is similar to the rules used to simulate random polymer walking, with the exception of introducing the criteria that polymers must maintain linearity.[186] A border, used as an FG source, encompasses the user defined grid space with a boundary condition of constant FG concentration. Following each timestep, the border is cleared and set to the user defined FG concentration. ErMP concentration was set at 0.5 and 1.0% and they were not allowed to move across the border during the simulation. Additionally, FB cells were also kept from migrating across the border.

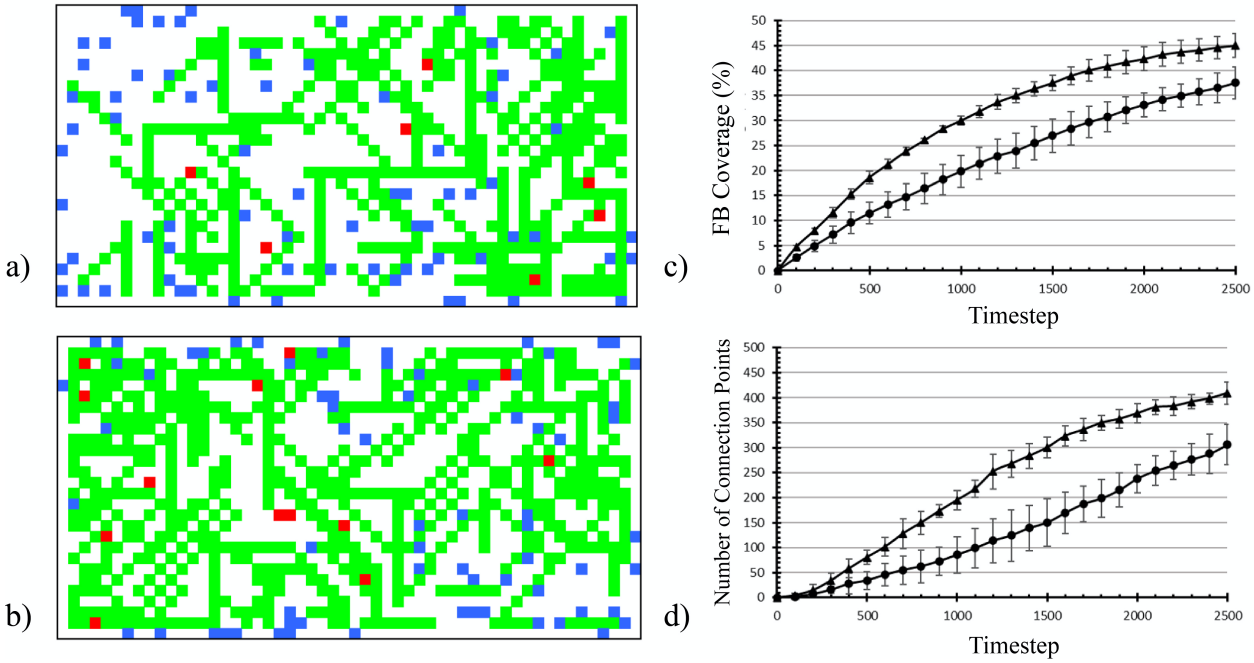

Simulation results comparing MP concentrations of 0.5% (n=5) and 1.0% (n=5) for a starting FG concentration of 10%. Shown are representative sample grids showing ErMP (red), FG (blue), and FB (green) configurations for a) 0.5% ErMP and b) 1.0% ErMP grids after 2500 timesteps, and average values of c) FB coverage ($p<0.01$ at 2500) and d) number of connection points ($p<0.01$ at 2500) for 0.5% ErMP (●) and 1.0% ErMP (▲).